Pore-Scale Investigation of Salt Precipitation during Evaporation from Porous Media

A thesis submitted to the University of Manchester for the degree of
Doctor of Philosophy
in the Faculty of Engineering and Physical Sciences

2014

Mansoureh Norouzi Rad

School of Chemical Engineering and Analytical Science

Contents

Total word count: 32081

List of Figures

within the first scanned block (3.3×3.3×1.7 mm3) is shown for five time steps. Isolated liquid clusters were filtered out to highlight continuous liquid phase only. In course of evaporation, water content decreases without breaking phase continuity" (Shokri et al., 2010) …… **148**

C.3.1 (a) A typical horizontal cross section above the surface, taken at the beginning of the experiment, illustrating the liquid [blue (dark gray)] and solid [brown (medium gray)] phases. (b) The same cross section after 17 h, showing the distribution of the solid [brown (medium gray)] and air (white) phases. (c) The image constructed by comparing the solid phases in (a) and (b) with the difference [orange (light gray)], corresponding to the precipitated salt. (d) A typical vertical close-up of the surface of the sand column saturated with 4 Molal NaCl solution, constructed by the same method as in (c) and applied to all cross sections. The spectrum of orange to yellow (medium to light grey) indicates the addition of precipitated salt in each scan. Brighter colours indicate longer times ……. **149**

C.3.2 "Cumulative mass of liquid water removed by evaporation from the sand columns, initially saturated with various NaCl solutions. The notably lower water evaporation from the 4.0 Molal solution might be due to the lower atmospheric demand. Although the evaporative demand was nearly constant during each round of the experiment, the relative humidity and temperature inside the x-ray chamber could not be controlled precisely. The inset shows the near surface (the top 0.5 mm) water saturation, confirming the presence of liquid at the surface during the entire course of the experiments". (Norouzi Rad *et al.* 2013) ……. **150**

C.4.3 "Cumulative mass of liquid water removed by evaporation from the columns packed with sand and glass beads initially saturated with NaCl solution. The symbols correspond to the cumulative mass loss measured during the experiments with X-ray microtomography determined from image analysis. In addition, three repetitions (written as rep. in the legend) were performed in the lab to measure the evaporation rate using digital balances to check the reproducibility of the observed behavior, *i.e.*, higher evaporation from sand

pack compared to the glass beads. The solid and dash lines indicate the data measured using the balance. The slight difference in the measured cumulative mass loss in each round is due to the slight fluctuation of the evaporative demand during each round affecting the evaporative mass losses during stage-1 evaporation". (Norouzi Rad *et al.*, 2014) ……. **151**

C.4.5 "(a) Water saturation profiles at different times from the onset of the evaporation experiments in the columns packed with sand and glass beads. (b) The average water saturation over the top 1 mm of the sand and glass beads columns confirming the presence of water close to the surface during the entire course of our experiments in both cases and also higher water saturation in the case of sand compared to glass beads." (Norouzi Rad *et al.*, 2014) ……. **152**

List of Tables

Abstract

of thesis submitted by **Mansoureh Norouzi Rad** for the degree of **Doctor of Philosophy** and entitled "**Pore-Scale Investigation of Salt Precipitation during Evaporation from Porous Media**" on 12 December 2014

Understanding the physics of water evaporation from saline porous media is important in many processes such as soil salinity, terrestrial ecosystem functioning, vegetation and crop production, biological activities in vadose zone, and CO_2 sequestration. Precipitation of salt is one of the possible outcomes of the evaporation process from saline porous media which may either enhance or interrupt the desired process depending on the localization and pattern of the precipitated salt. In the present study X-ray micro tomography was used to study the 3D dynamics and patterns of salt deposition in drying porous media under different boundary conditions and the effects of salt concentration, particle size distribution and shape of grains on the precipitation patterns and dynamics at pore-scale have been investigated. Evaporation process from porous media involves preferential invasion of large pores on the surface while the fine pores remain saturated serving as the evaporation sites to supply the evaporative demand. This results in increasing salt concentration in fine pores during evaporation. Precipitation starts when salt concentration exceeds the solubility limit in the preferential evaporation sites. At the early stages, the precipitation rate increases with time until all evaporation sites at the surface reach the solubility limit and turn into the precipitation sites. This is followed by a constant rate of precipitation proportional to the evaporation rate. We show that the formation of salt crust at the surface does not immediately interrupt the evaporation process due to the porous nature of the precipitated salt investigated using the scanning electron microscopy. Also, our results confirmed the formation of discrete efflorescence at the surface of porous media due to the presence of pores with different sizes. Distribution of these fine pores on the surface directly influences the patterns of salt precipitation and thickness of the salt crust such that in the media with more fine pores, precipitated salt forms a thinner crust as the solute transferred to the surface is distributed among more evaporation sites. In contrast, in the media with fewer evaporation sites at the surface the salt crust will be more discrete but thicker. A simple equation is also proposed to estimate the evolution if the thickness of the salt crust on the surface of porous media. Our results provide new insights regarding the physics of salt precipitation and its complex dynamics in porous media during evaporation.

Declaration

No portion of the work referred to in the thesis has been submitted in support of an application for another degree or qualification of this or any other university or other institute of learning.

Copyright Statement

i. The author of this thesis (including any appendices and/or schedules to this thesis) owns certain copyright or related rights in it (the "Copyright")[1] and s/he has given The University of Manchester certain rights to use such Copyright, including for administrative purposes.

i. Copies of this thesis, either in full or in extracts and whether in hard or electronic copy, may be made only in accordance with the Copyright, Designs and Patents Act 1988 (as amended) and regulations issued under it or, where appropriate, in accordance with licensing agreements which the University has from time to time. This page must form part of any such copies made.

ii. The ownership of certain Copyright, patents, designs, trademarks and other intellectual property (the "Intellectual Property") and any reproductions of copyright works in the thesis, for example graphs and tables ("Reproductions"), which may be described in this thesis, may not be owned by the author and may be owned by third parties. Such Intellectual Property and Reproductions cannot and must not be made available for use without the prior written permission of the owner(s) of the relevant Intellectual Property and/or Reproductions.

iv. Further information on the conditions under which disclosure, publication and commercialisation of this thesis, the Copyright and any Intellectual Property and/or Reproductions described in it may take place is available in the University IP Policy (see http://documents.manchester.ac.uk/DocuInfo.aspx?DocID=487), in any relevant Thesis restriction declarations deposited in the University Library, The University Library's regulations (see http://www.manchester.ac.uk/library/ aboutus/regulations) and in The University's policy on Presentation of Theses.

[1] This excludes the chapters which are already published in academic journals for which the publisher owns the copyright

Dedication

To the angels of my life! My mother, Forough, the strong and lovely woman, who helped me become the person I am. And my sister, Maryam, the best friend, who listened, believed and taught me to follow my dreams.

And

To my father, who would have been proud.

Acknowledgements

First and foremost, I would like to express my deepest gratitude to my supervisor, Dr. Nima Shokri. I am grateful for his patience, enthusiasm, immense knowledge and selfless dedication which helped both my personal and academic development. I have been extremely lucky to work with such a caring supervisor and cannot think of a better one to have.

I would like to thank the Department of Earth and Environment at Boston University, American Chemical Society Petroleum Research Fund (PRF 52054-DNI6) and School of Chemical Engineering and Analytical Science at The University of Manchester for funding my PhD.

I am also thankful to the staff members at the Center for Nanoscale Systems (CNS) at Harvard University and Manchester X-ray Imaging Facilities (MXIF) especially Dr. Fettah Kowsar and Dr. Samuel McDonald for their help in micro scale imaging and image reconstruction and Ms. Pen Richardson at The Computational Shared Facility for her help in using High Performance Computing cluster for image analysis.

And last but not least, I would like thank my husband, Siamak, for his support, encouragement and unwavering love.

Chapter 1

Introduction

Precipitation and deposition of salts in porous media during evaporation is important in many natural processes and industrial and environmental applications. Salt deposition may change the evaporation rate and modify the structure and transport properties of porous media. In soil, excessive accumulation of salt may result in soil salinity which affects the terrestrial ecosystem functioning, crop production, vegetation and biodiversity in vadose zone (Nassar and Horton, 1989l; Shimojimaa *et al.*, 1996; Gran *et al*., 2011). Also, soluble salts exist in porous materials such as food, paper, building materials which may precipitate when the product goes under drying influencing the quality as well as strength and durability of the materials (Farifteh *et al*., Zhao, *et al*., 2014, Kucuk *et al*., 2014, Fonseca and Scherer, 2014, Walters *et al*., 2014, Bickle, 2009). Crystallization and salt precipitation in porous media not only change the appearance of the material, but also may cause serious damages to its structure and modify its flow and transport characteristics motivating many researcher to investigate this phenomenon (Tsui *et al*., 2003, Espinosa-Marzal *et al*., 2011, Flatt, 2014). Although the topic of salt transport and precipitation patterns in drying porous media has motivated many studies owing to the significance of related practical issues, as stated in Veran-Tissoires *et al*. (2012), "the understanding of the efflorescence formation and growth at the surface of a porous material is surprisingly not very advanced".

The main objective of this thesis is to obtain a better physical understanding of salt precipitation patterns and dynamics during evaporation from porous media. To do so, one

should know the physics of the evaporation process from porous media as well as the effects of the presence of soluble salts on the process. In this chapter a brief introduction and background on evaporation from saline porous media is presented.

1.1 Evaporation from Water Surface

Water evaporation is a phase change from liquid to the gas state. It is a mass transfer process driven by the vapour pressure gradient between the water surface and the surrounding ambient. In stagnant air[2], this process may be explained by Fick's first law, where the vapour flux is proportional to the difference in the water vapour concentration between the surface of the water body and the bulk air (McCabe *et al*.,2004).

$$J\ \alpha\ (P_s^w - P_\infty) \tag{1.1}$$

where J is the vapour flux, and P_s^w and P_∞ are the partial pressure of water vapour close to the surface and in the bulk air, respectively. Since the air film on the surface of the water is saturated with water molecules, partial pressure of the water vapour on the surface is equal to the saturation vapour pressure of water in the ambient temperature. The partial pressure of water vapour in the ambient temperature may be calculated by measuring the relative humidity (RH%) of the air:

$$RH\% = \frac{P_\infty}{P_s^w} \tag{1.2}$$

When there is soluble salt in water, the saturated vapour pressure will be different due to the different bonding force between the water molecules and solute in the liquid phase. In this case P_s^w in equation 1.1 will be substituted with P_s^{sol} which is the vapour pressure of the solution. P_s^{sol} depends on both temperature and the salt concentration in the water phase

and may be estimated using thermodynamic equations or tables. Vapour pressure of water containing soluble salts is generally lower than that of pure water which leads to a smaller driving force for water evaporation and consequently lower evaporation rates (Nassar and Horton, 1989; Shimojimaa *et al*., 1996; Nachshon *et al*., 2011).

1.2 Evaporation of Pure Water from Porous Media

When the porous medium is saturated with water (*i.e.* all the pore space is completely filled with water) and exposed to air for natural evaporation, it experiences two distinctive stages of evaporation rates described briefly in the following. At the early stages of evaporation, larger pores are invaded preferentially by air as they have smaller capillary pressure and cannot retain the water. As a result, the evaporation process is supplied by the capillary-induced liquid flow from the saturated zone at bottom to the smaller water filled pores located at the surface. At this stage, the so-called stage-1 evaporation, the liquid vaporization mainly occurs in the small pores at the surface and vapour transports to the atmosphere via diffusion. This stage of evaporation is mainly limited by the atmospheric condition (ambient temperature and relative humidity, wind velocity, solar radiation). The evaporation rate during stage-1 is relatively constant which may fluctuate as the environmental conditions change.

During stage-1, there is a competition between upward capillary forces and downward gravity forces (the viscous force may be negligible in the case of large particles such as sandy media). When these two forces are balanced, capillary-induced liquid flow is no longer able to maintain the liquid connection between the saturated zone and the surface of porous media. This results in disconnection of hydraulic pathways which marks the end of stage-1 evaporation and onset of the transition to stage-2 evaporation (Nissan *et al*. 1959; Kowalski, 1999; Shokri *et al*., 2007; Lehmann *et al*., 2008; Or *et al* 2013).

During transition, the continuous liquid pathways disconnects from the surface gradually. When all the liquid connections are disconnected from the surface, a new vaporization plane forms below the surface marking the onset of stage-2 evaporation. During this period, liquid is transported from the wet zone at bottom to this new vaporization plane, liquid vaporization occurs at that level and vapour diffuses through the overlaying dry layer (Shokri *et al*., 2009). The two stage of evaporation rate as well the transition period is presented in Figure 1.1 which illustrates a typical evaporation curve measured during evaporation from sand pack.

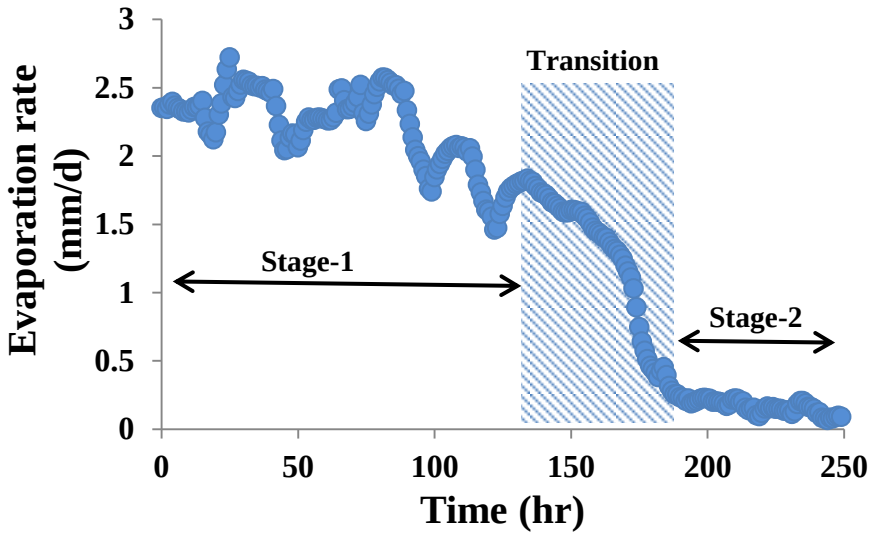

Figure 1.1 A typical evaporation curve measured during evaporation from sand pack (measured in the lab). Evaporation rate is relatively high and constant during stage-1 limited by the atmospheric condition, followed by a much lower rate controlled by the vapour diffusion through porous media during stage-2.

1.3 Evaporation from Saline Porous Media

In the presence of soluble salt in water during evaporation from porous media, salt is transported by convection induced by capillary liquid flow toward the evaporating surface where it accumulates, whereas diffusion tends to spread the salt and homogenize

concentrations in space (Huinink *et al*., 2002; Guglielmini *et al*., 2008). Therefore, the competition between the convection and diffusion affects the dynamics of salt distribution in porous media. This competition is often characterized by the dimensionless Peclet number which quantifies the relative importance of convective and diffusive transport. For large Peclet numbers (Pe > 1), convection is the dominant transport process and solute concentration increases close to the the surface of the medium while for smaller Peclet numbers (Pe < 1), the process is controlled by diffusion and concentration tend to distribute homogenously through the drying porous medium (Guglielmini, 2008).

During evaporation from saline porous media, when Peclet number is larger than 1, the solute concentration on the evaporation surface increases continuously. Higher concentrations lower the vapour pressure of the solution and as a result evaporation rate decreases. Therefore in saline porous media, during stage-1 evaporation, even though the surface is still wet, the evaporation rate may show a decreasing rate due to the increasing concentration over time (Bechtold *et al*, 2011). The change in the evaporation rate during stage-1 of evaporation from saline porous media depends on the initial concentration and the evaporative demand. Figure 1.2 shows a typical evaporation curve measured during evaporation from sand pack saturated with NaCl solution.

If at any stage of the evaporation, the concentration exceeds the solubility limit of salt and reaching super-saturation, crystallization may occur in a metastable state of equilibrium which may result in precipitation of salt. The degree of super-saturation where precipitation occurs can be affected by environmental conditions, and soluble and solid states of dissolved salt (Veran Tissoires *et al*, 2014; Shahidzadeh *et al* 2008). Salt precipitation may happen either on the surface of the porous media which is called efflorescence or inside the media which is called sub-florescence. Occurrence of

efflorescence or sub-florescence depends on the dominant process of salt transfer. If the convection is controlling (*i.e.* large Peclet numbers), then precipitation happens on the surface of the porous media. On the other hand, if the salt transport is controlled by diffusion (*i.e.* small Peclet numbers), precipitation is most likely happen inside the media (Huinink *et al.*, 2002). This process may be influenced by the parameters affecting the convective transport (*e.g.* the rate of evaporation, environmental conditions) and/or diffusive transport (*e.g.* nature of the salt, temperature). In this project, sodium chloride (NaCl) is used as the salt in our investigation. Also, we do not consider sub-florescence in this dissertation as the focus of the project was on efflorescence.

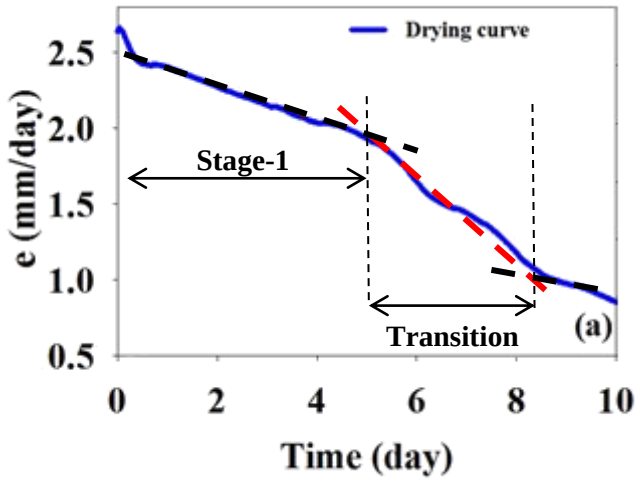

Figure 1.2 A typical evaporation curve measured during evaporation from sand pack saturated with NaCl solution of 2.5 Molal (Norouzi Rad and Shokri, 2012). Evaporation rate is decreasing during stage-1 due to the increasing salt concentration at the surface.

The precipitation patterns of sodium chloride at the surface of porous media depend on the evaporation rate, pore distribution and shapes, hydrophobicity and texture of the media. It has been shown that the thickness of the mass transfer boundary layer which affects the rate and consistency of evaporation rate affects the pattern of the efflorescence (Veran-Tissoires et al., 2012a). Preferential evaporation affecting the localization of salt precipitation on the surface of the porous media has been observed in previous papers.

Nachshon *et al.* (2012b) studied the evaporation from porous media with vertical textural contrasts (*i.e.* hydraulically connected vertical layers of porous media differing in particle sizes) and observed the salt precipitation on the surface of fine textured medium which is due to the higher capillarity of the finer medium. Similar results have been reported by Veran-Tissoires *et al.* (2012b). These studies confirm the influence of the locations of the small pores on the pattern and localization of the salt precipitation. Recently, a synchrotron X-ray microtomography study on the pore-scale dynamics of dissolved salt transport and distribution in drying porous media also confirmed the preferential accumulation of solute in fine pores on the surface of porous media during evaporation (Shokri, 2014).

The majority of the studies investigating salt precipitation and efflorescence patterns in drying porous media were conducted at macro-scale and mainly focused on twodimensional evaporating surfaces with a very few exception such as Nachshon *et al.,* (2011a). Three-dimensional (3-D) investigation of salt precipitation patterns in porous media is rare mainly because of the difficulty and limitation of the available techniques capable of visualization of the dynamics of salt precipitation in drying porous media which is precisely the objective of the present dissertation. .

1.4 Thesis Overview

The lay out of the thesis is as following. In chapter 2, the effect of salt concentration on evaporation rate in drying porous media and rate of efflorescence formation and its relation with drying rate have been investigated. Chapters 3, 4 and 5 are on pore scale study of salt precipitation dynamics and patterns in porous media during evaporation. Chapter 3 is on the dynamics of salt precipitation as influenced by salt concentration in the evaporating solution. In chapter 4, effects of the grain irregularity on the salt precipitation patterns is

investigated. Grain shape and irregularity modifies the pore size distribution which affects the pattern of efflorescence. Chapter 5 is on the effects of the pore size distribution on the salt precipitation patterns using porous media with different texture. This thesis is prepared in an "alternative format" and contains published papers (chapters 2, 3 and 4) and a manuscript which is in review (chapter5).

At the end, Appendix A is on the numerical solution of the Convection Diffusion Equation (CDE) which was used in both chapters 2 and 3 and the relevant MATLAB code used for that. And Appendix B which is on image analysis and use of Support Vector Machines (SVM) for image segmentation. Since these methods were used as the tools to achieve the information needed for the main data analysis, they are presented as the appendices on the thesis.

Throughout the thesis, adding or changing some of the statements and/or presenting some figures with more details was be required for better clarification. However, due to the copyright issues it was not possible to alter the texts. So these changes and additional information are presented as footnotes. The modified figures are presented in Appendix C.

Chapter 2

Nonlinear effects of salt concentrations on evaporation from porous media

This chapter has been published in the Geophysical Research Letters, volume 39 in 2012. The main objective of this chapter is to study the effects of salt concentration on evaporation from porous media and the relation between the salt crust formation and the rate of evaporation. This is a macro-scale study and the efflorescence formation was studied in 2D. Experiments were carried out using the glass columns packed with silica sand particles saturated with NaCl solutions varying in concentration.

The results presented in this chapter suggest that evaporation may be enhanced due to the salt crust formation which was observed by other researchers as well (Sghaier *et al*. 2009; Eloukabi *et al*. 2011). This is shown in section 2.4.1 but then corrected in section 2.5.Also the dynamics of salt precipitation on 2D surfaces as influenced by the salt concentration are investigated which resulted in proposing a non-destructive method to estimate the end of stage-1 evaporation based on the salt precipitation rate at the surface of porous media.

Nonlinear effects of salt concentrations on evaporation from porous media

Mansoureh Norouzi Rad and Nima Shokri

GEOPHYSICAL RESEARCH LETTERS, VOL. 39, L04403, doi:10.1029/2011GL050763, 2012

Abstract

Evaporation from porous media saturated with salt solution is influenced by the interactions among the transport properties of porous media, thermodynamics of the evaporating solution and environmental conditions. To study the effects of salt concentrations on the evaporation dynamics, we conducted a series of evaporation experiments under constant atmospheric conditions using columns packed with sand particles saturated with various NaCl solutions differing in concentrations. Results show that the evaporation rate decreases as NaCl concentration increases only up to a certain level. When exceeding this level, any further increase of NaCl concentration results in higher evaporation rates which is described theoretically using the thermodynamics of the solution. Results also reveal a nonlinear relation between NaCl concentrations and onset of efflorescence which is described by the numerical solution of the classical convection-diffusion equation. Moreover, we found a strong correlation between the growth dynamics of precipitated salt at the surface and the evaporation rate such that the maximum rate of surface coverage by salt coincide with the end of stage-1 evaporation. This potentially offers a new method to nondestructively study the evaporation process from saline porous media.

2.1 Introduction

Fundamental understanding of the evaporation process from porous media in the presence of soluble salt is important in various environmental and hydrological applications such as soil salinization, rock weathering, terrestrial ecosystem functioning, plant growth and vegetation, microbiological activities and biodiversity in vadose zone. Also complex dynamics of salt precipitation patterns affected by the salt concentration in pores of rock,

masonry, and porous building materials can generate stresses which may lead to severe damages (Scherer, 1999; Flatt, 2002; Scherer, 2004). Thus it is important to understand the effects of salt concentration on evaporation process and general dynamics of the salt precipitation patterns.

Several studies showed that the presence of salt lowers the evaporation rate from porous media (Nassar and Horton, 1989; Shimojimaa *et al.*, 1996; Nachshon *et al.*, 2011). For instance, Shimojimaa *et al*. [1996] reported that in the presence of water table, the evaporation rate from silica sands and glass beads saturated with NaCl solution of 0.3 Molal (*i.e.*, moles of salt per kilograms of water) was reduced 70% and 30%, respectively, compared to the evaporation rate from pure water. Nassar and Horton [1999] also reported reduction of the evaporation rate due to the presence of KCl in water. Despite the fact that areas such as salt-affected lands, salt marshes, and salt lakes may contain high salt concentrations, most of the previous evaporation studies focused on the situations in which salt concentrations were relatively low and very few studies attempted to quantify the evaporation process from porous media saturated with highly saline solutions.

Along with the evaporation rates, the dynamics of salt distribution and precipitation patterns depend significantly on the salt concentration. During evaporation from porous media, dissolved salt is transported via capillary induced liquid flow toward the evaporating surface where it preferentially accumulates (Shokri *et al.*, 2010). When salt concentration exceeds the saturation level, precipitation starts. The process is called efflorescence when taking place on the surface (Scherer, 2004; Guglielmini *et al.*, 2008)[2].

This paper was motivated by the important consequences of the presence of salt on many

[2] More recent studies on crystallization dynamics and efflorescence and sub-florescence processes may be find in Pel *et al*. [2013] and Gupta et al. [2014] and references therein.

hydrological processes. The main objectives of this paper are to address the nonlinear effects of salt concentrations on the a) evaporation rate from porous media and b) the dynamics of salt precipitation at the surface. Using thermodynamics of the salt solution, we describe quantitatively the effects of salt concentration on the evaporation rate. Also we use the convection-diffusion equation to analyze the effects of salt concentration in the liquid water that is transported from the deeper depths towards the evaporation surface on the onset of efflorescence at the evaporating surface. All the theoretical predictions are evaluated experimentally by conducting a series of laboratory evaporation experiments.

2.2 Theoretical Considerations

2.2.1 Effects of Salt Concentrations on the Evaporation Rate

Evaporation from porous media is characterized by a high evaporation rate at the early stage of the process when it is relatively constant and is close to that from an open pan, the so called-stage 1 evaporation (Scherer, 1990). At this stage, the evaporation rate is limited by the atmospheric demand and under isothermal condition is proportional to:

$$e\ \alpha\ (P_s - P_\infty) \tag{2.1}$$

with e the evaporation rate, and P_∞ and P_s the partial vapor pressure in the bulk air and saturated vapor pressure at the ambient temperature (corresponding to the vapor pressure immediately above the surface), respectively. P_s can be found from thermodynamic tables for pure water at different temperatures; however for saline solutions it changes based on salt nature and concentration. Raoult's law is widely used to calculate the saturated vapor pressure for solutions using the salt concentration as:

$$P_s^{sol} = xP_s \tag{2.2}$$

with x the molar fraction of water in solution and P_{ssol} the saturated vapor pressure of the solution. Equation (2.2) is valid only if the salt concentration is relatively low (dilute solution) in which the activity coefficient (indicating the deviation of the solution from an ideal solution) is close to 1. For high salt concentrations, Raoult's law is modified as (Smith *et al*., 2004):

$$P_s^{sol}\varphi = x\gamma P_s \tag{2.3}$$

with φ the fugacity coefficient indicating the deviation of the gas phase from ideal gas and γ the activity coefficient. Equation (2.3) shows that estimation of P_{ssol} requires predictions of γ as a function of salt concentration which may be approximated using virial expansion of Gibbs free energy (Pitzer *et al*., 1984). Depending on the nature of salt and its concentration, the activity coefficient may increase or decrease as salt concentration increases (Pitzer *et al*., 1984; Guendouzi and Mounir, 2003). Pitzer *et al*. [1984] obtained the activity coefficient for NaCl aqueous solution at different temperatures and concentrations. Their results showed that the activity coefficient decreases when NaCl concentration increases up to 1.2 Molal at 30°C. However, any increase above this threshold results in a higher activity coefficient (Figure 2.1a) thus higher evaporation rates (equations (2.1) and (2.3)). Note that the concentration for minimum evaporation rate is slightly higher than the one for minimum activity coefficient.

2.2.2 Salt Transport and Precipitation

During evaporation from porous media, convection induced by the capillary liquid flow transports salt toward the vaporization plane, while diffusion tends to spread the salt homogenously in the space. The resulting interplay between convection and diffusion affects the dynamics of salt distribution in porous media commonly characterized by the

dimensionless Peclet number, Pe (indicating the relative importance of convective to diffusive transport). Under the assumption of negligible ion adsorption on the pore wall, the equation governing the ions transport in liquid is given by the convection-diffusion equation (CDE). Assuming a 1-D vertical solute transport, the CDE will be (Guglielmini *et al*., 2008):

$$\frac{\partial(\rho\varepsilon SC)}{\partial t} = \frac{\partial}{\partial z}(\rho\varepsilon SD^{*}\frac{\partial C}{\partial z} - \rho\varepsilon SCU) \qquad (2.4)$$

with C(z, t) the mass fraction of salt, ε the porosity, D* the effective diffusion coefficient of solute in porous media, ρ the density of the solution, z the depth below surface, U the average velocity of the liquid, t the time, and S the saturation.

Using the analytical and numerical solutions of CDE, many researchers studied the dynamics of salt distribution in drying porous media. For example Huinink *et al*. [2002] and Guglielmini et al. [2008] illustrated that low Pe results in homogenizing salt concentration throughout porous media; while for high Pe salt is preferentially accumulated toward the evaporation surface. In the present study, we solve CDE numerically to study the onset of salt precipitation at the surface as a function of initial salt concentration. More details about the boundary conditions and assumptions we applied to solve the CDE will be presented in section 4.2.

2.3 Materials and Methods

A series of laboratory evaporation experiments were conducted in an environmental chamber in which the relative humidity and ambient temperature were kept constant at 30% and 30°C, respectively during the experiments. Reagent grade NaCl (from EMD Chemicals, Inc. NJ, USA) was used to make saline solutions. Sand particles with an

average particle size of 0.48 mm were used to pack the glass cylindrical columns (85 mm in diameter and 230 mm in height) saturated with various NaCl solutions of 0, 0.1, 0.5, 0.75, 1, 1.5, 2, 2.5, 3, 3.5 Molal. All boundaries of the columns were closed, except the top boundary which was exposed to air for evaporation. The sand grains were immersed in water to ensure complete initial saturation. The resulting packing porosity was 0.4 and the bulk density was about 1.55 g/cm^3. The columns were mounted on digital balances connected to a computer to record the evaporative water loss each 5 minutes. A camera was set vertically to take pictures from surface of sand columns automatically each 30 minutes for recording the general dynamics of salt deposition patterns on the surface. The same experiments were also conducted just with salt solutions (in the absence of sand particles) of 0, 0.1, 0.5, 2, 3, 4 and 5 Molal using plastic pans (160 mm in diameter and 70 mm in height) to study the effects of salt concentration on the evaporation from saline solutions.

2.4 Results and Discussions

2.4.1 Evaporation Rates as a Function of Salt Concentrations

The evaporation rate from each column was calculated using the data recorded by the balances. The stage-1 evaporation rates were determined following the procedure described by Shokri and Or [2011]. Figure 2.1b depicts the average evaporation rates measured during stage-1 evaporation from sand columns and also from the salt solutions as a function of initial salt concentrations. The rates were normalized with respect to the potential evaporation rate (*i.e.*, the evaporation rate in the absence of salt).

Results show that the evaporation rates decreased as the initial concentrations increased up to a certain concentration. Further increase of the salt concentration resulted in higher

evaporation rates. The solid line in Figure 2.1b shows the predicted relative evaporation rate as a function of salt concentration calculated as:

$$\frac{e}{e_0} \alpha \frac{P_s^{sol} - P_\infty}{P_s - P_\infty} \tag{2.5}$$

with e_0 the potential evaporation rate. The solution vapor pressure was determined using the modified Raoult's law (equation (2.3)) and considering ambient air as an ideal gas (*i.e.*, φ = 1). The activity coefficients of various NaCl solutions were calculated using the initial salt concentration of each sand column following the model described by Pitzer *et al.* [1984]. Figure 2.1b shows that the predicted evaporation rates as a function of the initial salt concentration were in reasonable agreement with the measured evaporation rates from both salt solutions and sand columns.

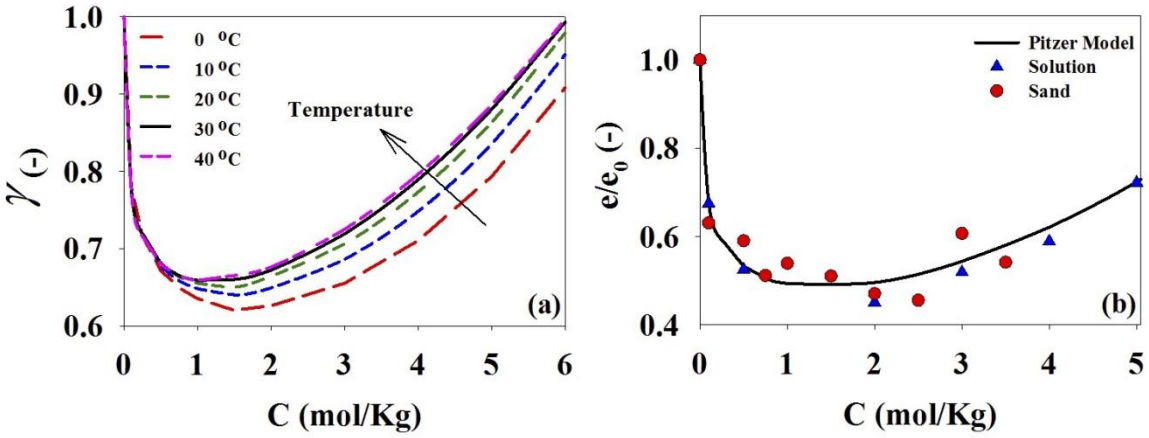

Figure 2.1 (a) Activity coefficient of the solutions as a function of the NaCl concentration under different temperatures based on Pitzer's model (Pitzer *et al.*, 1984). (b) Normalized evaporation rates measured during stage-1 evaporation from sand columns saturated with NaCl solutions together with the measured evaporation rates from NaCl solutions (in the absence of sand particles) as a function of initial concentrations.

2.4.2 Onset of Efflorescence

The onset of visible salt precipitation at the surface was determined experimentally using the pictures taken from surfaces of the columns. The experimental results are presented in Figure 2.2 showing the onset of salt precipitation at the surface as a function of the initial salt concentration[3]. We solved CDE numerically to describe this relation. For the numerical solution, at the boundaries, we assumed that the diffusive and convective fluxes are balanced, *i.e.*,$UC - D^* \frac{\partial C}{\partial z} = 0$ [4] at z = 0, L (L is the length of the column). We assumed negligible change in water saturation through the space, and also since the initial precipitation takes place during stage-1 evaporation, as a first order of approximation, we estimated the velocity term in the CDE by averaging the measured evaporation rate during stage-1 evaporation. Temporal change in liquid saturation is accounted as $S = 1 - \frac{e}{\rho L \varepsilon}$ (Huinink *et al*., 2002). We also used D* = 10^{-9} m^2 s^{-1} as a typical value for the effective diffusion coefficient in porous media according to Huinink *et al*. [2002], Pel *et al*. [2002] and Shokri *et al*. [2010]. More details about the numerical solution of CDE can be found in many previous studies describing the dynamics of salt distribution during evaporation from saline porous media such as Huinink *et al*. [2002] and Guglielmini *et al*. [2008], thus it is not repeated here. The result of the numerical solution is presented as the solid line in Figure 2.2. Considering the simplifying assumptions used for solving the CDE, the simulated non-linear relationship between onset of efflorescence and the initial salt concentration was in a reasonable agreement with the experimental data initial.

[3] It shall be noted that these values are not the onset of crystallization but the onset of visible precipitation which is limited by the imaging technique. The actual time of that precipitation starts might be smaller but not captured (not visible) by the camera used in the experiment.
[4] The parameters are the same as Eq. 2.4

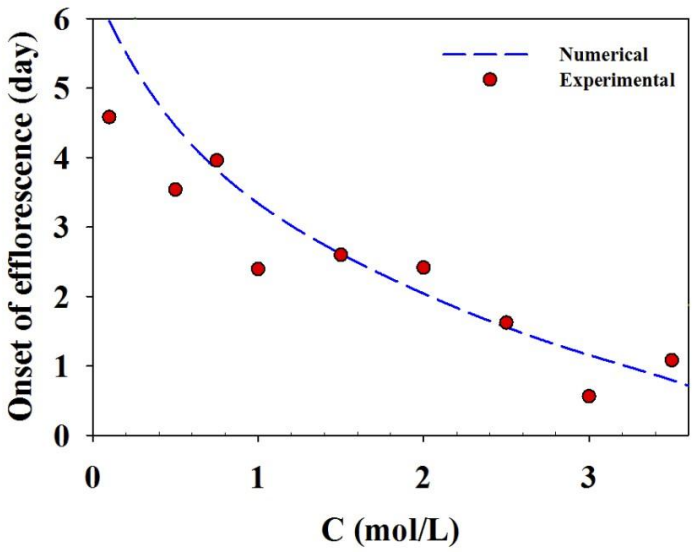

Figure 2.2 Time of onset of efflorescence at the surface of sand columns determined experimentally versus initial concentration compared with the numerical solution of the CDE (solid line).

2.4.3. Surface Coverage Rate versus the Evaporation Rate

The images of the sand columns were segmented to determine the lateral dynamics of precipitated salt at the surface (*i.e.*, the growth dynamics of the area covered by salt at the surface). A typical gray value image, its corresponding gray value frequency distribution denoted as histogram and the segmented image is depicted in Figure 2.3a. Typically each histogram consists of four zones (Figure 2.3a) indicating the background (*i.e.*, the scale), the glass wall of the column, sand particles without salt on top and regions covered by salt (*i.e.*, the last peak in the histogram). A similar methodology to the one described by Shokri *et al*. [2008] was used to determine the threshold value to segment the gray value images (inset of Figure 2.3a) to the black and white. The area covered by salt was then computed by counting the white pixels. The same algorithm was applied to all images to determine the dynamics of lateral propagation of the precipitated salt at the surface during drying of each column. Results show that the coverage rate as a function of time could be represented

by Gaussian distribution function unique to each initial salt concentration. The dynamics and evolution of the area covered by salt at the surface during evaporation may be affected[5] by the atmospheric condition, transport properties of porous media, and the nature of salt, among other factors. Typical surface salt coverage rates, r_{salt}, versus time are illustrated in Figure 2.3b showing the continuous increase of the coverage rate during stage-1 evaporation. This might be caused by the fact that during this period, salt is continuously transported to the evaporation surface via the capillary induced liquid flow. When the concentration at the surface exceeds the saturation limit, first salt crystal appears and the concentration will remain the same as the evaporation proceeds. Crystallization starts with a small crystal (Nuclei) which forms due to a quick change of the concentration in a part of the solution which is in a metastable state of equilibrium. Other crystals form due to the same reason as well as collisions with the previously formed crystals (McCabe *et al.*, 2004). Thus, having more crystals on the surface may result in a higher salt coverage rate. However, at the end of stage-1, the continuous liquid pathways connecting the receding drying front to the surface start to detach from the surface one after the other (*i.e.*, the transition period from stage-1 to stage-2 evaporation, see Shokri and Or [2011] for more detail). This results in a decreasing salt deposition rate at the surface during the transition period which continues until all liquid connections are disconnected from the surface marking the onset of stage-2 evaporation (Shokri and Or, 2011). At this point, the salt deposition rate at the surface goes to zero (since vaporization does not occur anymore at the surface).

[5] It is more correct to make the statement as : The dynamics and evolution of the area covered by salt at the surface during evaporation ***will*** be affected by the atmospheric condition, transport properties of porous media, and the nature of salt, among other factors.

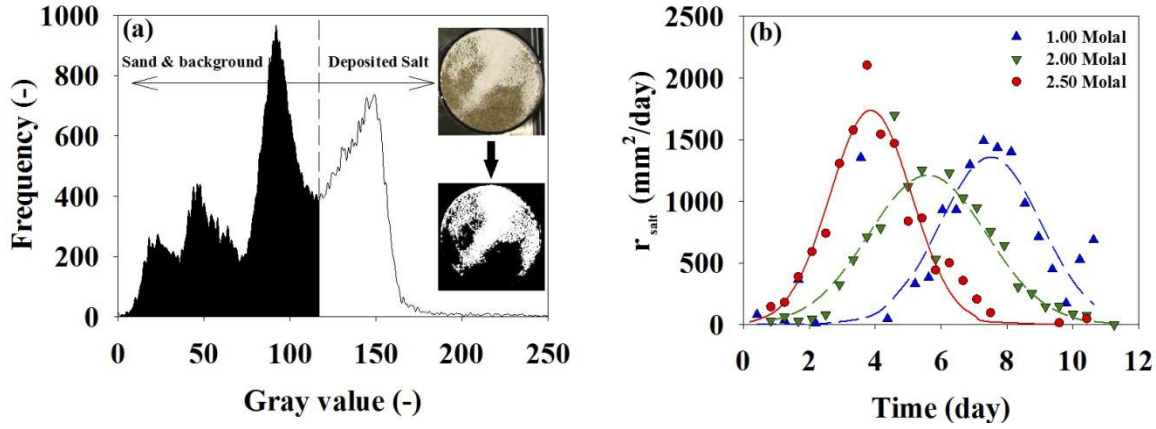

Figure 2.3 (a) Gray value histogram of a typical image taken from surface of the sand column illustrated as color image in the inset. The white color indicates the area covered by salt corresponding to the last peak in the histogram. The vertical line indicates the threshold used to segment the gray value image to black and white. The area covered by salt in the segmented image (*i.e.*, the white color) was used to calculate the rate of surface coverage by precipitated salt during evaporation. (b) Sample surface salt coverage rates (r_{salt}) versus time for the sand columns packed with salt solution of 1, 2, and 2.5 Molal. The coverage rates could be described by Gaussian distribution function (the solid lines).

We have found a relatively strong correlation between the time at which the salt coverage rate at the surface is maximum (*i.e.*, the peak of the Gaussian distribution) and the end of stage-1 evaporation determined from the drying curves. For example, Figure 2.4a shows a typical result illustrating the measured evaporation rate from the sand column saturated with a solution of 2.5 Molal of NaCl and the corresponding salt coverage rate at the surface.

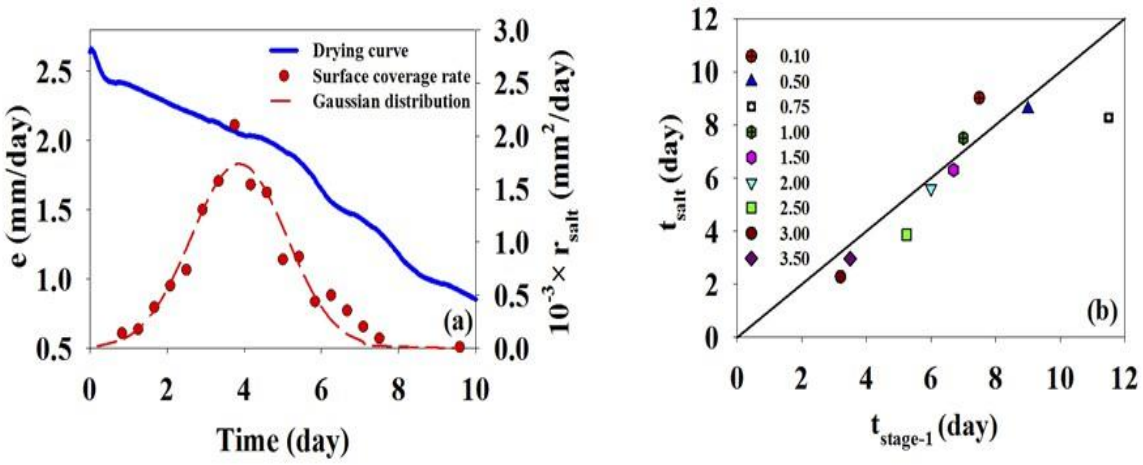

Figure 2.4 (a) The surface salt coverage rate and evaporation rates of the sand column saturated with the solution of 2.5 Molal versus time. Results show that the maximum surface coverage rate and the end of stage-1 occur nearly at a same time. (b) The time at which the surface salt coverage rate (t_{salt}) is maximum, versus the time of the end of stage-1 evaporation ($t_{stage\text{-}1}$) determined from the drying curves.

Figure 2.4b shows the time at which the salt coverage rate at the surface is maximum, t_{salt}, delineated by image analysis for each sand column, versus the prolongation of stage-1 evaporation, $t_{stage-1}$, determined from the drying curves following the procedure described by Shokri and Or [2011]. Except for the column saturated with the salt solution of 0.75 Molal, the other points indicate a linear 1-1 relation between the end of stage-1 evaporation and the time at which the surface salt coverage is the maximum. To the best of our knowledge, such a correlation was never reported in the past. This may potentially offer a new tool to non-destructively study the evaporation process from porous media by quantifying the dynamics of the salt coverage and deposition patterns at the surface. Further research is required to explore this possibility in more details[6].

[6] For example, using the remote sensing data and satellite images of a field, one may be able to find the surface salt coverage rate, which can result in determining the end of stage-1 (based on the current paper) which is the time that surface is starting to dry out. This might be of interest in soil science and agriculture applications at the first instance.

2.5 Conclusions

In this work, we have studied the effects of salt concentration on the evaporation rate from porous media and also the dynamics of salt deposition at the surface. We predicted the effects of salt concentration on the evaporation rate by considering the thermodynamics of the salt solution evaluated by a series of experiments. Our theoretical and experimental results show that increasing initial NaCl concentration up to ~1.5 Molal reduces the evaporation rate from porous media, but any further increase of NaCl concentration results in higher evaporation rates, a conclusion which may not seem trivial at first glance. Besides, we studied the nonlinear effects of NaCl concentration on the onset of efflorescence using the numerical solution of CDE and as expected, higher initial salt concentration leads to earlier salt precipitation at the surface which was confirmed by the experiments. We have also studied the growth dynamics of the area covered by precipitated salt on the evaporating surface under various initial salt concentrations. Our results showed that the surface salt coverage rate can be described reasonably by a Gaussian distribution function. We have found that the maximum rate of lateral deposition of precipitated salt at the surface occurs at the end of stage-1 evaporation. This result may offer new tools and also future research lines for nondestructive analysis of the evaporation from porous media. [7]

[7] It should be mentioned that there are other non-destructive methods of studying evaporation and precipitation, such as X-ray microtomography (Norouzi Rad *et al*., 2013), Non Magnetic Resonance Imaging or NMR (van der Heijden *et al*., 2007) but they are not applicable to the large samples especially field scale. Using acoustic technology however is another nondestructive method to determine the stages of evaporation in porous media. This method may be used for larger media depending on the device used, but it needs local measurements and should be installed in (or beside) the porous media of interest (Graspas and Shokri, 2014).

References

Flatt, R. J. (2002), Salt damage in porous materials: How high supersaturations are generated, J. Cryst. Growth, 242, 435-454, doi:10.1016/S0022-0248(02)01429-X.

Guendouzi, M., and A. Mounir (2003), Water activity, osmotic and activitycoefficients of aqueous solutions of Li2SO4, Na2SO4, K2SO4, (NH4)2SO4, MgSO4, MnSO4, NiSO4, CuSO4, and ZnSO4 at T = 298.15 K, J. Chem. Thermodyn., 35(2), 209-220, doi:10.1016/S0021-9614(02)00315-4.

Guglielmini, L., A. Gontcharov, J. A. Aldykiewicz, and H. A. Stone (2008), Drying of salt solutions in porous materials: Intermediate-time dynamics and efflorescence, Phys. Fluids, 20, 077101, doi:10.1063/1.2954037.

Huinink, H. P., L. Pel, and M. A. Michels (2002), How ions distribute in a drying porous medium: A simple model, Phys. Fluids, 14, 1389-1395, doi:10.1063/1.1451081.

McCabe, W. L., J. C. Smith, and P. Harriott (2004), Unit Operations of Chemical Engineering, McGraw Hill, New York.

Nachshon, U., E. Shahraeeni, D. Or, M. I. Dragila, and N. Weisbrod (2011), Infrared thermography of evaporative fluxes and dynamics of salt deposition on heterogeneous porous surfaces, Water Resour. Res., 47, W12519, doi:10.1029/2011WR010776.

Nassar, I. N., and R. Horton (1989), Water transport in unsaturated non-isothermal salty soil: II. Theoretical development, Soil Sci. Soc. Am. J., 53, 1330-1337, doi:10.2136/sssaj1989.03615995005300050005x.

Nassar, I. N., and R. Horton (1999), Salinity and compaction effects on soil water evaporation and water and solute distributions, Soil Sci. Soc. Am. J., 63, 752-758, doi:10.2136/sssaj1999.634752x.

Pel, N., H. Huinink, and K. Kopinga (2002), Ion transport and crystallization in inorganic building materials as studied by nuclear magnetic resonance, Appl. Phys. Lett.,81, 2893, doi:10.1063/1.1512329.

Pitzer, K. S., J. C. Peiper, and R. H. Busey (1984), Thermodynamic properties of aqueous

sodium chloride solutions, J. Phys. Chem. Ref. Data, 13,1-102, doi:10.1063/1.555709.

Scherer, G. W. (1990), Theory of drying, J. Am. Ceram. Soc., 73, 314,doi:10.1111/j.1151-2916.1990.tb05082.x.

Scherer, G. W. (1999), Crystallization in pores, Cem. Concr. Res.,29,1347-1358, doi:10.1016/S0008-8846(99)00002-2.

Scherer, G. W. (2004), Stress from crystallization of salt, Cem. Concr. Res., 34, 1613-1624, doi:10.1016/j.cemconres.2003.12.034.

Shimojimaa, E., R. Yoshika, and I. Tamagawa (1996), Salinization owing to evaporation from bare-soil surfaces and its influences on the evapora-tion, J. Hydrol.,178, 109-136, doi:10.1016/0022-1694(95)02826-9.

Shokri, N., and D. Or (2011), What determines drying rates at the onset of diffusion controlled stage-2 evaporation from porous media?, Water Resour. Res., 47, W09513, doi:10.1029/2010WR010284.

Shokri, N., P. Lehmann, P. Vontobel, and D. Or (2008), Drying front and water content dynamics during evaporation from sand delineated by neutron radiography, Water Resour. Res., 44, W06418, doi:10.1029/ 2007WR006385.

Shokri, N., P. Lehmann, and D. Or (2010), Liquid-phase continuity and solute concentration dynamics during evaporation from porous media: Pore-scale processes near vaporization surface,Phys. Rev. E, 81, 046308, doi:10.1103/PhysRevE.81.046308.

Smith, J. M., H. C. Van Ness, and M. M. Abbott (2004), Introduction to Chemical Engineering Thermodynamics , McGraw-Hill, New York.

2.6 Correction to "Nonlinear effects of salt concentrations on evaporation from porous media"

In the paper "Nonlinear effects of salt concentrations on evaporation from porous media" by Mansoureh Norouzi Rad and Nima Shokri (Geophysical Research Letters, 39, L04403, doi:10.1029/2011GL048153, 2011), in order to apply equation 2.3 to obtain saturated vapor pressure of the solution and its evaporation rate (Figure 2.1b) the activity coefficient of the solution should be used instead of the mean activity coefficient of NaCl. This will result in a decreasing vapor pressure for the solution and subsequently a decreasing evaporation rate which does not follow the observed experimental data in our experiments. The decreasing vapor pressure has been reported in other works (Clarke *et al.*, 1985). Similar trend between the evaporation rate from saline porous media and salt concentration has been observed in literature (Sghaier *et al*. 2009; Eloukabi *et al*. 2011). The increasing evaporation rate after 1 Molal NaCl concentration may be attributed to the salt crust formed at the surface of the sand column which may enhance the evaporation surface boosting the evaporation rate. In the case of saline solutions, averaging the bulk concentration instead of considering the concentration gradient in the solution might be the source of observed behavior. Additionally, the non-uniform distribution of the ambient temperature and relative humidity inside the environmental chamber might have affected the results too. Corrected figure and texts appear here.

In paragraph 1: When exceeding this level, any further increase of NaCl concentration results in higher evaporation rates.

In paragraph 5: The sentence "Using thermodynamics of the …" should be deleted.

In paragraph 6: However, any increase above this threshold results in a higher activity

coefficient.

In paragraph 6: At the end of the paragraph, the sentence " Note that the concentration for minimum…" should be deleted.

Figure 2.1b should be modified as:

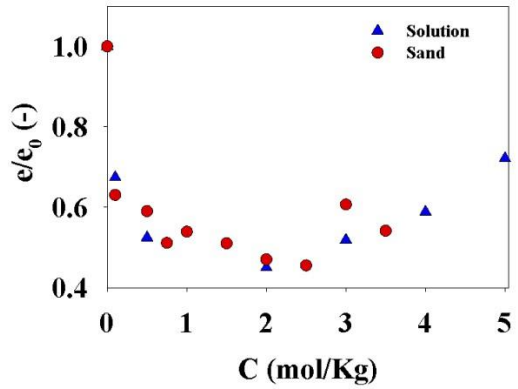

Figure 2.5 Normalized evaporation rates measured during stage-1 evaporation from sand columns saturated with NaCl solutions together with the measured evaporation rates from NaCl solutions (in the absence of sand particles) as a function of initial concentrations.

In paragraph 12: From the sentence "The solid line in Figure 2.1b shows …" till the end of the paragraph should be deleted.

In paragraph 17: The sentence "We predicted the effects of salt concentration …" should be deleted.

In paragraph 17: The sentence "Our theoretical and experimental results show …" should read as "Our experimental results show …"

References

Clarke, E. C. W., and D. N. Glew (1985), Evaluation of the thermodynamic functions for aqueous Sodium Chloride from equilibrium and calorimetric measurements below 154 ^{o}C, J. Phys. Chem. Ref. Data, 14, 489-610.

Eloukabi, H., N. Sghaier, M. Prat, and S. B. Nassrallah (2011), Drying experiments in a hydrophobic model porous medium in the presence of a dissolved salt, Chem. Eng. Tech., 34, 1085-1094, doi:10.1002/ceat.201100064.

Sghaier, N. and M. Prat (2009), Effects of efflorescence formation on drying kinetics of porous media, Transp. Porous Med., 80, 441-454, doi: 10.1007/s11242-009-9373-6.

Chapter 3

Pore-scale dynamics of salt precipitation in drying porous media

This chapter has been published in Physical Review E, volume 88, in 2013. The main objective of this chapter is to study the pore scale dynamics of salt precipitation in porous media during natural evaporation. This has been done using columns packed with silica sand saturated with solutions of NaCl of three different concentrations. 4D X-ray micro tomography imaging was performed to visualize the 3D network of the porous media and image analysis techniques were applied to quantify the evaporation and precipitation dynamics.

Results presented in this chapter show the preferential precipitation on the surface of the porous media which happens in two different stages of precipitation; an increasing rate period followed by a constant rate stage. The physics governing the precipitation rates and patterns in drying porous media is revealed in this study. Also using SEM imaging the structure and evolution of salt crust on the surface and its potential influences on the evaporation rates are investigated.

Pore-scale dynamics of salt precipitation in drying porous media

Mansoureh Norouzi Rad,[1]Nima Shokri,[1]* and Muhammad Sahimi [2]

[1] School of Chemical Engineering and Analytical Science, University of Manchester, Manchester M13 9PL, United Kingdom

[2] Mork Family Department of Chemical Engineering and Materials Science, University of Southern California, Los Angeles, California 90089-1211, USA

PHYSICAL REVIEW E 88 , 032404 (2013)

Abstract

We study the pore-scale dynamics of salt precipitation in three-dimensional drying porous media, utilizing high resolution x-ray microtomography and scanning electron microscopy. Our results illustrate that the salt precipitation patterns in drying porous media are nonuniform, manifesting the influence of the spatial distribution of pore sizes on the dynamics of salt crystallization and formation of discrete efflorescence. Results reveal that during stage-1 evaporation from saline porous media, the salt precipitation rate initially increases which is followed by a constant precipitation rate. This non-linear behaviour is attributed to the preferential liquid vaporization and salt precipitation in finer pores located at the surface of the porous medium contributing in evaporation according to the pore sizes. We also show that, contrary to common practice, the macroscopic convection-diffusion equation cannot provide accurate predictions for the dynamics of salt precipitation, at least at the early stages, due to the microscale heterogeneity of evaporation sites at the surface that results in salt precipitation exclusively in the finer pores.

3.1 Introduction

Understanding the physics of salt precipitation in porous media is of fundamental importance to many natural and industrial processes, such as preservation of pavement and historical monuments, mineral-fluid interactions, CO_2 sequestration in rock, and the evaporation rates from porous media (Scherer, 2004; Espinosa Marzal andScherer, 2008; Schiro *et al*. 2012; ,Nachson *et al*., 2011; Sghaier and Prat, 2009; Eloukabia *et al*., 2013; Norouzi Rad and Shokri, 2012). As water evaporates, the salt concentration in the pore space increases continuously until it exceeds the solubility limit, at which time it precipitates. The precipitation pattern modifies the morphology of the pore space and,

consequently, influences flow and transport processes in it. Despite their high importance, particularly to the problem of drinking water for the world's rapidly increasing population, direct pore-scale imaging and the study of salt precipitation and crystallization patterns in three-dimensional (3D) drying porous media are very rare, largely due to the imaging complexity of the dynamics of salt precipitation. Therefore, most of the previous studies were focused on the description of salt deposition patterns at the macroscale and were restricted mostly to two-dimensional (2D) imaging of evaporating surfaces (Nachshon *et al*., 2011; Sghaier *et al*., 2009; Eloukabia *et al*., 2013; Norouzi Rad and Shokri, 2012; Veran-Tissoires *et al*., 2012; Eloukabi *et al*., 2011).

We have employed x-ray microtomography to study the key effects of the pore sizes and the initial salt concentration on dynamics and patterns of salt precipitation in a drying porous medium. Detailed visualization of salt precipitation enables us to identify unambiguously the mechanism of discrete efflorescence on the evaporation surface as a result of the invasion of large pores by air and the subsequent capillary-induced liquid flow toward the fine pores on the surface, where water evaporation occurs preferentially. We establish that the pore-size heterogeneity at the surface of porous media results in heterogeneous distribution of the vaporization sites on the surface and the preferential efflorescence that occurs exclusively in the fine pores. In addition, we quantify the influence of the initial salt concentration on its deposition rate in 3D drying porous media. Finally, we demonstrate that, contrary to common practice, the observed trends cannot be accurately modeled by the convection-diffusion equation (CDE), at least at the early stages.

3.2 Experimental Considerations

The drying experiments were carried out in cylindrical plastic columns, 35 mm in height and 11 mm in diameter, packed with sand grains with particle sizes ranging from 0.17 to 1.0 mm, with an average size of 0.58 mm, saturated with NaCl (reagent grade powder from EMD Chemicals, Inc., New Jersey, USA) solutions of 3.5 Molal (moles of NaCl/kg of water), 4 Molal, and 6 Molal. The drying of the sand columns was visualized by means of a HMXST x-ray microtomography system (at 70 kV and 140 μÅ) with spatial and temporal resolutions of 0.021 mm and 30 min. The duration of each round of the experiments was nearly 24 h.

Each 3D scan included 1500 horizontal cross sections. We used the standard machine learning technique of a support vector machine (SVM) (Cortes and Vapnik, 1995; Platt, 1999) with a quadratic kernel to segment each cross section into solid, liquid, and air. The SVMs were trained using sequential minimal optimization from MATLAB's machine learning package. More details about the method are given elsewhere) (Cortes and Vapnik, 1995; Platt, 1999). To distinguish the precipitated salt from the sand grains, each 2D cross section was compared to its corresponding image obtained at the beginning of the experiment, when there was no solid salt in the sample, with the difference indicating the precipitated salt.

The resulting typical cross sections are illustrated in Figure. 3.1(a)–3.1(c). Figure 3.1(d) shows a typical example of the vertical growth of the precipitated salt above the sand surface. The spectrum of yellow to orange (light to medium gray) indicates the time of the scan such that the closer the color is to yellow (light gray), the later the column was scanned. Using this method, we quantify the dynamics of salt growth above the evaporation surface at various times and locations.

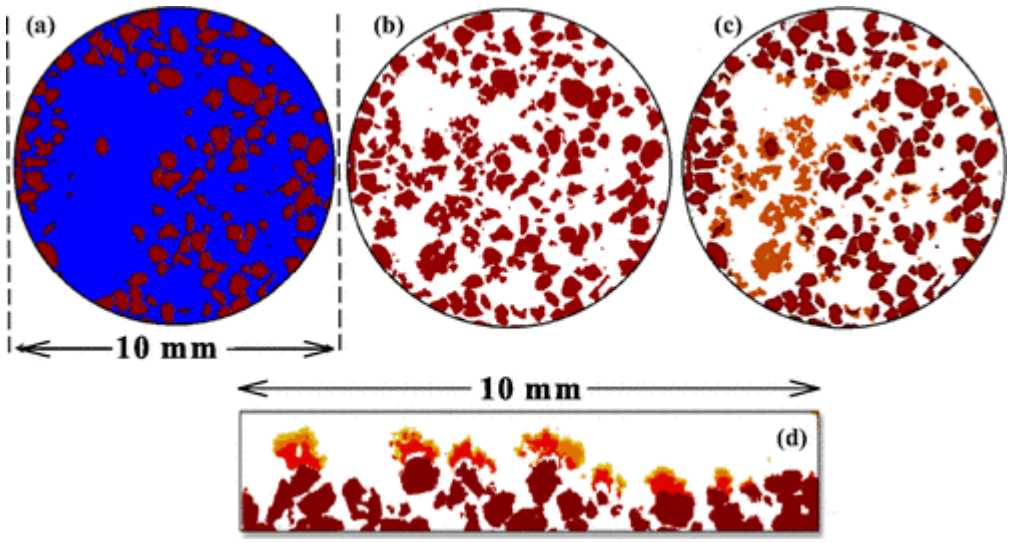

Figure 3. 1 (a) A typical horizontal cross section above the surface, taken at the beginning of the experiment, illustrating the liquid [blue (dark gray)] and solid [brown (medium gray)] phases. (b) The same cross section after 17 h, showing the distribution of the solid [brown (medium gray)] and air (white) phases. (c) The image constructed by comparing the solid phases in (a) and (b) with the difference [orange (light gray)], corresponding to the precipitated salt. (d) A typical vertical close-up of the surface of the sand column saturated with 4 Molal NaCl solution, constructed by the same method as in (c) and applied to all cross sections. The spectrum of orange to yellow (medium to light gray) indicates the addition of precipitated salt in each scan. Brighter colors indicate longer times.[8]

3.3 Results and Discussions

A. Evaporative water losses

Figure 3.2 illustrates the cumulative water loss calculated by image analysis. The nearly constant slope of the curves indicates that in all cases the process was in the stage-1 evaporation. The inset in Figure 3.2 shows the evolution with time of water saturation at the surface for various initial salt concentrations, confirming the presence of liquid at the surface during the experiments, consistent with the previously reported data (Shokri *et al.*, 2010; Shokri and Sahimi, 2012; Shokri *et al.*, 2012; Lehman *et al.*, 2008; Shokri and Or, 2013;

[8] A modified version of this figure is presented in Appendix C as Figure C.3.1.

Shokri and Salvucci, 2011; Yiotis *et al.*, 2004). The recorded pore-scale images indicate that, at the early stages of the evaporation process, large pores at the surface are invaded preferentially by air, while the fine pores remain saturated due to required higher capillary pressures. These are the characteristics of stage-1 evaporation in which the evaporation rate remains relatively constant and the medium behaves as if it were saturated (Shokri et al., 2010; Shokri and Sahimi, 2012; Shokri et al., 2012; Lehman et al., 2008; Shokri and Or, 2013; Shokri and Salvucci, 2011). Results similar to what was reported in Figure 3.3 of Shokri *et al.* (2010) [9]were obtained in the present study, confirming the presence of continuous liquid pathways between the water-filled fine pores at the surface and the saturated zone at the bottom (which are not repeated here).

In the presence of salt, water evaporation from fine pores at the surface results in a continuous increase of salt concentration in the preferential "evaporating spots." When salt concentration reaches the solubility limit, which is 6.12 Molal for NaCl at 25◦C, precipitation takes place, as supersaturation effects are negligible for NaCl (Chatterji, 2000). Due to the limited number and discrete nature of the evaporating spots at the surface, salt precipitation occurs at discrete positions that coincide with the locations of the fine pores.

[9] Figure is presented in Appendix C as Figure C.1.

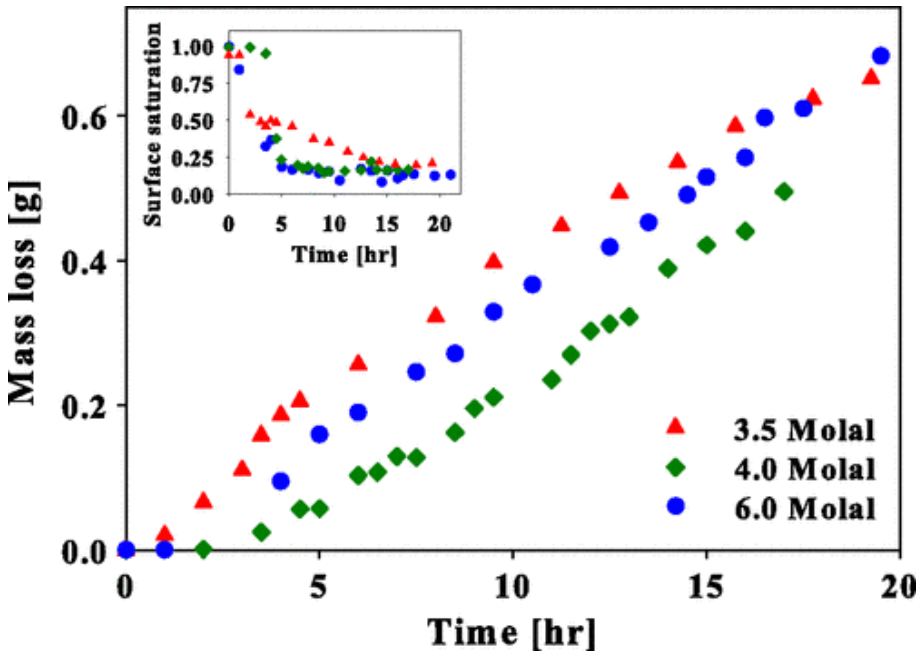

Figure 3.2 Cumulative mass of liquid water removed by evaporation from the sand columns, initially saturated with various NaCl solutions. The notably lower water evaporation from the 4.0 Molal solution might be due to the lower atmospheric demand. Although the evaporative demand was nearly constant during each round of the experiment, the relative humidity and temperature inside the x-ray chamber could not be controlled precisely. The inset shows the near surface (the top 0.5 mm) water saturation, confirming the presence of liquid at the surface during the entire course of the experiments.[10]

[10] A modified version of this figure is shown in Appendix C as Figure C.3.2 with straight lines to better visualization of the constant slopes of the mass loss curves and stage-1 evaporation.

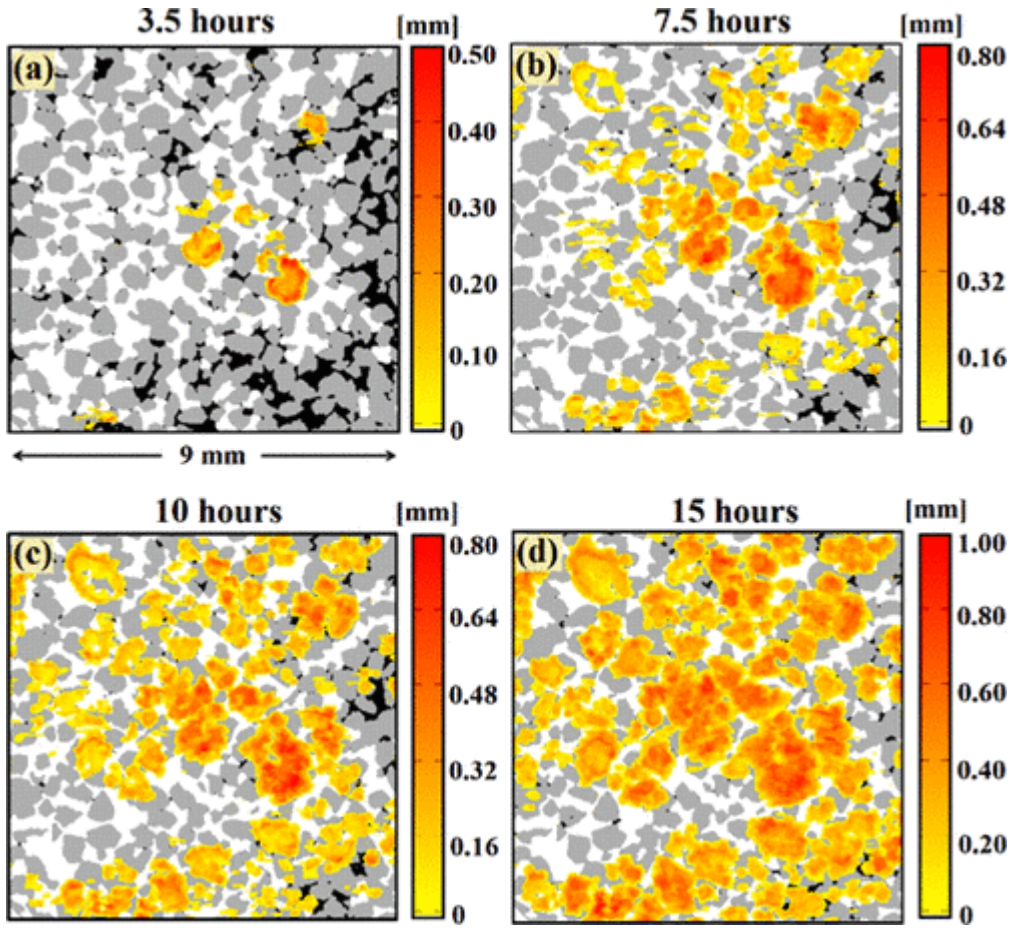

Figure 3.3 Patterns and distribution of precipitated salt at the surface of the sand column at various times, saturated with the 4 Molal NaCl solution. The color scale indicates the height of the precipitated salt. Black, gray, and white indicate, respectively, the regions filled with the liquid, sand grains, and the air phase. All other colors correspond to the precipitated salt and the color spectrum indicates the thickness of the precipitated salt such that the closer the color is to orange (darker color), the thicker is the salt crust.

B. Salt precipitation patterns and dynamics

In Figure 3.3 the patterns of the deposited salt at various times from the onset of the experiment are shown, along with the liquid (shown by black) distribution, at the surface of the sand column that was saturated with a 4 Molal solution. The color scale represents the

thickness of the precipitated salt, such that the closer to orange (darker) it is, the larger the thickness is. Figure 3.3 demonstrates that the nonuniform distribution of the precipitated salt at the surface is influenced by the distribution of the pore sizes. Over time, each evaporating spot turned into a precipitation spot, when the salt concentration exceeded the solubility limit. Therefore, the number of precipitation spots increased with time, as indicated by Figure. 3.3(a)–3.3(c). When the NaCl concentration exceeded the solubility limit at all the evaporation spots, the number of active pores that contributed to salt precipitation remained constant.

Let us emphasize that what is shown in Figure 3.3 is *solely* related to the flow of the liquid toward the evaporating surface, either in the bulk or by film flow, driven by capillary action. A simple analysis clearly demonstrates this. Consider a fully saturated cylindrical pore of radius r with complete evaporation within it. In the absence of convective transport to replenish the evaporating liquid, the volume per unit length occupied by the precipitated salt is $\pi r^2 \gamma/\rho_s$, with γ being the solubility and ρ_s being the salt density. Thus, assuming that salt precipitates uniformly on the pore's surface, the available pore volume is $\pi r^2 \ (1-\gamma/\rho_s)$, implying a relative reduction $1-\gamma/\rho_s$ of the pore volume. With $\gamma \approx 0.36$ g/cm ^{3} and $\rho_s \approx 2.165$ g/cm ^{3} for salt density, the fraction is about 0.17. This calculation shows that even after salt precipitation, a part of the pore volume at the surface is still open. Therefore, the evaporating pore could be still hydraulically connected to the wet zone at the bottom via the capillary-induced liquid flow supplying the evaporative demand.

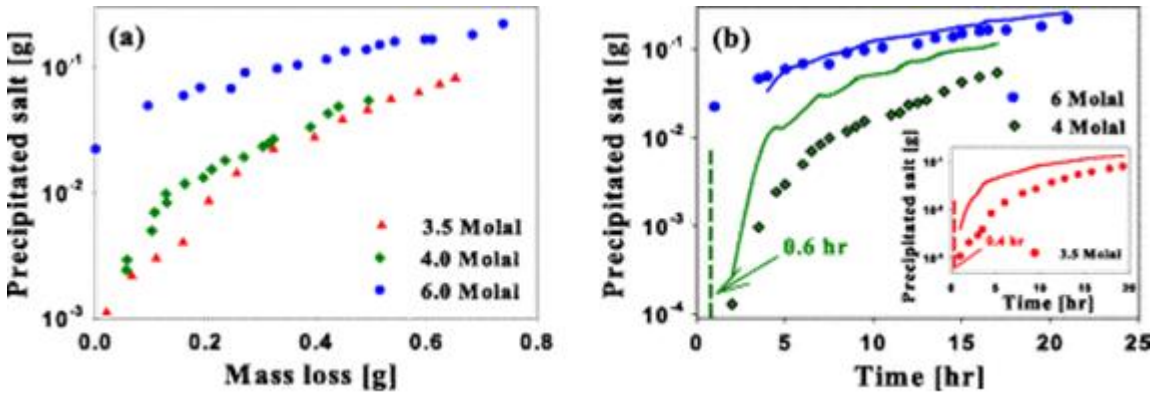

Figure 3.4 (a) Cumulative precipitated salt as a function of the cumulative mass of liquid water lost by evaporation. The legend indicates the initial salt concentration in each evaporating sand column. (b) Time dependence of the cumulative precipitated salt in each sand column. The precipitation rate (the slope of the curves) changes with time until it becomes nearly constant in the cases of the columns saturated with 3.5 and 4 Molal solutions. The transition time to a constant precipitation rate is the time at which all the evaporation spots at the surface turn into precipitation spots. Solid lines correspond to the precipitated salt at the surface over time predicted by convection. The vertical dash lines indicate the onset of NaCl precipitation at the surface predicted by the numerical solution of the CDE which is in a reasonable agreement with the experimental data.

Using the pore-scale data, the salt growth rate at the evaporating surface in each 3D sand column was computed. Figure 3.4(a) presents the cumulative precipitated salt as a function of the cumulative mass of liquid water lost due to drying. In the case of the sand column initially saturated with a higher salt concentration, more salt has precipitated at the surface for the same mass loss. Figure 3.4(b) presents the time dependence of the precipitated salt in each sand column indicating that, in the cases of sand columns saturated with 3.5 and 4 Molal NaCl solutions, the salt precipitation rate (the *slope* of the line) initially changes with time, followed by a nearly constant value (confirmed by regression analysis). The transition point corresponds to the time at which all evaporation spots serve as the precipitation spots, hence giving rise to a relatively constant precipitation rate. In other words, prior to the transition time, due to water evaporation, salt concentration continuously increases at the surface until it

reaches the solubility limit. Therefore, evaporation spots continually turn into precipitation spots at the early stages, resulting in higher precipitation rates, even though the evaporative flux remains nearly constant, as indicated by Figure 2. After the transition, however, the number of the precipitation spots does not change anymore, and salt continues to deposit on the already existing spots, and hence, the salt precipitation rate remains relatively constant due to the constant drying rate. Interestingly, in the case of the sand column saturated with a 6 Molal solution, the salt deposition rate remains nearly constant during the entire course of the experiment because the initial salt concentration is very close to the solubility limit of NaCl, and all the evaporation spots are quickly (within a few minutes) transformed into precipitation spots after the onset of the experiment.

C. Numerical analysis

During stage-1 evaporation, the ions are transported by convection toward the evaporation surface via the capillary-induced liquid flow. However, diffusion tends to spread the salt uniformly through the entire space. Therefore, the dynamics of the salt distribution is determined by the competition between convective and diffusive fluxes. To quantify the dynamics, the *macroscale* CDE has traditionally been used, but it has never been established that the CDE can actually model the phenomenon quantitatively. Thus, to test this possibility we solved the continuum CDE numerically and estimated the time required to reach the limit of NaCl solubility at the evaporation surface that marks the onset of salt precipitation. The one-dimensional CDE, traditionally used for this purpose, for a porous medium of length L is given by (Guglielmini *et al*., 2008; Huinink *et al.,* 2002; Sahimi 2011)

$$\frac{\partial}{\partial t}(\varepsilon\rho SC) = \frac{\partial}{\partial z}\left(\varepsilon\rho SD\frac{\partial C}{\partial z}\right) - \frac{\partial}{\partial z}(\varepsilon\rho SCU)) \tag{3.1}$$

where ρ is the solution density, ε is the porosity, S is the liquid saturation, C is the salt's mass fraction dissolved in the liquid phase, D is the solute's effective diffusivity, and U is the average liquid velocity. The initial porosity is 0.4, and we neglect its mild changes as salt precipitates. The boundary conditions are that the diffusive and convective fluxes are equal at $z = 0$ and $z = L$, as the ions cannot escape the liquid phase. D was taken to be 10^{-9} m^2s^{-1}. We assume that the liquid saturation is spatially uniform and varies with time as $S = 1-E/(\rho\varepsilon L)t$, (Guglielmini *et al.*, 2008; Huinink *et al.*, 2002) where E is the evaporation rate. As the evaporation is slow, the spatial variation of S is very slow and thus is neglected. More details of the numerical simulation of the CDE are given elsewhere (Guglielmini *et al.*, 2008; Huinink et al., 2002; Sahimi 2011).

As shown in Figure 3.4, the CDE predicts 0.4 and 0.6 h as the times required to reach the salt solubility limit at the surface of sand columns saturated with 3.5 and 4 Molal NaCl solutions, respectively. Solid lines correspond to the predicted precipitated salt at the surface as a result of convection. As the comparison indicates, the macroscale convective flux cannot by itself describe the dynamics of precipitation at the early and intermediate stages because it cannot account for the pore-scale effect that pores at the surface do not reach the salt solubility limit at the same time (shown in Figure 3.3) because they have different sizes and contribute differently to water evaporation. One must carry out pore-scale simulation to account for such an effect. We note that, in the case of the 6 Molal solution, the macroscale convective flux provides a reasonable estimate of the precipitated salt at the surface because in this case the salt concentration is very close to the solubility limit, and thus, most of the evaporating spots act as the precipitation sites. This means that as water evaporates, the salt transferred to the surface by capillary flow precipitates there, but this is not necessarily the case in the 3.5 and 4 Molal columns.

D. Structural evolution of the precipitated salt

A puzzling question is why during stage-1 evaporation the drying rate remains nearly constant, whereas the surface is covered by the precipitated salt. For example, in the case of the 6 Molal NaCl solution, the evaporation surface is covered quickly by the precipitated salt, but as illustrated by Figure 3.2, the evaporation rate remains relatively constant. This phenomenon may be explained by considering two main factors, namely, the preferential locations of salt precipitation and the structure of the precipitated salt. The initiation and growth of the salt crystals occur on the grains, not inside the pores, as illustrated in Figure 3.1(d), because the energy of heterogeneous nucleation (the formation of the crystal nuclei on preferential nucleation sites, such as solid particles or the surface) is lower than that of the homogeneous process of nucleation in the supersaturated liquid under the conditions of our experiment (Liu, 2000).

The second factor can be related to the structure of the precipitated salt. We used scanning electron microscopy (SEM) to image the evolution of the precipitated salt structure at various times and length scales, down to a few hundred nanometers. The SEM images indicate that the growing precipitated salt has a porous structure during stage-1. Figure 3.5 illustrates the SEM images of the precipitated salt at the surface with different magnification factors after 18 h and 1 week. They indicate that the precipitated salt is porous even after 18 hours. At later stages of drying, however, the structure is modified, with the pores being blocked by further salt precipitation. Therefore, during stage 1, the precipitated porous salt may draw the liquid to the surface where evaporation actually occurs, maintaining the hydraulic connections between the receding front and the evaporation surface, despite the existence of the precipitated salt at the surface (Lehmann *et al*., 2008; Shokri and Or, 2013; Shokri *et al*., 2011; Shokri and Salvucci, 2011; Yiotis *et al*., 2004).. As evaporation proceeds,

however, further salt precipitation eventually blocks the pores of the efflorescence, resulting in the interruption of capillary flow to the surface.

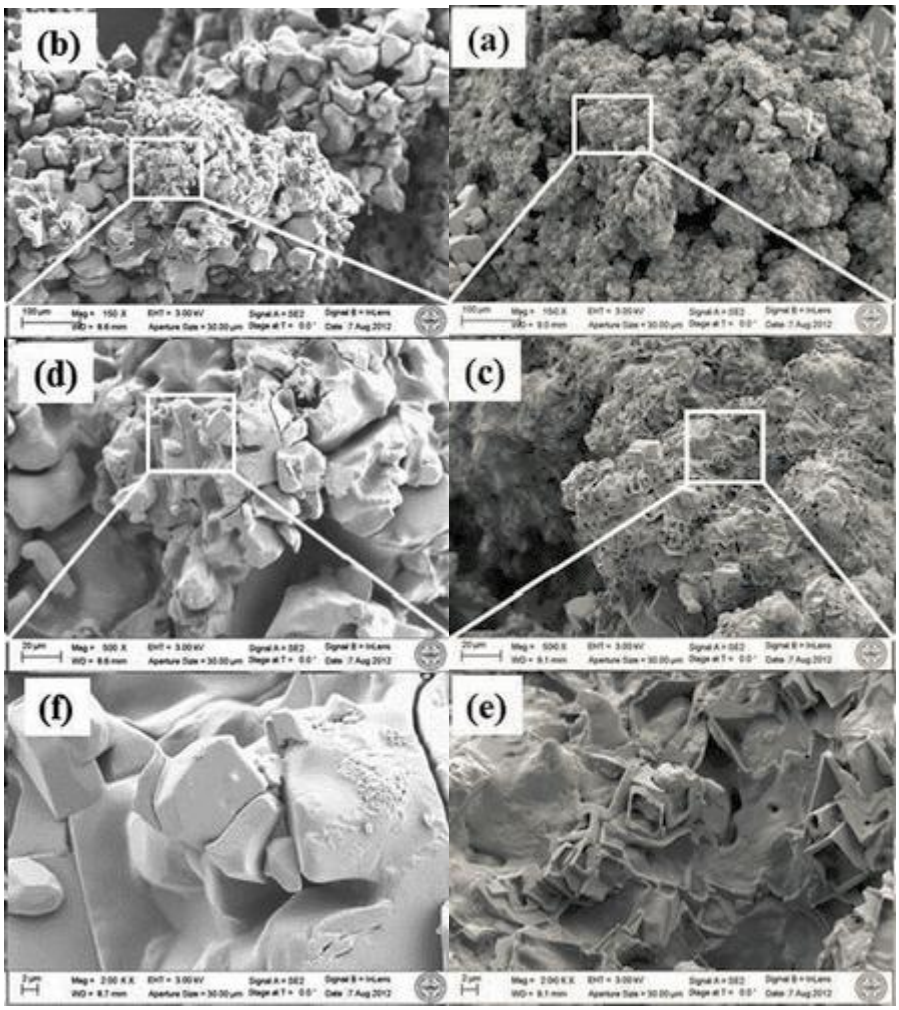

Figure 3.5 The SEM images, showing the structure of the precipitated salt at the surface of the sand column, saturated with a 3.5 Molal NaCl solution after (left) 18 and (right) 168 h with magnification factors of (a) and (b) 150, (c) and (d) 500 and (e) and (f) 2000.

3.4 Summary and Conclusions

In summary, using direct pore-scale imaging, we investigated the 3D dynamics of salt crystallization in drying porous media and delineated the governing mechanisms that affect salt growth and precipitation patterns in saline porous media. Moreover, the SEM imaging confirms unambiguously the porous nature of the precipitated salt, its evolution at the

evaporation surface, and its role in maintaining a relatively constant evaporation rate, even when the surface is covered by the precipitated salt.

Acknowledgments

We are grateful to Peng Zhou, who conducted the SEM imaging at the Boston University Photonics Center. The x-ray microtomography experiments were performed at the Center for Nanoscale Systems at Harvard University. This work was supported in part by the ACS Petroleum Research Fund (PRF No. 52054-DNI6).

References

Espinosa Marzal, R. M., and G. W. Scherer, Crystalization of Sodium Sulfate salt in lime stone, Environ. Geol. 56, 605 (2008);

Schiro, M., E. Ruiz-Agudo, and C. Rodriguez-Navarro, Damage mechanisms of porous materials due to in-pore salt crystallization, Phys. Rev. Lett. 109, 265503 (2012).

Nachshon, E. Shahraeeni, D. Or, M. Dragila, and N. Weisbrod, Infrared thermography of evaporative fluxes and dynamics of salt deposition on heterogeneous porous surfaces, Water Resour. Res. 47, W12519 (2011);

Sghaier, N. and M. Prat, Effect of efflorescence formation on drying kinetics of porous media, Transp. Porous Media 80, 441 (2009);

Eloukabi, H., N. Sghaier, S. Ben Nasrallaha, and M. Prat, Experimental study of the effect of sodium chloride on drying of porous media: The crusty–patchy efflorescence transition, Int. J. Heat Mass Transfer 56, 80 (2013)

Norouzi Rad, M., and N. Shokri, Nonlinear effects of salt concentrations on evaporation from porous media, Geophys. Res. Lett. 39, L04403 (2012).

Veran-Tissoires, S., M. Marcoux, and M. Prat, Discrete salt crystallization at the surface of a porous medium, Europhys. Lett. 98, 34005 (2012); Phys. Rev. Lett. 108, 054502 (2012);

Eloukabi, H., N. Sghaier, M. Prat, and S. B. Nassrallah, Drying experiments in a hydrophobic model porous medium in the presence of a dissolved salt, Chem. Eng. Technol. 34, 1085 (2011).

Cortes, C., and V. Vapnik, Support-vector networks, Mach. Learn. 20, 237 (1995)

Platt, J.C., in Advances in Kernel Methods: Support Kernel Machine, edited by B. Scholkopf, C. Burges, and A. J. Smola (MIT Press, Cambridge, MA, 1999), Chap. 12, p. 185.

Shokri, N., P. Lehmann, and D. Or, Liquid-phase continuity and solute concentration dynamics during evaporation from porous media: Pore-scale processes near vaporization surface, Phys. Rev. E 81, 046308 (2010);

Shokri, N., and M. Sahimi, Structure of drying fronts in three-dimensional porous media, Phys. Rev. E., 85, 066312 (2012);

Shokri, N., M. Sahimi, and D. Or, Morphology, propagation dynamics and scaling characteristics of drying fronts in porous media, Geophys. Res. Lett. 39, L09401 (2012).

Lehmann, P., S. Assouline, and D. Or, Characteristic lengths affecting evaporative drying of porous media, Phys. Rev. E 77, 056309 (2008);

Shokri, N., and D. Or, Drying patterns of porous media containing wettability contrasts, J. Colloid Interface Sci. 391, 135 (2013);

Shokri, N., and D. Or, What determines drying rates at the onset of diffusion controlled stage- 2 evaporation from porous media?, Water Resour. Res. 47, W09513 (2011);

Shokri, N., and G. Salvucci, Evaporation from porous media in the presence of a water table, Vadose Zone J. 10, 1309 (2011).

Yiotis, A. G., Boudouvis, A. K. Stubos, I. N. Tsimpanogiannis, and Y. C. Yortsos, Effect of liquid films on the drying of porous media, AIChE J. 50, 2721 (2004).

Chatterji, S., On the applicability of Fick's second law to chloride ion migration through Portland cement concrete, Cem. Concr. Res. 30, 669 (2000).

Guglielmini, L. , A. Gontcharov, A. J. Aldykiewicz, Jr., and H. A. Stone, Drying of salt solutions in porous materials: Intermediate-time dynamics and efflorescence, Phys. Fluids 20, 077101 (2008);

Sahimi, M., Flow and Transport in Porous Media and Fractured Rock, 2nd ed. (Wiley-VCH, Weinheim, Germany, 2011); Rev. Mod. Phys. 65, 1393 (1993).

Liu, X. Y., Heterogeneous nucleation or homogeneous nucleation?, J. Chem. Phys. 112, 9949 (2000).

Chapter 4

Effects of grain angularity on NaCl precipitation in porous media during evaporation

This chapter has been published in Water Resources Research, volume 50, in 2014, and investigates the effects of the angularity of the grains forming the porous media, on evaporation and precipitation dynamics and efflorescence patterns during evaporation. In order to do so two columns packed with different fully hydrophilic grains of silica sands (angular grains) and glass beads (spherical), with the same average grain size, were used as model porous media. The grains were saturated with the same NaCl solutions. The same method of X-ray micro-tomography was used as in chapter 2. To ensure the similar environmental conditions, both columns went through evaporation and imaging at the same time to ensure the similar atmospheric conditions.

Results presented in this chapter show that the angularity of the grains which enhances the corner flow may slightly modify the evaporation rate, however its effects on the precipitation dynamics and patterns is significant. It influences the distribution of the precipitated salt at the surface as well as the thickness of the salt crust formed above the evaporation surface due to the preferential evaporation and precipitation processes in porous media.

Effects of grain angularity on NaCl precipitation in porous media during evaporation

Mansoureh Norouzi Rad[1] and Nima Shokri[1]

[1]School of Chemical Engineering and Analytical Science, University of Manchester, Manchester, UK

Water Resour. Res., 50, doi:10.1002/2014WR016125

Abstract

Three dimensional pore-scale analysis was carried out using X-ray microtomography to investigate the effects of grain angularity on NaCl precipitation dynamics and patterns during evaporation from saline porous media. To do so, quartz sand and glass beads with almost similar average particle size and porosity were used enabling us to constrain the effects of grain angularity on NaCl precipitation since the glass beads were spherical and smooth whereas the sand consisted of irregularly shaped grains. Presence of angularity resulted in different pore sizes and shapes influencing the dynamics of evaporation and NaCl precipitation. Our results demonstrate that the preferential evaporation exclusively in fine pores at the surface of porous media results in discrete efflorescence. We observed a higher cumulative NaCl precipitation in the case of glass beads at the early stages of precipitation due to the presence of a fewer number of evaporation sites at the surface. This phenomenon resulted in formation of a thicker and more discrete NaCl crust at the surface of glass beads compared to sand grains. Also, computed water saturation profiles reveals formation of a wider unsaturated zone above the receding drying front in the case of sand compared to glass beads due to the presence of finer pores affecting the capillary flow though the partially wet zone. Our results provide new insights regarding the effects of grain angularity on NaCl precipitation dynamics and patterns during evaporation from saline porous media.

4. 1 Introduction

Understanding salt precipitation during evaporation from saline porous media is of major concern in many hydrological and environmental applications. Some examples include soil salinity, terrestrial ecosystem functioning, vegetation and crop production, biological activities in vadose zone, and CO_2 sequestration (Rodriguez-Navarro and Doehne, 1999*;*

Prasad *et al.,* 2001*;* Il'ichev *et al.,* 2008*;* Shahidzadeh-Bonn *et al.,* 2008*;* Nachshon *et al.,* 2011a*).*

Dynamics of water evaporation from saline porous media is not only dependent on the nature of the soluble salt, but also on the drying behavior of porous media, which is influenced by atmospheric conditions, structure and the transport properties of the porous medium (van Brakel, 1980*;* Scherer, 1990*;* Petković *et al.,* 2007*;* Or *et al.,* 2013). Thus describing salt transport and precipitation patterns requires knowledge of the mechanisms controlling water evaporation. Early stages of evaporation from porous media involves preferential invasions of large pores by air while the fine pores at the surface remain saturated, the so-called stage-1 evaporation (van Brakel, 1980). During this period, capillary induced liquid flow from the large pores located at a receding drying front (defined as the interface between saturated and unsaturated zone) to the fine pores at the surface supplies the evaporative demand (Scherer, 1990; Shokri *et al*., 2010; Yiotis *et al*., 2012). Stage-1 evaporation is terminated when the downward gravity and viscous forces equal the upward capillary driving forces resulting in the disconnection of continuous hydraulic connections between the receding drying front and the evaporation surface that marks the onset of stage-2 evaporation in which the evaporative flux is limited by vapour diffusion through porous media (Fisher, 1923; Saravanapavan and Salvucci, 2000; Lehmann *et al*., 2008; Shokri and Or, 2011). More details on evaporation from porous media can be found in reviews by Prat [2002] or a more recent one by Or *et al*. [2013 and references therein], thus it is not repeated here.

Presence of salts makes the drying of porous media more complicated. The vapour pressure above the evaporation surface is modified by the type of salt and its concentration in the solution influencing the evaporation dynamics. Besides, during evaporation dissolved salt is convected from the bulk liquid (saturated zone) to the surface via capillary induced liquid

flow while the diffusion tends to spread the salt uniformly in space (see Huinink *et al*. [2002] and Guglielmini *et al*. [2008] for more detail on this). Since evaporation takes place in the fine pores at the surface of porous media, salt concentration preferentially increases in those evaporation sites (Shokri, 2014). When salt concentration exceeds the solubility limit, it precipitates (Scherer, 2004; Norouzi Rad *et al*., 2013). When salt precipitation occurs at the surface of porous media, it is called efflorescence, and it refers specifically to evaporatively driven soluble salt from the interior of the porous media to the surface where evaporation takes place (Scherer, 2004; Guglielmini *et al*., 2008; Norouzi Rad *et al*., 2013). In other cases, salt may deposit inside porous media, the so-called subflorescence, which can create extensive damage to materials under certain conditions (Scherer, 2004). Subflorescence is not discussed in the present study.

The precipitation patterns at the surface of porous media strongly depend on the pore size distribution of the porous medium and pore shapes among other factors. Eloukabi *et al*. [2013] distinguished between two types of precipitation patterns at the surface of porous media referred as crusty and patchy efflorescence. They observed formation of a crusty efflorescence in the case of a porous medium consisting of small particles limiting the evaporation rate as opposed to patchy efflorescence when the particles were larger. In the latter case, the evaporation rate was even enhanced due to the salt precipitation at the surface. Also, *Veran*-Tissoires *et al*. [2012a] illustrated the discrete nature of efflorescence and its relation with the evaporation rates. Veran-Tissoires *et al*. [2012b] studied precipitation patterns in the presence of vertical textural interfaces and observed preferential solute deposition at the surface of finer-textured medium due to the higher capillary pressure compared to the coarse-textured medium. Similar results were observed in Nachshon *et al*. [2011b]. Norouzi Rad *et al*. [2013] showed the effects of NaCl concentration on the dynamics

of salt precipitation in drying porous media. Using pore-scale images obtained by X-ray microtomography, they could relate the occurrence of discrete efflorescence at the surface to the location of the fines pores at the surface serving as the preferential vaporization sites. Also, using Scanning Electron Microscopy (SEM) imaging, they could visualize the evolving porous structure of the precipitated NaCl at the surface of a porous medium. More recently, Shokri [2014] used synchrotron X-ray microtomography to study the pore-scale dynamics of dissolved salt transport and distribution in drying porous media with a high spatial and temporal resolution and experimentally established the preferential accumulation of solute exclusively in fine pores (specially at the grains' contacts) at the surface of the drying porous media.

As shown in several papers (some mentioned above) efflorescence patterns in drying porous media are influenced by the location of the small pores at the surface in which preferential salt precipitation and evaporation takes place. Building on this concept, the specific objective of the present paper is to investigate the effects of grain angularity on salt precipitation in drying porous media as the grain angularity modifies the shape and size of the pores. The majority of previous studies investigating solute precipitation patterns and accumulation during evaporation from porous media were conducted at macro scale and mainly focused on two-dimensional evaporating surfaces (*e.g.*, Norouzi Rad *and* Shokri, 2012; Veran-Tissoires *et al*., 2012a, 2012b; Eloukabi *et al*., 2013). With a very few exception (Nachshon *et al*., 2011a; Norouzi Rad *et al*., 2013), three-dimensional (3-D) investigation of salt precipitation patterns in porous media is rare largely due to the difficulty of visualization of the dynamics of salt precipitation and limitations imposed by available techniques. Therefore, in the present work, we carried out a comprehensive pore-scale study using X-ray microtomography to map

the dynamics of efflorescence patterns during evaporation from packs of spherical glass beads and irregularly shaped sand grains.

4.2 Experimental Considerations

Glass columns of 35 mm in height and 10 mm in diameters were used to run the evaporation experiments and investigate the effects of grain angularity influencing the size and shape of the pores on NaCl precipitation dynamics. To do so, quartz sand and glass beads with almost similar average particle size and porosity but different shapes were used enabling us to constrain the effects of grain angularity affecting pore size and shape on NaCl precipitation patterns since the glass beads were spherical and smooth whereas the sand consisted of irregularly shaped grains resulting in different pore size and shape which affect the distribution of the vaporization sites at the surface of porous media. Figure 4.1a illustrates the particle size distribution of sand and glass beads used in our experiments with the average particle size of ~0.6 mm and Figure 4.1b illustrates the porosity variation through both columns computed by image analysis using the pore scale data obtained by X-ray microtomography (explained in following section). The lower porosity at the lower depths observed in both columns might be due to the tighter grains' arrangement as opposed to the ones located close to the surface.

Sand grains and glass beads were carefully washed and dried for 24 h in an oven at 105°C. Both particles were hydrophilic. The grains were packed into the cylindrical glass columns following the procedure explained in Grapsas and Shokri [2014]. The packed beds were saturated with 3 Molal solutions of reagent grade NaCl (from EMD Chemicals, Inc., NJ, USA). All boundaries of the evaporating columns were closed except the top which was open to air for evaporation. To visualize the 3-D dynamics and patterns of NaCl precipitation

during evaporation, we have used the X-ray microtomography technique. The X-ray imaging was carried out using a HMXST device at the Harvard University Centre for Nanoscale Systems (CNS). Both columns were taped together and were scanned at a same time as a bundle to ensure similar evaporative conditions during evaporation. There was no air flow above the surface of the column. We were not able to measure the relative humidity and temperature inside the X-ray chamber (which was close to the room temperature), but since both columns were scanned at a same time, they were under similar evaporative conditions. The experiment was continued for 22 h. The entire column was scanned roughly every 1.5 h during evaporation resulting in 3-D pore-scale information about the patterns and dynamics of NaCl precipitation during evaporation from saline porous media with a spatial resolution of 0.017 mm. The general experimental and imaging procedures were similar to the one described in Norouzi Rad *et al*. [2013].

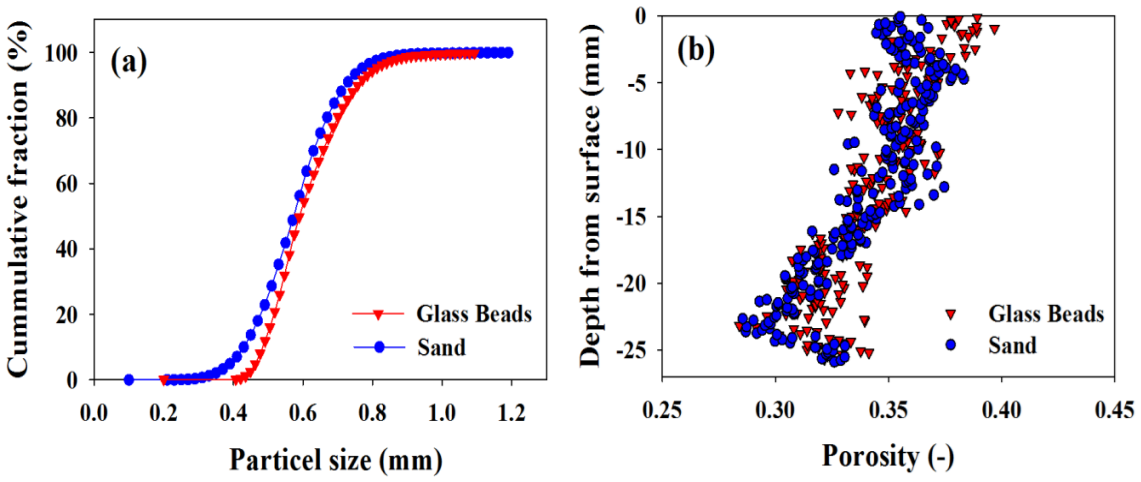

Figure 4.1 (a) Particle size distribution of sand and glass beads used in the experiments (b) porosity variation though the columns packed with sand and glass beads. Porosity was calculated using the pore-scale data obtained by X-ray microtomography. As illustrated, two materials share nearly similar average particle size and porosity.

As for the image analysis, we used the standard machine learning technique of a support vector machine (SVM) (Cortes and Vapnik, 1995) with a quadratic kernel to segment each cross section into solid, liquid, and air. The SVMs were trained using sequential minimal optimization (Platt, 1999) from MATLAB's machine learning package. The segmentation algorithm is the same as the one explained in Norouzi Rad *et al*. [2013]. The gray-scale images were segmented into images with three colors of white, blue, and brown indicating air, liquid and solid phases, respectively. A typical example of the segmented images is presented in Figure 4.2. To distinguish the precipitated NaCl from the grains, each 2-D cross section was compared to its corresponding image obtained at the beginning of the experiment with the difference of the solid phase indicating the precipitated NaCl. A similar method was used in Norouzi Rad *et al*. [2013].

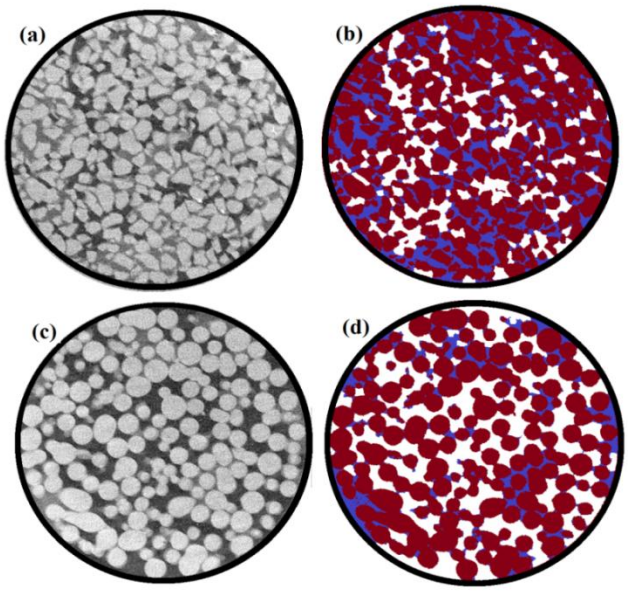

Figure 4.2 (a, c) Original and (b, d) segmented two-dimensional horizontal cross sections of the columns packed with sand (Figure 4.2a) and glass beads (Figure 4.2c). White, blue and brown in Figures 4.2b and 4.2d correspond to air, liquid and solid phases, respectively. The images illustrate the phase distributions after 5.7 h from the onset of the experiment at 0.44 mm below the surface.

4.3 Results and Discussion

4.3.1 Evaporative Mass Loss

Evaporative mass losses from the evaporating sand and glass bead columns were computed using the segmented images. Figure 4.3 shows the cumulative water losses due to evaporation versus time. The evaporation process was in stage-1 during the entire course of the experiments, so the evaporative flux was mainly controlled by the atmospheric conditions (Smits *et al*., 2012; Haghighi *et al*., 2013). Therefore, stage-2 evaporation in which the evaporative flux is limited by vapour diffusion through porous media was not observed in our experiments (this is confirmed later according to the computed water content profiles). As shown in Figure 4.3, water evaporation was higher in the case of sand compared to glass beads especially at the later stages of the evaporation process in our experiments. To confirm the reproducibility of this result, we have conducted three more rounds of experiments using the same sand and glass beads in our laboratory. The results are included in Figure 4.3. In all cases, more water was evaporated from the sand pack despite of having the same average particle size and porosity as the glass beads. Besides, the presented cumulative mass loss curves in Figure 4.3 show slightly decreasing evaporation rates in all cases over time (indicated by the decreasing slope of the tangent lines to the cumulative mass loss curves) over time. The slight decrease of the evaporation rates is due to the continuous increase of the NaCl concentration resulting in decreasing saturated vapour pressure above the surface which eventually leads to decreasing evaporation rates during drying of saline porous media.

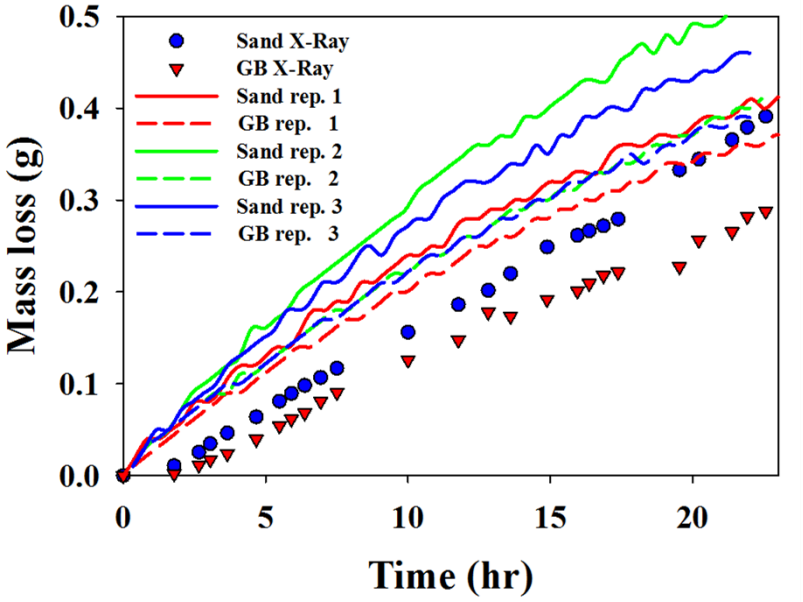

Figure 4.3 Cumulative mass of liquid water removed by evaporation from the columns packed with sand and glass beads initially saturated with NaCl solution. The symbols correspond to the cumulative mass loss measured during the experiments with X-ray microtomography determined from image analysis. In addition, three repetitions (written as rep. in the legend) were performed in the lab to measure the evaporation rate using digital balances to check the reproducibility of the observed behavior, *i.e.*, higher evaporation from sand pack compared to the glass beads. The solid and dash lines indicate the data measured using the balance. The slight difference in the measured cumulative mass loss in each round is due to the slight fluctuation of the evaporative demand during each round affecting the evaporative mass losses during stage-1 evaporation.[11]

Higher evaporation from sand pack is due to the presence of more evaporation sites at the surface of sand compared to glass beads due to the grain angularity. In other words, as a result of the grains' irregularity in sand pack, more fine pores and preferential evaporation sites were formed at the surface of the sand pack compared to the glass beads especially at the grains' contacts and crevices. While the larger pores at the surface are invaded by air, these fine preferential evaporation sites remain saturated (due to the higher capillary pressure)

[11] A modified version of this figure is presented in Appendix C as Figure C.4.3 with straight lines to better visualizing of the constant slopes of mass loss curves and stage-1 evaporation.

and hydraulically connected to the wet zone at bottom enhancing the evaporation and liquid flow through corners and crevices compared to the smooth glass beads pack.

To evaluate the above explanation, the pore size distribution in sand and glass beads pack were quantified using the pore-scale data obtained by 3-D X-ray microtomography. To compute the pore size distribution, the pore network extraction code described in Dong and Blunt [2009] was used in this study. We have computed the pore size distribution over the top ~0.5 mm and 12 mm of the sand and glass beads to represent the pore size distribution close to the surface and the bulk medium respectively. The obtained results are presented in Figure 4.4. Figures4. 4a and 4.4b confirm the presence of finer pores in sand compared to glass beads pack as a result of the sand grains angularity.

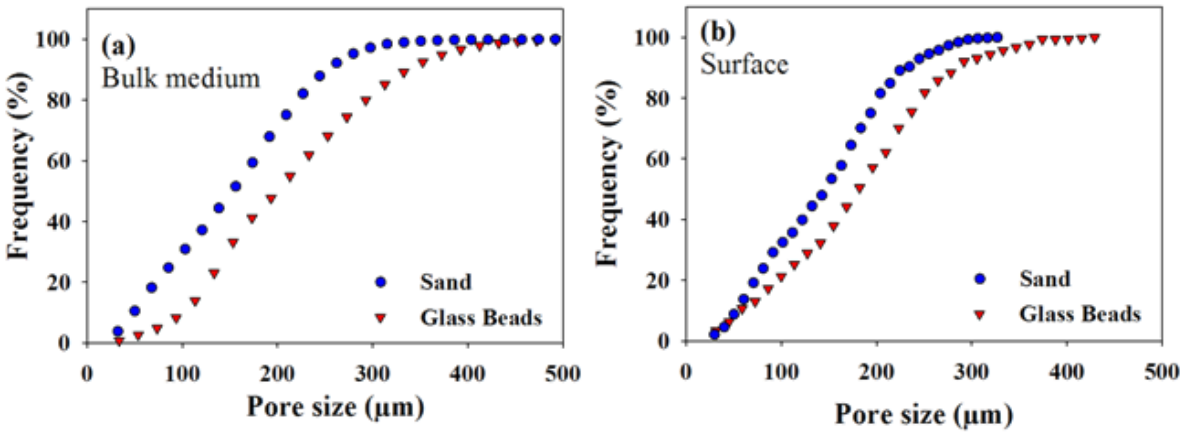

Figure 4.4 The pore size distribution computed from the 3-D X-ray images determined using the network extraction code developed by Dong and Blunt [2009]. (a) The pore size distribution of the bulk medium and (b) the pore size distribution over the top 0.5 mm of the columns.

4.3.2 Water Saturation Profiles

We calculated the water saturation distribution through each evaporating column using the pore-scale images obtained by X-ray microtomography. Figure 4.5a illustrates typical water

saturation profiles measured during evaporation from sand and glass beads at four different elapsed times from the onset of the experiment with the temporal evolution of the water saturation averaged over the top 1 mm of the evaporating samples presented in Figure 4.5b confirming the existence of more water at (or close to) the surface of the column packed with sand compared to glass beads.

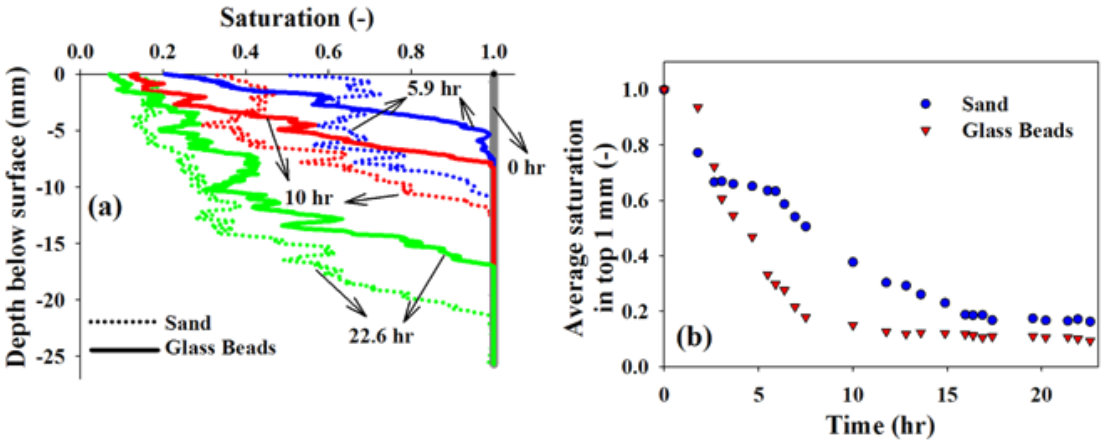

Figure 4.5 (a) Water saturation profiles at different times from the onset of the evaporation experiments in the columns packed with sand and glass beads. (b) The average water saturation over the top 1 mm of the sand and glass beads columns confirming the presence of water close to the surface during the entire course of our experiments in both cases and also higher water saturation in the case of sand compared to glass beads.[12]

The results presented in Figure 4.5 reveal the presence of liquid water at the surface of both evaporating columns at the end of the experiment (~22 h) which is an indication of stage-1 evaporation. The results also show the presence of a sharper and more distinct interface between saturated and unsaturated zone in the column packed with glass beads. Also, the length of the unsaturated zone (the area invaded by air during evaporation) was shorter in the case of glass beads compared to sand for a given elapsed time from the onset of the experiment. This is due to the presence of finer pores in sand pack compared to glass beads as

[12] The x-axis of (a) is "water saturation" which is presented in the modified version of the figure as Figure C.4.5 in Appendix C.

a result of the grain angularity which maintains a longer capillary length between the receding drying front (*i.e.*, the interface between saturated and unsaturated zone) and the evaporation surface. The observed fluctuation in the calculated water saturation profiles is due to the porosity variation though the column and also presence of disconnected liquid clusters above the saturated zone in both cases as a result of pinning-unpinning of air-liquid interfaces through the unsaturated zone during evaporation (Shokri *et al*., 2012).

4.3.3 Pore-Scale NaCl Precipitation Patterns

Figure 4.5 confirmed the presence of less water at the surface of the column packed with glass beads compared to sand. Also, the pore-scale images (see *e.g.* Figure 4.2) confirmed the presence of a fewer preferential evaporation sites at the surface of glass beads pack. This should eventually result in more discrete but thicker efflorescence at the surface of glass beads since the advected salt toward the surface are accumulated in fewer preferential deposition sites. Using the 3-D pore-scale information obtained by X-ray tomography, the patterns and dynamics of precipitated NaCl could be visualized. Figure 4.6 shows a close-up of the surface of the column packed with sand and glass beads at different times from the onset of the experiment with the light gray indicating the precipitated NaCl. This figure clearly shows less area is covered at the surface of glass beads compared to sand at the end of the experiment due to the presence of less fine pores at the surface to serve as evaporation and precipitation sites.

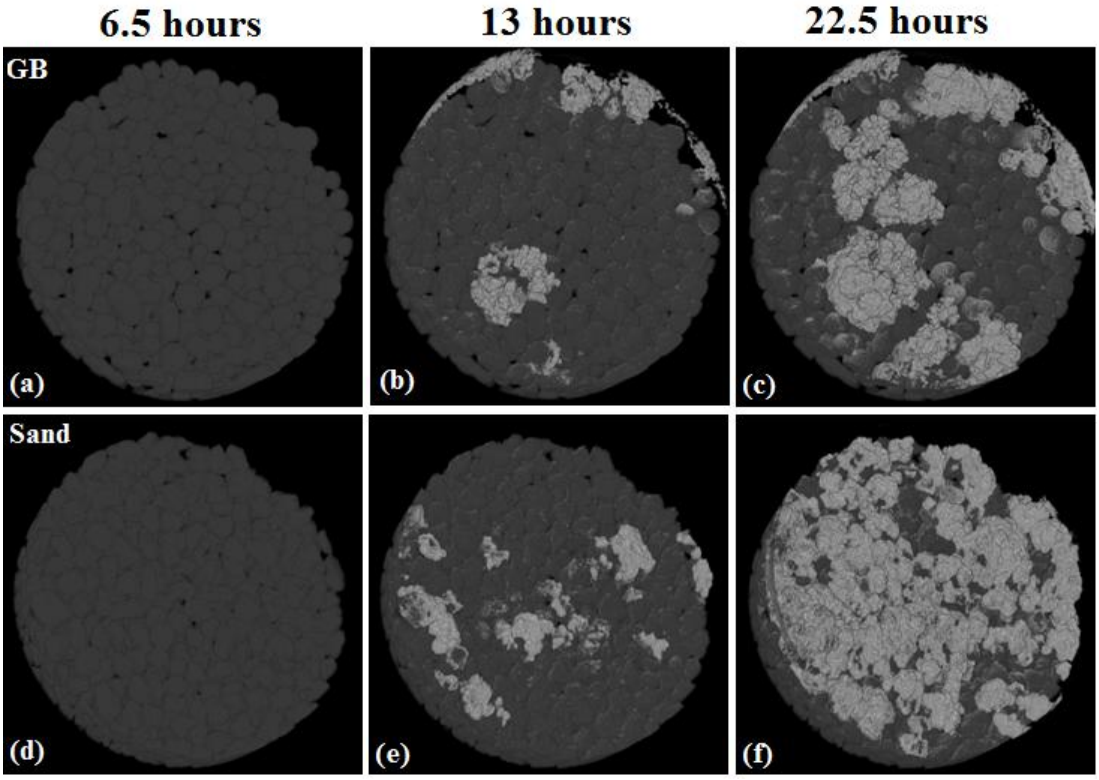

Figure 4.6 Efflorescence at the surface of the column packed with (a) glass beads and (d) sand at different times from the onset of the evaporation experiments. The numbers at top indicate the elapsed time from the beginning of the experiment. The dark and light gray indicates the grains and precipitated NaCl respectively. The efflorescence at the end of the experiment in the case of glass beads is more discrete compared to sand column due to the presence of fewer evaporation and precipitation sites at the surface of the column.

Figure 4.7 quantitatively shows the distribution and thickness of the precipitated NaCl at the surface of the column packed with glass beads and sand at the end of the evaporation experiment. The color-map indicates the thickness of the precipitated NaCl. Figure 4.7 confirms that the total area covered by NaCl is larger in the case of sand compared to glass beads. Also, it shows that the NaCl crust formed above the surface of glass bead is thicker than the sand column. The average crust thickness in the case of glass beads and sand was 0.34 mm and 0.27 mm, respectively. Besides, the maximum thickness of the NaCl crust is roughly 25% more in the case of glass beads pack compared to the sand column. Due to the

existence of less precipitation sites at the surface of glass beads as a result of the smooth glass beads, a thicker NaCl crust is formed at the end of the evaporation experiment in the column packed with the glass beads. This is quantitatively shown in Figure 4.8 illustrating the histograms of the thickness of the precipitated NaCl above the surface of the sand and glass beads together with the cumulative distributions. Figure 4.8a confirms formation of thicker NaCl crusts above the surface of the glass beads. Also, due to the presence of more small pores (preferential evaporation sites) at the surface of sand pack (as illustrated quantitatively in Figure 4.4b), the covered area by precipitated NaCl is notably more in the case of sand compared to glass beads shown in Figure 4.8b. Figure 4.8 shows that nearly 64 mm^2 of sand surface was covered by the precipitated NaCl as opposed to 36 mm^2 in the case of glass beads pack. However only less than 5% of the deposited salt above the sand surface has a thickness of 0.5 mm or more whereas this ratio is about 20% in the case of the glass beads pack. This illustrates the significant effect of pore size and shape (influenced by the grain angularity) on NaCl precipitation patterns in drying saline porous media.

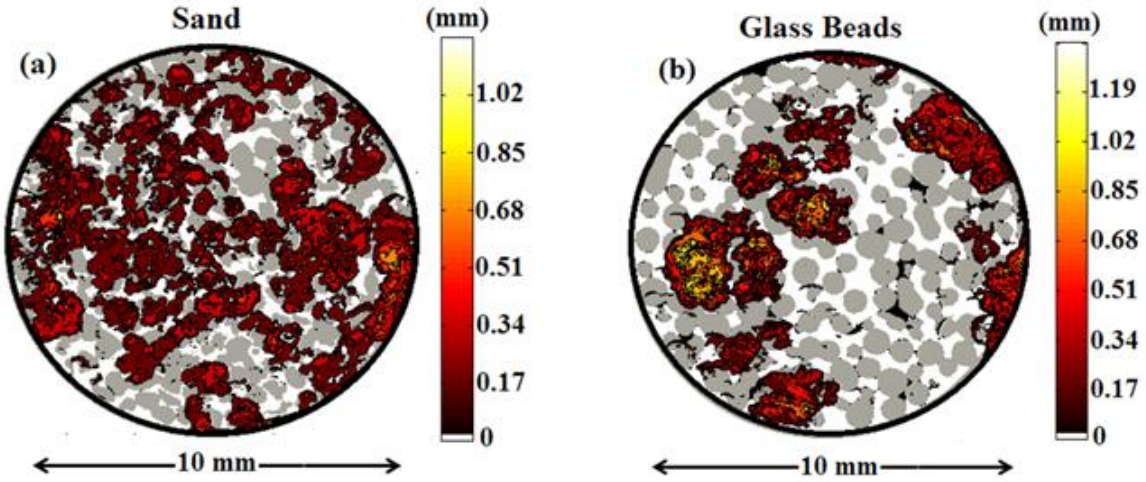

Figure 4.7 Patterns and distribution of the precipitated NaCl on the surface of the columns. The color bar indicates the thickness of the precipitated NaCl such that the closer the color is to yellow, the thicker is the salt crust. Black, white, and gray corresponds to regions filled with water, air and grains, respectively. Less precipitation sites existed at the surface of the columns packed with glass beads resulted in formation of a thicker and more discrete NaCl crusts.[13]

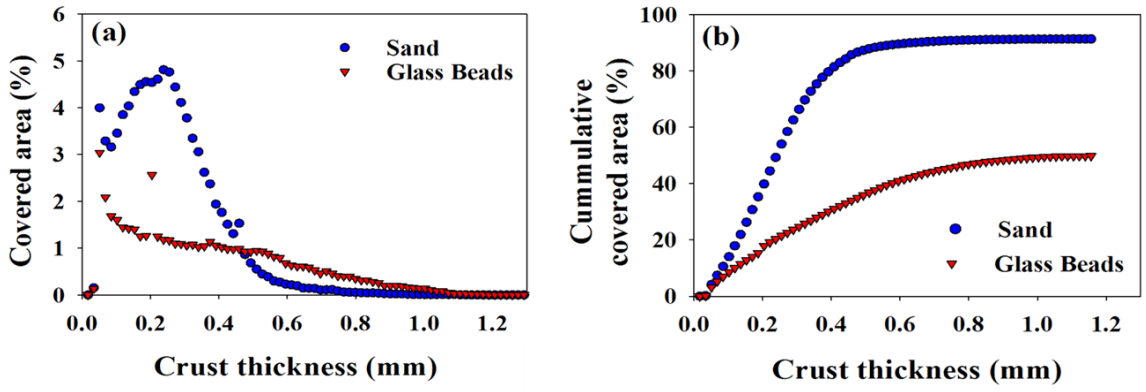

Figure 4.8 (a) Histogram of the thickness of the precipitated NaCl with the corresponding cumulative distribution presented in Figure 4.8b.

[13] The circles show the cross section of the surface of the columns with the grains (shown in gray). This surface is defined as where the porosity is representative of the average porosity of the column. The yellow to red shades of the colors shows the precipitated salt which was formed (only) on top of the surface.

Figure 4.9 shows the volume of the deposited NaCl versus its distance from the surface at the end of the experiment. At larger distances from the surface of the column (smaller *Y* values) more NaCl is deposited on the glass beads compared to sand which confirms the formation of a thicker NaCl crust on the glass bead pack, while in shorter distances (*Y* values between 0.7 mm and 1.25 mm), volume of precipitated salt above the sand column is more due to the formation of a thinner but 'crustier' salt.

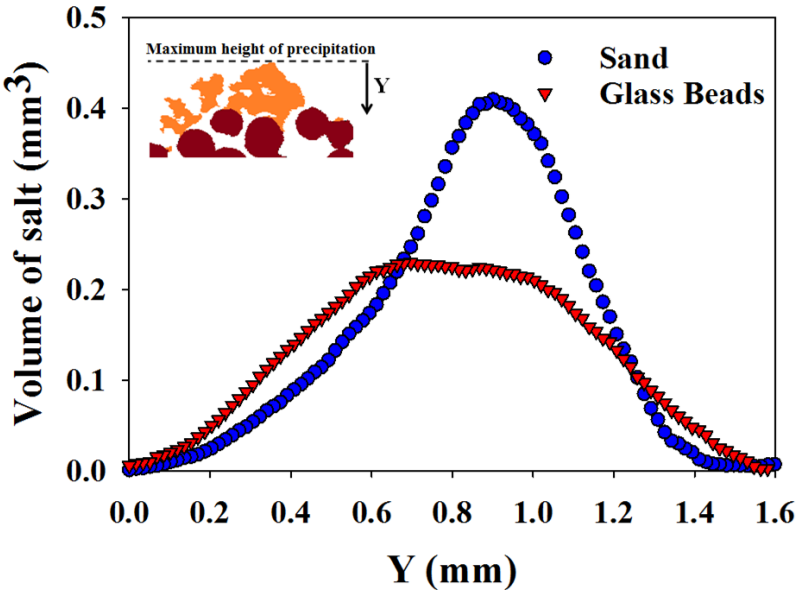

Figure 4. 9 Volume of precipitated NaCl formed above the surface of the columns packed with glass beads and sand grains (*Y* is the distance measured from the highest point of the crust formed above the surface as indicated in the legend with the downward direction corresponding to the positive value).

4.3.4 Effects of Grain Angularity on NaCl Precipitation Dynamics

As mentioned before, during stage-1 evaporation, smaller pores on the surface remain saturated and evaporation takes place mainly in these fine pores serving as preferential evaporation sites. As a result, NaCl concentration continuously increases in the fine pores at the surface. This mechanism has been experimentally verified in Shokri *et al*. [2010] and

Shokri [2014]. As evaporation proceeds, the NaCl concentration eventually reaches the salt solubility limit (6.12 Molal at 25°C) that marks the onset of precipitation. Using the pore-scale data, we could delineate the dynamics of NaCl precipitation and growth above the evaporation surface as influenced by the grain angularity. Figure 4.10 shows the cumulative precipitated NaCl versus time and cumulative water losses in both columns.

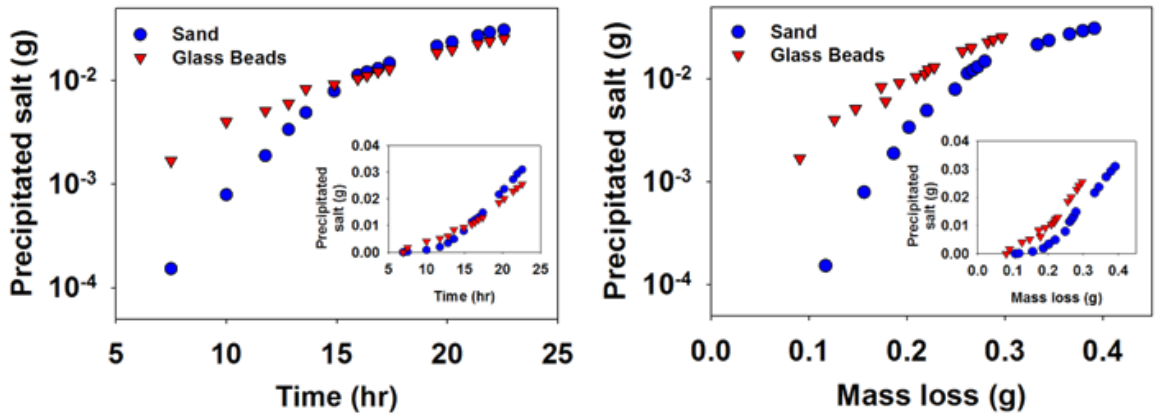

Figure 4.10 Cumulative precipitated NaCl above the surface for both glass bead and sand columns versus (a) time and (b) cumulative mass of liquid water removed by evaporation. In both cases, the precipitation rate increases at the early stages followed by a constant precipitation rate. Note, more NaCl precipitation in the case of glass beads compared to sand under a same evaporative water loss. This is due to the presence of a fewer evaporation sites on the surface of glass beads (see the text for further explanation). The insets present the same data but in a linear scale.

Results in Figure 4.10a show an increasing precipitation followed by a nearly constant precipitation rate in both cases similar to the behavior observed in Norouzi Rad *et al*. [2013] in which the effects of NaCl concentration on precipitation dynamics was investigated. This behavior is due to the fact that the evaporation sites at the surface do not reach NaCl solubility limit at the same time since they contribute differently in supplying the evaporative demand depending on their pore sizes (Norouzi Rad *et al*., 2013). The finer pores reach the solubility limit earlier than the larger pores. Thus, at the early stages of the evaporation, the

number of the precipitation sites increases as the evaporation sites turn into the precipitation sites sequentially resulting in an increasing precipitation rate despite of a relatively constant evaporation rate. However, when NaCl concentration in all evaporation sites exceeds the solubility limit, the number of the precipitation sites remains constant resulting in a constant precipitation rate. Since more evaporation sites exist at the surface of sand column compared to the glass beads, more water should evaporate to have all evaporation sites converted to precipitation sites in the column packed with sand grains. Therefore the transition from the increasing to constant precipitation rate regime occurs at a higher evaporative mass losses in sand compared to the glass bead column as reflected in Figure 4.10b.

Also, Figure 4.10b shows more precipitation in the case of glass beads compared to sand under a same cumulative mass loss. This is not a trivial result as one may expect same amount of precipitated NaCl above the surface when same amount of water is evaporated from the columns. This behavior can be explained considering the fact that the number of the evaporation sites at the surface of glass beads is less than sand column due to the grain angularity in the sand pack. Therefore, due to the existence of a fewer evaporation sites at the surface of glass beads, less salt is required to reach the NaCl solubility limit at the surface; consequently the transported ions will contribute to the NaCl precipitation earlier than the sand pack.

4.4 Summary and Conclusions

To investigate the effects of grain angularity on the dynamics and patterns of NaCl precipitation in 3-D porous media, X-ray microtomography was used during evaporation from saline porous media. Glass beads and sand particles sharing a similar average particle size and porosity but different grain angularity were used in this study. The resulted 3-D

pore-scale images were segmented to quantify the evaporative water losses and the dynamics and patterns of NaCl precipitation and water distribution during evaporation as influenced by the grain angularity, pore shape and size. Despite of the similar average particle size and porosity of the two columns used in this study, the resulting dynamics and patterns of NaCl precipitation was significantly different reflecting the dominant role of the pore size and shape influenced by the grain angularity on evaporation from saline porous media.

We observed that at early stages of the evaporation, larger pores on the surface are invaded preferentially by air while fine pores remain saturated due to the higher capillarity followed by liquid vaporization exclusively in the fine pores similar to what was observed in other studies cited earlier in the paper. As the evaporation proceeds, NaCl concentration in the fine pores increases until it reaches the solubility limit when the precipitation starts. Since fine pores at the surface contribute in evaporation depending on their sizes, evaporation sites at the surface do not reach the solubility limit at a same time causing a nonlinear behavior in the precipitation rate. Therefore, initially the precipitation rate increases as the evaporation sites turn into precipitation sites sequentially. Once all evaporation sites turned into precipitation sites, the precipitation rates remained relatively constant due to the relatively constant evaporation rate observed in our experiments.

More precipitation was observed in the case of glass beads compared to the sand column under same cumulative water losses. This was due to the presence of a fewer fine pores (serving as evaporation sites) on the surface of glass beads compared to the sand column as a result of the irregularly shaped sand grains. Thus less water had to evaporate to have all evaporation sites converted to precipitation sites in the case of glass beads; consequently most of ions transferred to the surface contributed to the NaCl precipitation earlier than the sand column. Presence of a fewer evaporation sites at the surface of glass beads also resulted

in formation of a thicker and more discrete NaCl crust at the surface compared to the sand column. The presence of more fine pores in the sand pack compared to glass beads was confirmed by the computed pore size distribution of porous media extracted from the 3-D X-ray images.

The findings of this paper progress our physical understanding of NaCl precipitation patterns in saline porous media during evaporation which is important in various hydrological applications especially in soil processes as many chemical reactions in relation to nutrient availability and mobility in soil are modified due to the presence of salt in the environment (Sarmadian *et al*., 2010). Unfavorable salt accumulation can inflict severe damages to the ecosystem. Salt-affected land is considered as an ecosystem under stress, where decreases in the nutrient cycling, and increases in the dominance of exotic biota are evident. Such effects can adversely change disease prevalence in plant, animal, and human populations as the ecosystem begins to deteriorate and natural protective mechanisms break down (Jardine *et al*., 2007). Therefore, improving the ability to describe the effects of various parameters (in this paper grain angularity and pore size and shape) on the fate and precipitation of salt in porous media under different boundary conditions could provide benefits to a large global society affected by the problem of soil salinity.

Acknowledgments

We express our gratitude to Siamak Tazari for his helpful discussion regarding the use of SVMs for the image processing, Martin Blunt for sharing the network extraction code developed in his group and Ali Q. Raeini for his help to run the code used to compute the pore size distribution. The X-ray microtomography experiments were performed at the Center for Nanoscale Systems (CNS) at Harvard University, a member of the National Nanotechnology Infrastructure Network (NNIN). We gratefully acknowledge many insightful

and constructive comments made by the Associate Editor and anonymous reviewers. The data used in this manuscript will be available freely via sending a request to the corresponding author. Acknowledgment is made to the donors of the American Chemical Society Petroleum Research Fund for partial support of this research (PRF 52054-DNI6).

References

Cortes, C., *and* V. Vapnik *(*1995*),* Support-vector networks, Mach. Learning, 20, 273–297.

Dong, H., *and* M. J. Blunt *(*2009*),* Pore-network extraction from micro-computerized-tomography images, Phys. Rev. E., 80, 036307.

Eloukabi, E., N. Sghaier, S. Ben Nassrallah, *and* M. Prat *(*2013*),* Experimental study of the effect of sodium chloride on drying of porous media: The crusty–patchy efflorescence transition, Int. J. Heat Mass Transfer, 56, 80–93.

Fisher, R. A. *(*1923*),* Some factors affecting the evaporation of water from soil, J. Agron. Sci., 13, 121–143.

Grapsas, N., *and* N. Shokri *(*2014*),* Acoustic characteristics of fluid interface displacement in drying porous media, Int. J. Multiphase Flow, 62, 30–36.

Guglielmini, L., A. Gontcharov, A. J. Aldykiewicz Jr., *and* H. A. Stone *(*2008*),* Drying of salt solutions in porous materials: Intermediate-time dynamics and efflorescence, Phys. Fluids, 20, 077101, *doi:*10.1063/1.2954037.

Haghighi, E., E. Shahraeeni, P. Lehmann, *and* D. Or *(*2013*),* Evaporation rates across a convective air boundary layer are dominated by diffusion, Water Resour. Res., 49, 1602–1610, *doi:*10.1002/wrcr.20166.

Huinink, H. P., L. Pel, *and* M. A. Michels *(*2002*),* How ions distribute in a drying porous medium: A simple model, Phys. Fluids, 14, 1389–1395, *doi:*10.1063/1.1451081.

Il'ichev, A. T., G. G. Tsypkin, D. Pritchard, *and* C. N. Richardson *(*2008*),* Instability of the salinity profile during the evaporation of saline groundwater, J. Fluid Mech., 614, 87–104.

Jardine, A., P. Speldewinde, S. Carver, *and* P. Weinstein *(*2007*),* Dryland salinity and ecosystem distress syndrome: Human health implications, EcoHealth, 4, 10–17.

Lehmann, P., S. Assouline, *and* D. Or *(*2008*),* Characteristic lengths affecting evaporative drying of porous media, Phys. Rev. E, 77, 056309.

Nachshon, U., E. Shahraeeni, D. Or, M. Dragila, *and* N. Weisbrod *(*2011a*),* Infrared thermography of evaporative fluxes and dynamics of salt deposition on heterogeneous porous surfaces, Water Resour. Res., 47, W12519, *doi:*10.1029/2011WR010776.

Nachshon, U., N. Weisbrod, M. Dragila, *and* A. Grader *(*2011b*),* Combined evaporation and salt precipitation in homogeneous and heterogeneous porous media, Water Resour. Res., 47, W03513, *doi:*10.1029/2010WR009677.

Norouzi Rad, M., *and* N. Shokri *(*2012*),* Nonlinear effects of salt concentrations on evaporation from porous media, Geophys. Res. Lett., 39, L04403, *doi:*10.1029/2011GL050763.

Norouzi Rad, M., N. Shokri, *and* M. Sahimi *(*2013*),* Pore-scale dynamics of salt precipitation in drying porous media, Phys. Rev. E, 88, 032404.

Or, D., P. Lehmann, E. Shahraeeni, *and* N. Shokri *(*2013*),* Advances in soil evaporation physics—A review, Vadose Zone J., 12*(*4*),* *doi:*10.2136/vzj2012.0163.

Petković, J., H. P. Huinink, L. Pel, K. Kopinga, *and* R. P. J. van Hees *(*2007*),* Salt transport in plaster/substrate layers, Mater. Struct., 40*(*5*),* 475–490.

Platt, J. C. *(*1999*), in* Advances in Kernel Methods: Support Kernel Machine, *edited by* B. Scholkopf, C. Burges, *and* A. J. Smola, *chap. 12, 185 pp., MIT Press*, Cambridge, Mass.

Prasad, A., D. Kumar, *and* D. V. Singh *(*2001*),* Effect of residual sodium carbonate in irrigation water on the soil sodication and yield of palmarosa (Cymbopogon martinni) and lemongrass (Cymbopogon flexuosus), Agric. Water Manage., 50*(*3*),* 161–172.

Prat, M. *(*2002*),* Recent advances in pore-scale models for drying of porous media, Chem. Eng. J., 86, 153–164, *doi:*10.1016/S1385-8947(01)00283-2.

Rodriguez-Navarro, C., *and* E. Doehne *(*1999*),* Salt weathering: Influence of evaporation rate, super saturation and crystallization pattern, Earth Surf. Processes Landforms, 24, 191–209.

Saravanapavan, T., *and* G. D. Salvucci *(*2000*),* Analysis of rate-limiting processes in soil evaporation with implications for soil resistance models, Adv. Water Resour., 23, 493–502.

Sarmadian, F., A. Keshavarzi, *and* A. Malekian *(*2010*),* Continuous mapping of topsoil calcium carbonate using geostatistical techniques in a semi-arid region, Aust. J. Crop Sci., 4*(*8*),* 603–608.

Scherer, G. W. *(*1990*),* Theory of drying, J. Am. Ceramic Soc., 73, 3–14.

Scherer, G. W. *(*2004*),* Stress from crystallization of salt, Cement Concr. Res., 34, 1613–1624.

Shahidzadeh-Bonn, N., S. Rafai, D. Bonn, *and* G. Wegdam *(*2008*),* Salt crystallization during evaporation: Impact of interfacial properties, Langmuir, 24, 8599–8605.

Shokri, N. *(*2014*),* Pore-scale dynamics of salt transport and distribution in drying porous media, Phys. Fluids, 26, 012106.

Shokri, N., *and* D. Or *(*2011*),* What determines drying rates at the onset of diffusion controlled stage-2 evaporation from porous media?, Water Resour. Res., 47, W09513, *doi:*10.1029/2010WR010284.

Shokri, N., P. Lehmann, *and* D. Or *(*2010*),* Liquid phase continuity and solute concentration dynamics during evaporation from porous media- pore scale processes near vaporization surface, Phys. Rev. E., 81, 046308.

Shokri, N., M. Sahimi, *and* D. Or *(*2012*),* Morphology, propagation dynamics and scaling characteristics of drying fronts in porous media, Geophys. Res. Lett., 39, L09401, *doi:*10.1029/2012GL051506.

Smits, K. M., V. V. Ngo, A. Cihan, T. Sakaki, *and* T. H. Illangasekare *(*2012*),* An evaluation of models of bare soil evaporation formulated with different land surface boundary conditions and assumptions, Water Resour. Res., 48, W12526, *doi:*10.1029/2012WR012113.

van Brakel, J. *(*1980*),* Mass transfer in convective drying, *in* Advances in Drying, *vol.* 1, *edited by* A. S. Mujumdar, *pp.* 217–267, *Hemisphere*, Washington, D. C.

Veran-Tissoires, S., M. Marcoux, *and* M. Prat *(*2012a*),* Discrete salt crystallization at the surface of a porous medium, Phys. Rev. Lett., 108, 054502.

Veran-Tissoires, S., M. Marcoux, *and* M. Prat *(*2012b*),* Salt crystallisation at the surface of a heterogeneous porous medium, Europhys. Lett., 98, 3400.

Yiotis, A. G., D. Salin, E. S. Tajer, *and* Y. C. Yortsos *(*2012*),* Drying in porous media with gravity-stabilized fronts: Experimental results, Phys. Rev. E, 86, 026310.

Chapter 5

Effects of Texture of Porous Media on Salt Precipitation during Evaporation: A Pore Scale Investigation

This chapter is a manuscript submitted to the Transport in Porous Media for possible publication. The objective of this paper is to investigate the effects of the texture of the porous media on the precipitation dynamics and patterns during evaporation. Six types of quartz sand different in particle size distribution (average grain size varying from 0.2 mm to 2.1 mm) were used to pack glass columns. All sand columns were saturated by 3 Molal sodium chloride solutions. The columns were left for natural evaporation and the 3D visualization was performed using X-ray micro-tomography during evaporation enabling us to investigate salt precipitation patterns as influenced by the texture of porous media in 4D. Obtained images were segmented and dynamics of evaporation and precipitation were delineated using the segmented images.

Results show that even though the evaporation rates are close in different samples, the precipitation patterns are significantly different, such that for samples with a larger average grain size, smaller surface area is covered by a thicker salt crust. This can be explained by analysing the pore size distribution of the porous media and localization of the preferential evaporation/precipitation sites. To estimate the average thickness of the salt crust, a simple equation is proposed and its performance is evaluated against experimental data. Findings of this paper extend our physical understanding of the salt precipitation in porous media during evaporation as influenced by the texture of porous media.

Effects of Texture of Porous Media on Salt Precipitation during Evaporation: A Pore Scale Investigation

Mansoureh Norouzi Rad[a], Nima Shokri[a], Amir Keshmiri[b], and Philip J. Withers[c]

[a]School of Chemical Engineering and Analytical Science, University of Manchester, Manchester, United Kingdom

[b]School of Engineering, Manchester Metropolitan University, Manchester, United Kingdom

[c]School of Materials, University of Manchester, Manchester, United Kingdom

Abstract

Salt precipitation in saline porous media during evaporation is important in many processes including CO_2 sequestration, soil salinity which is a global problem as well as the preservation of monuments and buildings. In this study, X-ray micro-tomography (CT) was used to investigate the evolution of salt precipitation during evaporation to study the effects of particle and pore sizes on salt precipitation patterns and dynamics. The packed beds were saturated with NaCl solution of 3 Molal and the time-lapse X-ray imaging was continued for one day to obtain pore scale information associated with the evaporation and precipitation dynamics and patterns. The results show that the presence of preferential evaporation sites (associated with fine pores) on the surface of the sand columns influences significantly the patterns and dynamics of NaCl precipitation. They confirm the formation of an increasingly thick and discrete salt crust with increasing grain size in the sand column due to the presence of fewer fine pores (preferential precipitation sites) at the surface compared to the sand packs with finer grains. Fewer fine pores on the surface also results in shorter stage-1 precipitation for the columns with larger grain sizes. A simple model for the evolution of salt crust thickness based on this principle shows a good agreement with our experiments. The findings of this study offer new insights about the dynamics and patterns of salt precipitation in drying porous media.

5.1 Introduction

Evaporation from saline porous media is important in many industrial and environmental processes including soil salinization (relating to the excess accumulation of salts in soil), food drying, the drying of porous building materials, and geological carbon storage (Farifteh *et al*., Zhao, *et al*., 2014, Kucuk *et al*., 2014, Fonseca and Scherer, 2014, Walters *et al*., 2014,

Bickle, 2009). The transportation and accumulation of salt in soil may adversely influence the plant growth, vegetation and crop production. The excess accumulation of salt in soil is a global problem and is one of the most widespread soil degradation processes in the world [Zhaoyong *et al*., 2014] thus it is important to understand the parameters and mechanisms controlling salt transport and precipitation patterns in porous media during evaporation.

During evaporation from porous media saturated with water, large pores at the surface are invaded by air at the early stages of the process, while smaller pores remain saturated due to the capillarity effects. The evaporative demand is supplied by the capillary-induced liquid flow transferring water toward the fine pores at the surface, the so-called stage-1 evaporation (van Brakel, 1975, Scherer, 1990). During this period, liquid vaporization occurs mainly in the smaller pores filled with water at the surface. Such a transport mechanism continues as long as the downward resisting gravity and viscous forces are less than the upward capillary force (Or *et al*., 2013, Shokri and Sahimi, 2012, Lehman *et al*., 2008).

In the presence of dissolved salt in the evaporating solution, the capillary induced liquid flow transports the solute towards the evaporation surface (convective transport), while diffusive transport tends to spread the salt homogenously in the porous medium affecting the salt distribution. This is explained by the dimensionless Peclet number which quantifies the competition between convective and diffusive transport. When the salt concentration exceeds its solubility limit, it precipitates. Depending on the value of the Peclet number, salt precipitation may occur on the surface (efflorescence) or below the surface (subflorescence) of the porous media (Huinink *et al*., 2002, Sghaier *et al*., 2014). Salt precipitation may affect the transport properties of porous media by changing the exterior or interior structures. Efflorescence alters the façade of the porous media (Espinosa-Marzal and Scherer, 2010) and may influence the liquid and vapour transport ability in porous media (Zahnge *et al*., 2014;

Mercury *et al*., 2014). On the other hand, subflorescence changes the pore structure inside the media forming an obstruction for the flow (Espinosa-Marzal and Scherer, 2013) and it may cause serious damages to the porous structures depending on the crystallization stress (Flatt *et al*., 2014). The present study is restricted to efflorescence.

There have been a number of studies on the physics of efflorescence and patterns of salt deposition on the surface of porous media which is influenced by several factors such as the environmental conditions, characteristics of the porous material and physicochemical properties of the salt and its concentration (Petković *et al*., 2007). Previous work suggests that efflorescence depends highly on the location of the preferential evaporation sites on the surface (Shokri and Or, 2013; Veran-Tissoires *et al*., 2012b; Nachshon *et al*., 2011). Norouzi Rad *et al*. (2013) established the direct association of the preferential efflorescence with the location of the fine pores on the surface acting as evaporating sites. These sites are actively engaged in evaporation, which leads to an increase in the salt concentration and eventually its precipitation. Using synchrotron X-ray tomography, Shokri (2014) illustrated the dynamics of dissolved salt distribution and the preferential increasing of solute concentration in finer pores on the surface of porous media during evaporation.

The majority of the previous experiments investigating efflorescence under different boundary conditions have been conducted at the macro-scale with the visualization of the precipitation patterns based on 2D evaporation surfaces (*e.g.* Norouzi Rad and Shokri, 2012; Veran-Tissoires *et al*., 2012a, 2012b; Eloukabi *et al*., 2013; Hidri *et al*., 2013). However, due to advances in 3D and time-lapse 3D imaging techniques, a few papers have begun to investigate the dynamics of evaporation from saline porous media in 3D (Shokri, 2014; Norouzi Rad and Shokri, 2014; Norouzi Rad *et al*., 2013; Nachshon *et al*., 2011). These have revealed the effects of parameters such as salt concentration, angularity of the grains and

structure of porous media on the salt transport and precipitation patterns. The specific objective of the present paper is to quantify the effects of the texture of porous media on salt transport and precipitation patterns by employing advanced time-lapse (4D) x-ray microtomographic imaging to investigate the physics and dynamics of this complex problem at the pore-scale.

5.2 Experimental Considerations

Six types of quartz sand each differing in particle size distribution were prepared by sieving. The average particle size of each sand sample was determined using a laser diffraction particle size analyzer (LS 13 320, Beckman Coulter, Germany). Table 5.1 presents the sieve sizes as well as the average particle size of each sand sample. Cylindrical glass columns 35 mm in height and 10 mm in diameter were used to pack sand grains saturated with 3 Molal reagent grade sodium chloride solutions following the procedure described in Grapsas and Shokri (2014). The resulting porosity of each sand pack computed from the measured 3D X-ray images is presented in Table 5.1. The sand columns were closed at all boundaries except for the top, which was kept open for natural evaporation.

X-ray micro-tomography was used to visualise the 3D dynamics and pattern of salt precipitation. Two rounds of experiments were carried out. In each round, the 'field of view' comprised only the top 25 mm of the sand columns. The first round was performed using sand samples with the average particle size of 0.20, 0.60, 1.0 and 2.10 mm with the spatial and temporal voxel size of 14^3 μm^3 and about 1 hour, respectively. The X-ray scanner was HMXST x-ray microtomography system and the scans were performed at 70 kV and 140 μÅ with 720 projections which took 25 minutes to acquire a 3D data set. The second round was carried out in a Nikon Custom Bay (at 100 kV and 200 μÅ with 1000 projections and 17

minutes per scan) using the sand samples with the average particle size of 0.85 and 1.40 mm with spatial and temporal voxel size of 16.7^3 μm^3 and 1 hour respectively. In each round, the sand columns were taped together and scanned at the same time as a bundle to ensure consistency in the atmospheric conditions. Typical virtual cross-sections of each sand sample are shown in Figure 5.1.

Table 5.1 Average particle size of each sand pack (measured by a laser diffraction particle size analyser) and the upper and lower limit of the sieve sizes used to prepare each sand sample.

Average particle size (mm)	0.20	0.60	0.85	1.0	1.4	2.1
Range of particle sizes (mm)	0.09-0.34	0.36-	0.71-	0.8-1.4	1.2-1.6	1.3-2.7
Average porosity	--	0.37	0.4	0.38	0.4	0.41

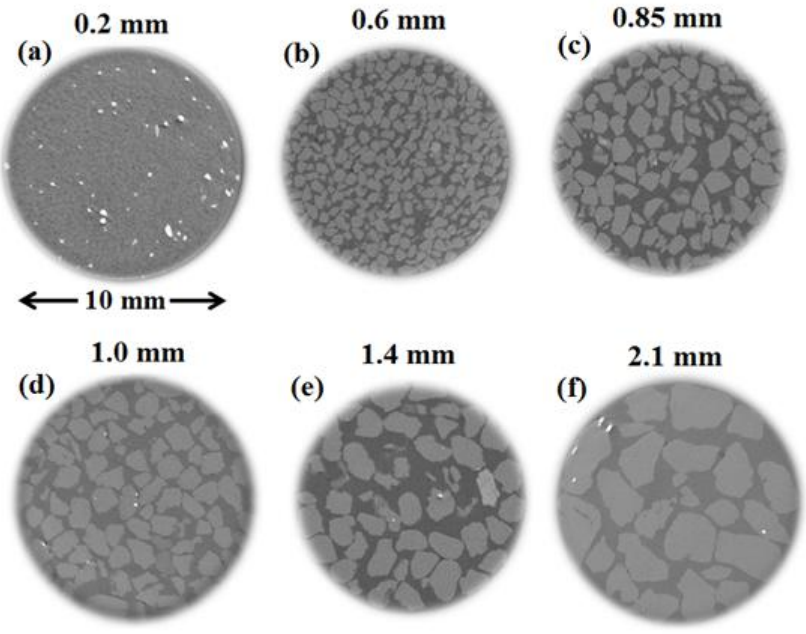

Figure 5.1 Typical virtual 2D horizontal cross-sections of the middle of each sand pack used in our experiments obtained by X-ray micro-tomography. The numbers indicate the average particle size of each sand sample.

To quantify the dynamics of evaporation as well as salt precipitation, the pore-scale X-ray images were analysed following the procedure used in Norouzi Rad *et al*. (2013) described briefly in the following. For quantifying the liquid phase distribution in the media, each 2D cross section was segmented into three distinct phases (solid, liquid and air). In order to do so, the standard machine learning technique of classification via Support Vector Machines (SVM) was used (Cortes and Vapnik, 1995). Each SVM was trained via a number of labelled examples (*i.e.* inputs with predetermined outputs) enabling it to predict the results for further inputs. For each pixel in the original images, its spatial coordinates and grey value were taken as discriminating features for the classifier and a quadratic kernel transformation was applied. For each column, we built two separate SVM classifiers, one to distinguish solid from non-solid and one to distinguish air from non-air; parts not classified as solid or air were deemed to be liquid. For the training, we used a selection of images segmented via determining a threshold manually and doing careful pre- and post-processing to ensure accuracy in the results. It is important to make sure that the SVM sees all three phases during training; but also over-fitting due to too many examples should be carefully avoided. The typical outcome of such a segmentation method was presented in Norouzi Rad and Shokri (2014) and so is not repeated here. The SVMs were trained using the Sequential Minimal Optimization (SMO) algorithm from MATLAB's machine learning package. More technical details on SMO can be found in Platt (1998). As for the quantification of the precipitated salt, segmentation was performed following the method described in Shokri and Sahimi (2012) to segment each image into two phases (solid and non-solid); the difference in the solid phase between each cross-section and its initial reference state (*i.e.* the image scanned at the onset of the experiment), represents the precipitated salt. Figure 5.2 demonstrates a typical visualisation of the surface of the sand column with the precipitated salt presented dark grey in Figure

5.2(c). The same algorithm was used to segment all the images enabling us to delineate the effects of the texture of porous media on salt precipitation patterns during evaporation.

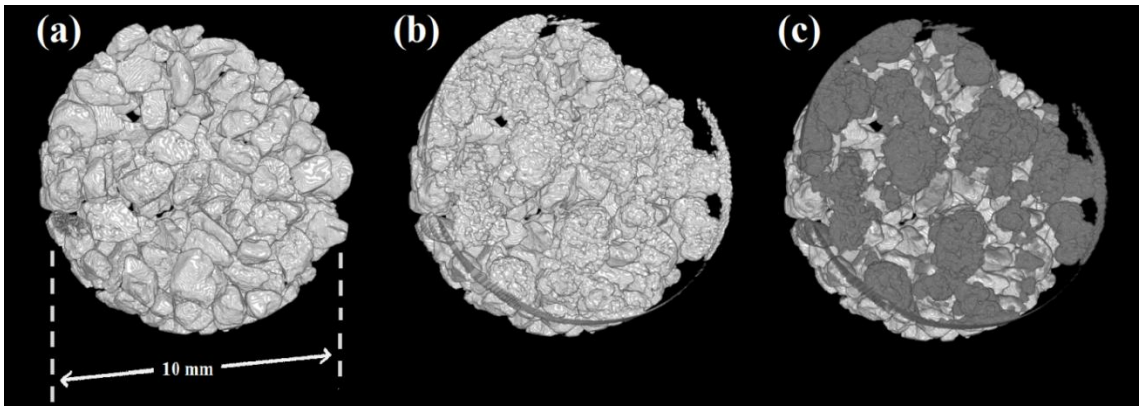

Figure 5.2 3D visualization of the solid phase close to the top of the column packed with sand grains with the average particle size of 0.85 mm at the onset of the evaporation experiment (a) and after 17 hrs from the onset of the experiment (b). The difference between (a) and (b) represents the precipitated salt and is delineated by the darker color in (c).

5.3 Results and Discussions

5.3.1 Evaporation rates

Using the segmented images we could quantify the evaporative mass losses from each sand column as well as the dynamics of the air and liquid phase distribution. The obtained results are presented in Figure 5.3 and 5.4, respectively. Note that due to the technical limitation, the quality of the images in the sample with the average particle size of 0.20 mm was not good enough to distinguish between the liquid and air phase, therefore, it was not possible to compute the evaporative mass losses from this particular column. The negligible mass loss from the sand column in the early stages (within the first ~2-3 hrs) in Figure 5.3 corresponds to the evaporation of ponding water above the surface of the columns (added at the beginning of the experiment to ensure the complete saturation condition in all sand columns). The difference among the evaporation rates from the sand columns (*i.e.* the gradient of the

cumulative mass loss curves) could have at least two explanations: a) we did not have control of the ambient temperature and relative humidity inside the X-ray chamber causing slight differences in the evaporative demand influencing the evaporation rate, b) due to different grain sizes used in our experiments, the empty space above the surface of each sand pack and the top of the column (which was filled by the ponding water at the beginning of the experiment) was slightly different affecting the diffusion length; consequently the evaporation rate (Schlunder, 1980; Yiotis *et al*., 2007; Shokri *et al*., 2008).

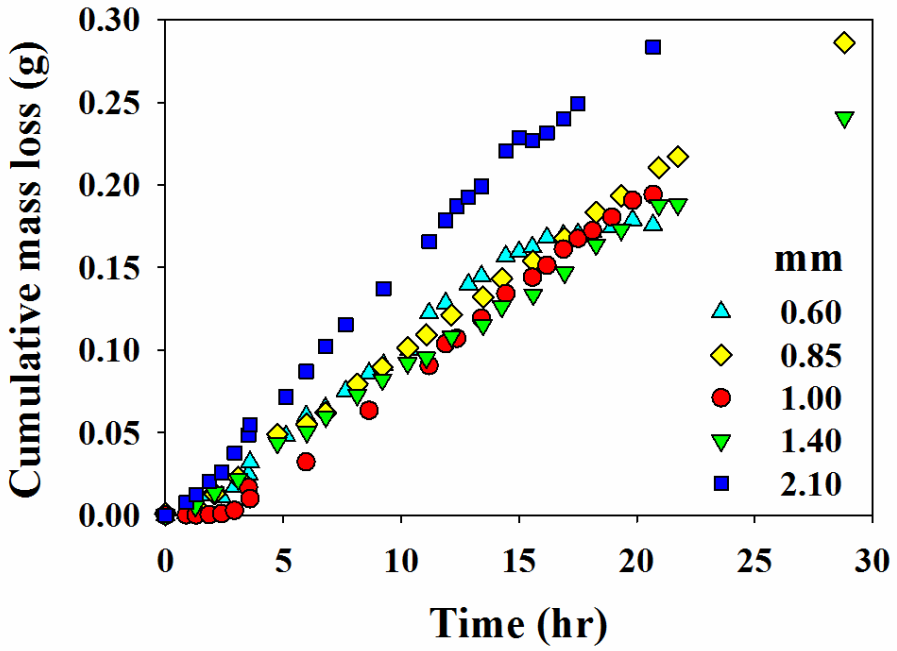

Figure 5.3 Evaporative mass loss from each sand pack computed from the segmented images. The legend shows the average grain size. The slope of the line indicates the evaporation rate.

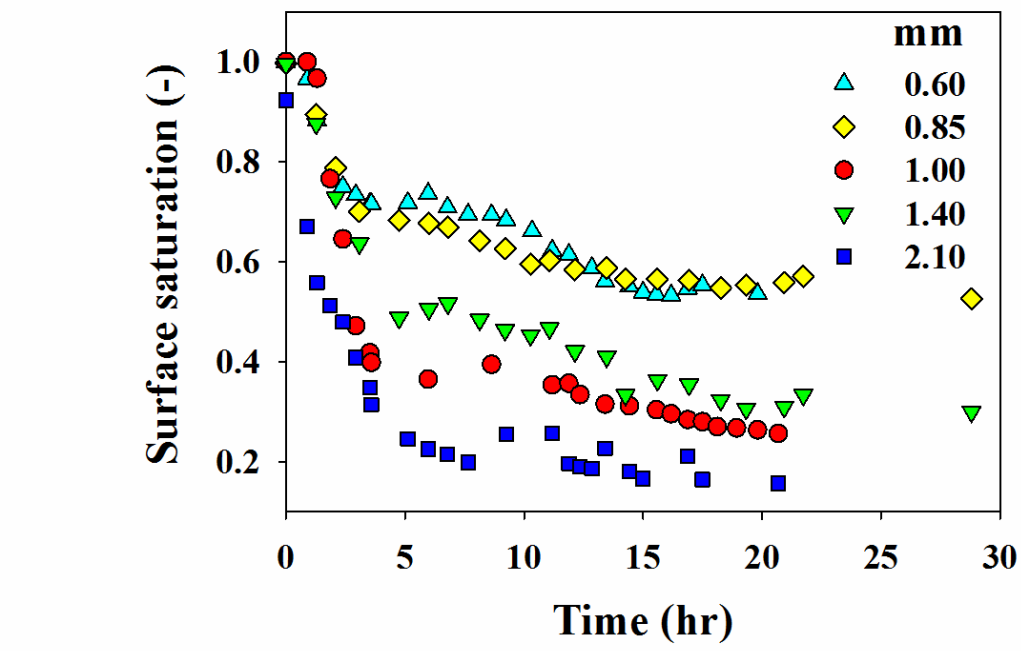

Figure 5.4 Water saturation profiles averaged over the top 1 mm of each sand pack. Presence of water at the surface even at the end of the experiments indicates stage-1 evaporation in all cases in our experiments. Legends show the average particle size of each sand pack.

The constant slope of the computed mass loss curves in Figure 5.3 indicates that in all cases the evaporation process was in stage-1 keeping the surface of the sand columns wet during the entire course of the experiments. However, there is a slight change in the gradient of the mass loss curve for the sand sample with the average particle size of 0.60 mm which is because of air breakthrough in the field of view that was considered for the image analysis (*i.e.* the top 25 mm of the sand column). Figure 5.4 further confirms that in all the sand columns the evaporation process remained in stage-1 because the computed water saturation profiles averaged over the top 1 mm of each sand column (referred to as the surface saturation) reveal that the surface of all sand samples remained wet throughout the entire duration of the experiments. This is an indication of stage-1 evaporation (Norouzi Rad and Shokri, 2014). Besides, Figure 5.4 shows that for any given time, as the average particle size increases, the surface saturation decreases. This is explained by the presence of fewer small

pores at the surface of the columns packed with larger grains. This results in the presence of fewer evaporation sites at the surface which are the pores filled with water located at the surface of porous media (Norouzi Rad and Shokri, 2014).

5.3.2 Precipitation dynamics

During stage-1 evaporation, as the solvent evaporates from the active evaporation sites at the surface, the solute concentration increases continuously in the preferential evaporation sites until it reaches the salt solubility limit (6.1 Molal at 25^{o}C). Figure 5.5 shows the cumulative salt precipitation computed using the 3D pore-scale images obtained by X-ray tomography during the evaporation process from each sand column. Since the experiments were run in two rounds (one round included the sand pack with the average particle size of 0.85 mm and 1.40 mm and the other one included all other sand packs), the corresponding precipitation dynamics are presented separately in Figure 5.5(a) and 5.5(b).

As already explained by Norouzi Rad *et al*. [2013] and Norouzi Rad and Shokri [2014], during evaporation each evaporation site may reach the precipitation state at a different time depending on its size and contribution to the evaporation. This phenomenon results in two stages in the precipitation rate as reflected in Figure 5.5. As long as new precipitation sites are arising, the precipitation rate will continue to increase due to the addition of new precipitation sites. We call this period the stage-1 precipitation period during which the precipitation rate increases despite the presence of a relatively constant evaporation rate. The increasing precipitation rate period will continue until all evaporation sites turn into precipitation sites marking the transition to the second stage of precipitation rate. During the second stage, if the process is in the stage-1 evaporation and the evaporation rate remains constant, the precipitation rate will remain constant as the constant evaporation rate leads to a constant rate of salt transport to the surface and precipitation.

The duration of the first stage of precipitation for different sand columns is presented in Figure 5.6. The result shows that as the particle size increases the duration of the stage-1 precipitation decreases. The columns packed with finer sand grains have more small pores (see Figure 5.7), therefore it takes longer for the surface to reach the salt solubility limit for all preferential evaporation sites therefore giving a longer stage-1 precipitation period.

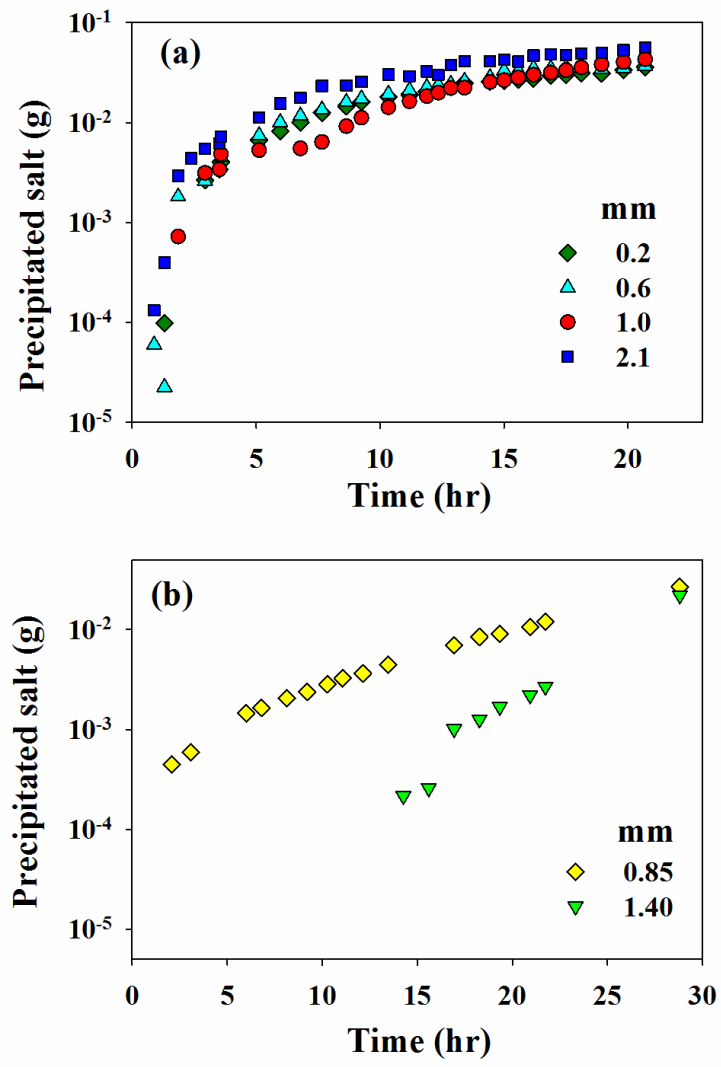

Figure 5.5 Dynamics of salt precipitation in each sand pack with the average particle sizes presented in the legend. Since the sand pack with the average particle size of 0.85 and 1.40 were in a separate round of experiments (hence different environmental conditions), they are presented separately in (b).

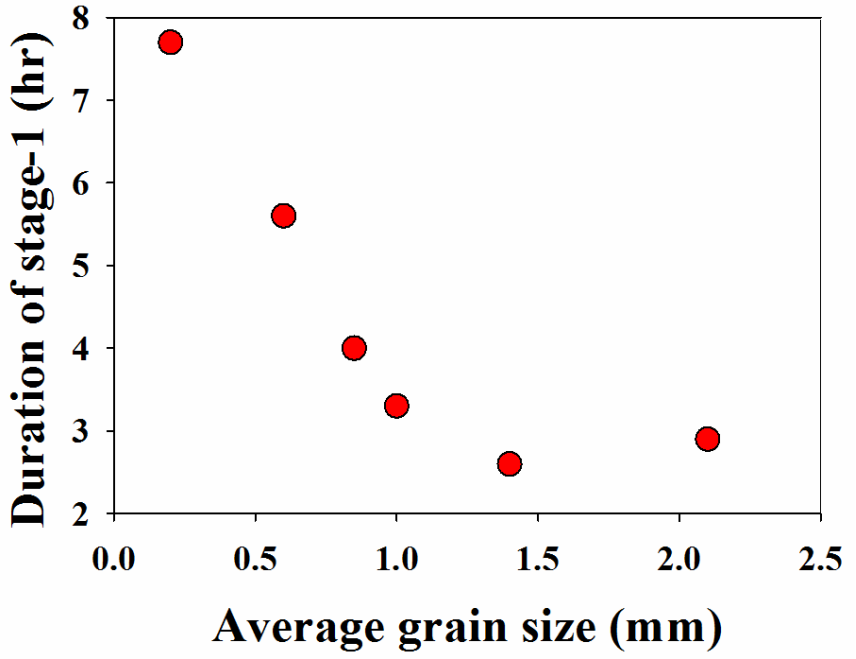

Figure 5.6 Duration of the stage-1 precipitation versus the average grain size. The presence of more evaporation sites on the surface of the columns packed with smaller sand grains extended the duration of the stage-1 precipitation.

To confirm the presence of more pores in the columns packed with smaller grains, the segmented 3D images obtained by X-ray tomography were used to determine the pore size distribution of each sand pack. To do so, we used The Network Extraction Code developed by Dong and Blunt (2009). The computed average pore sizes (μ), standard deviation (σ) of pore sizes, and the total number of the connected pores in the sand packs are presented in Figure 5.7. As mentioned above, the results show that the larger the average grain size of the sample, the fewer connected pores found in the porous media. Figure 5.7 also shows that the standard deviation of pore sizes in the sand packs used in our experiments increased as the average particle size increased.

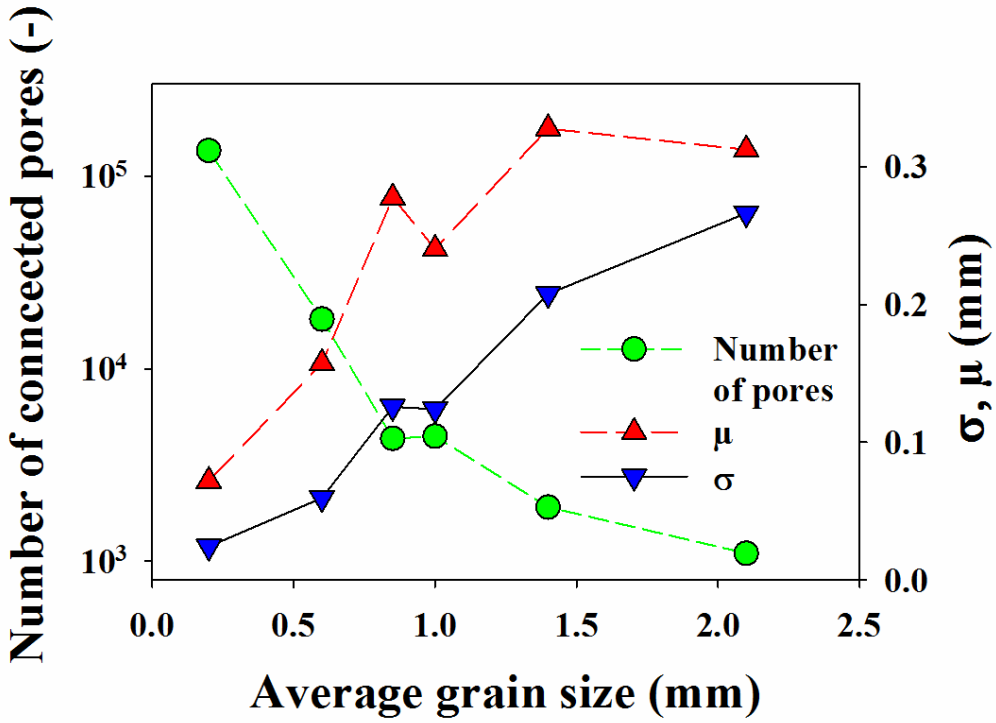

Figure 5.7 Number of the connected pores, mean (μ) and standard deviations (σ) of the pore diameters in each sand pack. This information was extracted from the 3D X-ray images.

According to Figure 5.6, the duration of stage-1 precipitation which is the result of a pore-scale phenomenon described above is relatively short compared to the processes simulated at the field-scale especially for larger particles. Therefore, for practical purposes or macro-scale numerical simulations, one may ignore such effects especially for larger particles for which stage-1 occurs only for the first ~2-3 hours of the experiment (Figure 5.6).

5.3.3 Salt Crust Thickness Influenced by the Grain and Pore Size of Porous Media

During evaporation when a certain amount of dissolved salt is transferred to the surface, the ions are distributed amongst the active evaporating and precipitating pores. Therefore, it is expected that with an increase in the average grain size, the thickness of the salt crust on the surface increases since there are fewer fine active pores on the surface (serving as preferential evaporation sites). Figure 5.8 shows qualitatively the thickness and patterns of salt crust for

the columns containing different average grain sizes. Note that in Figure 5.8 the cumulative amount of precipitated salt is the same in all cases (0.036 g) but the efflorescence patterns as well as the crust thickness is significantly different due to the differences in the pore size distributions of the sand packs used in our experiments. As illustrated in Figure 5.7, the sand pack with a larger grain size contains fewer pores. This results in the formation of thicker salt crust above the surface of the sand as shown qualitatively in Figure 5.8. However, the salt crust at the surface is more discrete as the particle size increases in contrast to the presence of a "crusty" efflorescence (Eloukabi *et al*., 2013) in the case of sand packs with smaller grain sizes. This is the result of the presence of fewer preferential evaporation (and consequently precipitation) sites at the surface of the sand packs with larger grain sizes (Norouzi Rad and Shokri, 2014).

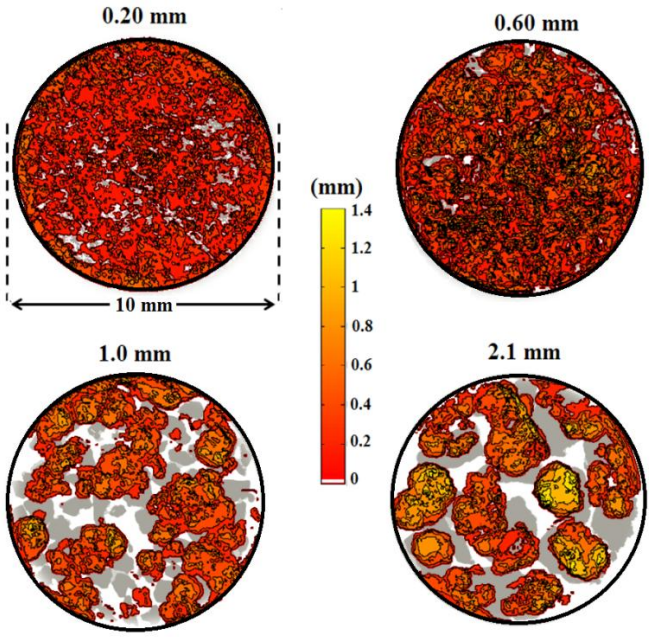

Figure 5.8 Precipitation patterns and salt distribution at the surface for the 0.2, 0.6, 1.0 and 2.1mm grain sized sand columns. The gray and white colour indicates the sand grains and air respectively. The colour bar indicates the thickness of the salt crust such that the brighter the colour, the thicker the salt crust. Note that the cumulative precipitation in all cases is 0.036 g but due to different pore size distributions the patterns of the precipitated salt are significantly different.

Figure 5.9 shows quantitatively the thickness of the salt crust as a function of the average particle size as well as the temporal evolution of the salt crust thickness during evaporation from each sand pack. Figure 5.9(b) shows that the rate of the increase in the salt crust thickness is higher in the sand pack with larger grain sizes leading to a more vertical growth. However, the lower rate in the sand pack with smaller grains leads to a more lateral growth of the salt crust as a result of the presence of more precipitation sites at the surface.

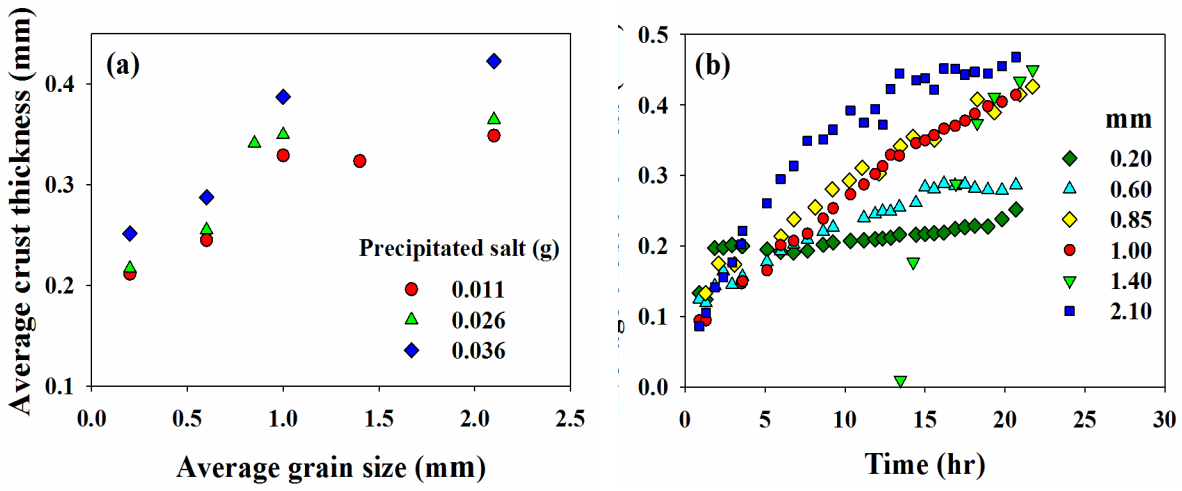

Figure 5.9 (a) Average thickness of the salt crust as a function of the average grain size. The legend indicates the computed cumulative water losses. Results show the formation of a thicker crust as the particle size increases (for the same cumulative mass loss) (b) Evolution of the thickness of salt crust at the surface over time. The legend indicates the average particle size in the column.

5.3.4 Estimation of the Salt Crust Thickness

As explained earlier, efflorescence occurs on the active pores at the surface which are those pores that remain saturated during the evaporation process. Such a phenomenon was previously shown in Shokri *et al*. (2010) and Norouzi Rad *et al*. [2013] using pore-scale images obtained by X-ray tomography thus it not repeated here. In the following, we provide

a relatively simple argument to estimate the evolution of the salt crust thickness over time. Immediately after the start of the experiments, the liquid saturation at the surface drops attaining a level that remains relatively constant as long as the evaporation remains in the stage-1 as illustrated in Figure 5.4. Using this constant surface saturation, the area at the surface saturated (occupied) by liquid phase can be estimated as $S\varepsilon A$ with S, ε and A representing the liquid saturation at the surface, porosity and the total surface area of the sand column, respectively. Dividing the area at the surface occupied by the liquid phase by the average area of a pore provides us with an estimation of the number of the pores participating in the precipitation. Additionally, at the pore-scale the precipitation initiates at the solid-air-liquid contact lines. The width of the precipitated salt $l(t)$ increases on the grain surface over time as evaporation proceeds. This is illustrated schematically in Figure 5.10(a). Following conservation of mass and representing the total mass of precipitated salt by M_s, one may estimate the average thickness of the salt crust ω over time as

$$\omega \sim \frac{M_s d}{S\rho_s \varepsilon l(t)} \tag{5.1}$$

where d is the average pore diameter and ρ_s is the precipitated salt density. The width of the crust on each grain may increase from zero to the diameter of the grain D. We propose the following equation to describe $l(t)$

$$l(t) = \mathrm{D}(1 - e^{-\tau t}) \tag{5.2}$$

where t indicates the time of precipitation and τ is a factor affecting the lateral spreading of the precipitated salt. In this study, we calculated the value of τ by fitting the measured experimental data to Eq. (1).

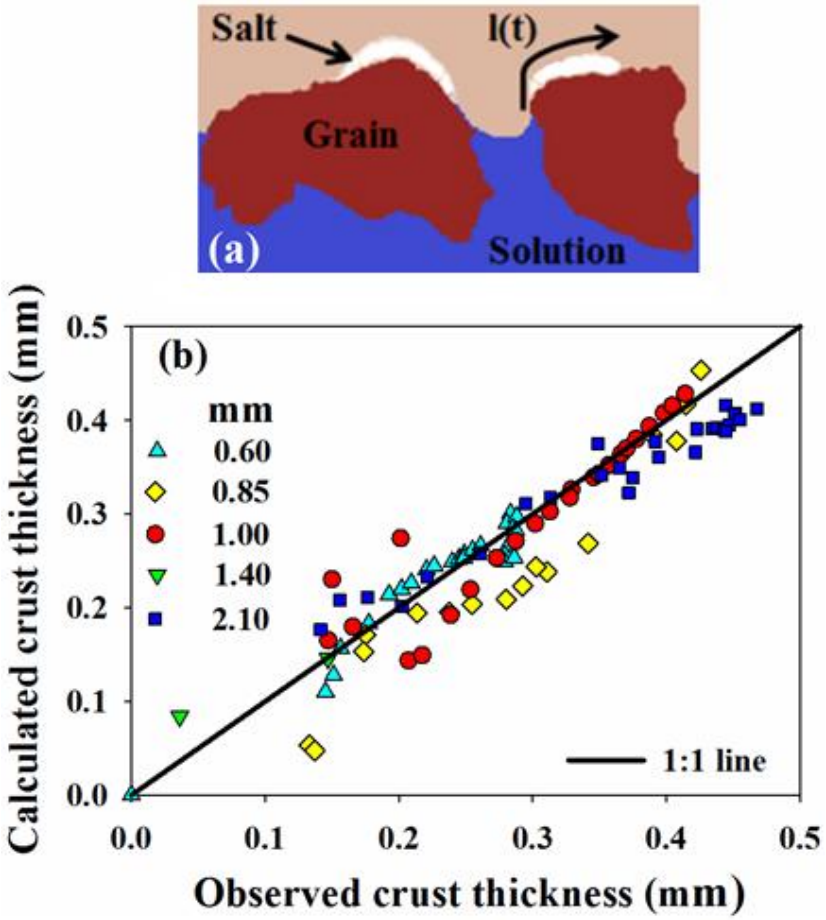

Figure 5.10 (a) A conceptual picture illustrating salt precipitation at the surface of the grains during evaporation into the air (pink) from porous media with the grain (dark red), evaporation solution (blue), and precipitated salt (white). Precipitation starts at the solid-liquid-air interface. As evaporation proceeds, the precipitation width of the salt $l(t)$ increase on the grain. (b) Estimated average thickness of the salt crust over time using Eq. (1) compared with the experimental data measured by X-ray micro-tomography. The legend indicates the average particle size of each sand pack.

The obtained τ values for each sand pack are presented in Table 5.2. The results in Table 5.2 reveals that the value of τ may not only be influenced by the particle size but also by the atmospheric conditions (influencing the evaporative demand) as the atmospheric conditions were not the same during the two rounds of experiments conducted in our study. The salt crust thickness measured experimentally and those calculated using Eq. (1) in each sand pack is compared in Figure 5.10(b). Note that the data from the sand sample with the average

particle size of 0.20 mm is not included in Figure 5.10(b) since the water saturation data was not available. It can be seen that the data are predominantly scattered around the 1:1 line, which shows a good correlation between the observed and estimated values of the crust thickness. Therefore, Eq. (1) may be considered as a promising method to describe the physics governing salt precipitation in drying porous media saturated with NaCl solution. The proposed equation is independent of the direct measurement of the evaporation rate since it only accounts for the amount of precipitation.

Table 5.2 The value of τ (with the unit of s^{-1}) in each sand sample obtained by fitting of the experimental data on Eq. (1).

Sample	τ (s^{-1})
0.60	0.016
0.85	0.003
1.00	0.024
1.40	0.006
2.10	0.034

5.4 Summary and Conclusions

X-ray micro-tomography (CT) has been used to investigate the pore-scale dynamics of the evaporation process for six sand columns having a systematic variation in particle sizes each saturated with NaCl solution enabling us to delineate the effects of grain and pore size of porous media on the efflorescence patterns. The results show that the presence of preferential evaporation sites on the surface of the porous media influences significantly the patterns and dynamics of NaCl precipitation at the surface of the sand columns. Our results confirm the formation of an increasingly thick and discrete salt crust with increasing grain size in the sand column due to the presence of fewer fine pores at the surface compared to the sand packs with finer grains. A simple equation is proposed to estimate the average thickness of the salt crust based on the pore size characteristic of the porous media. The estimated crust thickness

using the proposed equation is in a good agreement with the experimental data which supports the key role of the capillary-induced liquid flow toward the surface, vaporization in the fine pores at the surface and salt precipitation at preferential sites located at the surface of porous media. These results may be of particular interest in agricultural and industrial applications. For example the thicker salt crust on the surface is easier to be eroded by wind which may be of interest for agricultural practices in the arid and semi-arid areas or in preserving of buildings and monuments.

Acknowledgment

We express our gratitude to Dr. Siamak Tazari for his helpful discussion regarding the use of SVMs for the image processing, Prof. Martin Blunt for sharing the network extraction code developed in his group and Dr. Ali Q. Raeini for his help to run the code used to compute the pore size distribution using the X-ray images. We would like to thank Prof. Dani Or and Mr. Dani Breitenstein from EHT Zurich for enabling us to use their laser diffraction particle size analyzer. The X-ray micro-tomography experiments in HMXST x-ray microtomography system were performed at the Center for Nanoscale Systems (CNS) at Harvard University, a member of the National Nanotechnology Infrastructure Network (NNIN). We would like to acknowledge the assistance provided by the Manchester X-ray Imaging Facility to use the Nikon Custom Bay micro tomography system, which was funded in part by the EPSRC (grants EP/F007906/1, EP/F001452/1 and EP/I02249X/1). Acknowledgment is made to the donors of the American Chemical Society Petroleum Research Fund for partial support of this research (PRF No. 52054-DNI6).

References

Bickle, M.J: Geological carbon storage. Nat. Geosci. 2, 815-818 (2009)

Cortes, C., Vapnik, V.N.: Support-Vector Networks. Mach. Learn. 20, 273-297 (1995)

Dincer, I., Midilli, A., Kucuk, H.: Progress in Exergy, Energy, and the Environment. Springer (2014)

Dong, H, Blunt, M. J.: Pore-network extraction from micro-computerized-tomography images. Phys. Rev. E. 80, 036307 (2009)

Eloukabi, E., Sghaier, N., Ben Nassrallah, S., Prat, M.: Experimental study of the effect of sodium chloride on drying of porous media: The crusty–patchy efflorescence transition. Int. J. Heat Mass Transfer 56, 80-93 (2013)

Espinosa-Marzal, R.M., Scherer, G. W.: Mechanisms of damage by salt. Geol. Soc. Lon. 331, 61-77 (2010)

Espinosa-Marzal, R.M, Scherer, G. W.: Impact of in-pore salt crystallization on transport properties. Environ. Earth. Sci. 69, 2657–2669 (2013)

Farifteh J., Van der Meer, F., Atzberger, C., Carranza, E.J.M.: Quantitative analysis of salt-affected soil reflectance spectra: A comparison of two adaptive methods (PLSR and ANN). Remote Sens. Environ. 110 (1), 59–78 (2007)

Flatt, R. J., Caruso, F., Aguilar Sanchez, A. M., Scherer, G. W.: Chemomechanics of salt damage in stone. Nat. Com. 5823 (2014)

Fonseca, P.C., Scherer, G. W.: An image analysis procedure to quantify the air void system of mortar and concrete. Mater. Struct. 47, 10.1617/s11527-014-0381-9 (2014)

Grapsas, N., Shokri, N.: Acoustic characteristics of fluid interface displacement in drying porous media. Int. J. Multiphas. Flow 62, 30-36 (2014)

Hidri, F., Sghaier, N., Eloukabi, H., Prat, M., Ben Nasrallah, S.: Porous medium coffee ring effect and other factors affecting the first crystallisation time of sodium chloride at the surface of a drying porous medium. Phys. Fluids. 25, 127101 (2013)

Huinink, H. P., Pel, L., Michels, M. A. J.: How ions distribute in a drying porous medium: A simple model. Phys. Fluids 14, 1389 (2002)

Lehman, P., Assouline, S., Or, D.: Characteristic lengths affecting evaporative drying of porous media. Phys. Rev. E 77, 056309 (2008)

Nachshon U., Weisbrod, N., Dragila, M., Grader, A.: Combined evaporation and salt precipitation in homogeneous and heterogeneous porous media. Water Resour. Res. 47, W03513 (2011)

Norouzi Rad, M., Shokri, N.: Nonlinear effects of salt concentrations on evaporation from porous media. Geophys. Res. Lett. 39, L04403 (2012)

Norouzi Rad, M., Shokri, N.: Effects of grain angularity on NaCl precipitation in porous media during evaporation. Water Resour. Res. 50, 9020–9030, doi:10.1002/ 2014WR016125 (2014)

Norouzi Rad, M., Shokri, N., Sahimi, M.: Pore-Scale dynamics of salt precipitation in drying porous media. Phys. Rev. E 88, 032404 (2013)

Or, D., P. Lehmann, Shahraeeni, E., Shokri, N.: Advances in soil evaporation physics – a review. Vadose Zone J., vzj2012.0163 (2013)

Petković,J., Huinink, H.P., Pel, L., Kopinga, K.,Van Hees, R.P.J.: Salt transport in plaster/substrate layers. Mater. Struct. 40(5), 475-490 (2007)

Platt, J.C.: Advances in Kernel Methods: Support Kernel Machine. edited by B. Scholkopf, C. Burges, and A. J. Smola, MIT Press, Chap. 12, p. 185 (1999)

Prat, M.: Evaporation from a Porous Medium in the Presence of Salt Crystallization. NATO Science Peace Secur: Env. Sec. (8), 223-229 (2014)

Scherer, G. W.: Theory of drying. J. Am. Ceramic Soc. 73, 3 –14 (1990)

Schlunder, E.U.: On the mechanism of the constant drying rate period and its relevance to diffusion controlled catalytic gas phase reactions. Chem. Eng. Sci. 43, 2685-2688 (1988)

Sghaier, N., Geoffroy, S., Prat, M., Eloukabi, H., Ben Nasrallah, S.: Evaporation-driven growth of large crystallized salt structures in a porous medium, Phys. Rev. E. 90, 042402 (2014)

Shokri, N., Or, D., Drying patterns of porous media containing wettability contrasts, J. Colloid Interface Sci. 391, 135-141 (2013)

Shokri, N., Sahimi, M.: Structure of drying fronts in three-dimensional porous media. Phys. Rev. E. 85, 066312 (2012)

Shokri, N. Lehmann, P., Vontobel, P., Or, D.: Drying front and water content dynamics during evaporation from sand delineated by neutron radiography. Water Resour. Res. 44, W06418 (2008)

Shokri, N: Pore-scale dynamics of salt transport and distribution in drying porous media. Phys. Fluids. 26, 012106 (2014)

Veran-Tissoires, S., Marcoux, M., Prat, M., Discrete salt crystallization at the surface of a porous medium, Phys. Rev. Lett. 108, 054502 (2012a)

Veran-Tissoires, S., Marcoux, M., Prat, M., Salt crystallisation at the surface of a heterogeneous porous medium, Europhys. Lett. 98, 3400 (2012b)

Walters R. H., Bhatnagar, B., Tchessalov, S., Izutsu, K., Tsumoto, K., Ohtake, S.: Next Generation Drying Technologies for Pharmaceutical Applications. J. Pharm. Sci. 103, 2673–2695 (2014)

Yiotis, A.G., Tsimpanogiannis, I.N., Stubos, A.K., Yortsos, Y.C.: Coupling between internal and external mass transfer during drying of a porous medium. Water Resour. Res. 43, W06403 (2007)

Zahnge, C., Li, L., Lockington, D.: Numerical study of evaporation-induced salt accumulation and precipitation in bare saline soils: Mechanism and feedback. Water Resour. Res. 50, 2013WR015127 (2014)

Zhao, P., Ge, S., Ma, D., Areeprasert, C., Yoshikawa, K.: Effect of Hydrothermal Pretreatment on Convective Drying Characteristics of Paper Sludge. ACS Sustainable Chem. Eng. 2, 665−671 (2014)

Zhaoyong, Z., Abuduwaili J., Yimit H.: The Occurrence, Sources and Spatial Characteristics of Soil Salt and Assessment of Soil Salinization Risk in Yanqi Basin, Northwest China. PLoS ONE 9(9), e106079 (2014)

Chapter 6

Conclusions

The main objective of this thesis is to investigate the precipitation dynamics and patterns of sodium chloride in drying porous media. Precipitation dynamics during evaporation from porous media may be affected by several parameters such as salt concentration, environmental conditions, and physical characteristics of the media. In this work, the physics of salt precipitation was studied through the effects of the salt concentration, grain shapes and texture of the porous media.

It was shown that the presence of NaCl in the porous media during evaporation modifies the evaporation rate. NaCl begins to precipitate when the concentration on the surface exceeds the solubility limit of salt. The onset of precipitation may be estimated using the convection diffusion equation which shows a non-linear decreasing relation with the initial salt concentration, such that a higher initial salt concentration leads to an earlier salt precipitation at the surface. This was confirmed by the experiments.

The evolution of the area covered by the precipitated salt on the evaporating surface under various initial salt concentrations was investigated using the images taken from the surface of the saline porous media during evaporation. Results showed that the surface salt coverage rate can be described reasonably by a Gaussian distribution function. We have found that the maximum rate of lateral deposition of precipitated salt at the surface occurs at the end of stage-1 evaporation. This result offers a nondestructive method to investigate evaporation from saline porous media.

Following the macro-scale studies, a series of pore scale experiments were carried out to

investigate the salt precipitation dynamics and patterns in porous media during evaporation by visualizing the porous media in 3D using X-ray micro computed tomography imaging.

Using segmented pore scale images, solid, liquid and air phases in the porous media could be quantified in order to govern the dynamics and patterns of salt precipitation during evaporation.

It was observed that at early stages of the evaporation, larger pores on the surface are invaded preferentially by air while smaller pores remain saturated due to the higher capillarity followed by liquid vaporization exclusively in the fine pores. As the evaporation continues, NaCl concentration in the fine pores increases until it reaches the solubility limit when the precipitation starts. Since small pores at the surface contribute in evaporation depending on their sizes, evaporation sites at the surface do not reach the solubility limit at a same time causing a nonlinear behaviour in the precipitation rate. Therefore, precipitation of salt starts with an increasing rate as the evaporation sites turn into precipitation sites sequentially. Once all evaporation sites turned into precipitation sites, the precipitation rates remained relatively constant due to the relatively constant evaporation rate observed in our experiments.

The patterns of the salt precipitation are highly dependent on the pore size distribution of the porous media. Under same evaporation rates which result in the same amount of salt transferred to the surface, salt crust will be thicker and more discrete on the porous medium with fewer small active pores on the surface (serving as the preferential evaporation sites). Also, the transition in the precipitation rate takes place sooner in such medium. Therefore any factor affecting the pore size distribution may modify the salt precipitation pattern and average thickness of the crust on the surface of the porous media during evaporation. For example in two porous media, one consisting of angular grains and

the other of the spherical grains of the same average size, more small pores exists on the surface of medium consisting of the angular grains due to the grains' irregularity. Hence the salt crust on this medium will be thinner and more uniform compared to the medium with spherical grains. Or in the media with textural contrasts, the medium with the finer texture will have the smaller average crust thickness due to the presence of more fine pores on its surface.

A simple equation was proposed based on the physical characteristics of the porous media to estimate the average thickness of the salt crust on the surface. This equation is independent of the direct measurement of the evaporation rate since it only accounts for the amount of precipitation. The estimated values were in a good agreement with the experimental data.

The findings of this dissertation progress the physical understanding of NaCl precipitation patterns and dynamics in saline porous media during evaporation which is important in various hydrological and natural and industrial applications.

References

Bechtold, M., S. Haber-Pohlmeier, J. Vanderborght, A. Pohlmeier, T.P.A. Ferre, and H. Vereecken (2011), Near-surface solute redistribution during evaporation, Geophys. Res. Lett., 38 (17), L17404.

Bickle, M.J (2009), Geological carbon storage. Nat. Geosci., 2, 815-818. Chatterji, S (2000), A discussion of the paper "Crystallisation in pores" by G.W. Scherer, Cem. Concr. Res., 30, 669-671.

Clarke, E. C. W., and D. N. Glew (1985), Evaluation of the thermodynamic functions for aqueous Sodium Chloride from equilibrium and calorimetric measurements below 154 ^{o}C, J. Phys. Chem. Ref. Data, 14, 489-610.

Cortes, C., and V. Vapnik (1995), Support-vector networks, Mach. Learning, 20, 273-297.

Dincer, I., A. Midilli, H. Kucuk, (2014), Progress in Exergy, Energy, and the Environment. Springer.

Dong, H., and M. J. Blunt (2009), Pore-network extraction from micro-computerized-tomography images, Phys. Rev. E., 80, 036307.

Eloukabi, E., N. Sghaier, S. Ben Nassrallah, and M. Prat (2013), Experimental study of the effect of sodium chloride on drying of porous media: The crusty-patchy efflorescence transition, Int. J. Heat Mass Transfer, 56, 80-93.

Eloukabi, H., N. Sghaier, M. Prat, and S. B. Nassrallah (2011), Drying experiments in a hydrophobic model porous medium in the presence of a dissolved salt, Chem. Eng. Tech., 34, 1085-1094.

Espinosa-Marzal, R.M, G. W. Scherer (2008), Crystallization of sodium sulphate salts in limestone, Environ. Geol., 56, 605-621.

Espinosa-Marzal, R.M., A. Hamilton, M. McNall, K.Whitaker, and G. W. Scherer (2011), The chemomechanics of crystallization during rewetting of limestone impregnated with sodium sufate, J. Mater. Res., 26 (12) 1472-1481. Espinosa-Marzal, R.M, G. W. Scherer (2013), Impact of in-pore salt crystallization on transport properties. Environ. Earth. Sci. 69, 2657-2669.

Espinosa-Marzal, R.M., G. W. Scherer (2010), Mechanisms of damage by salt. Geol. Soc. Lon. 331, 61-77.

Farifteh J., F. Van der Meer, C. Atzberger, E. J. M. Carranza (2007), Quantitative analysis of salt-affected soil reflectance spectra: A comparison of two adaptive methods (PLSR and ANN). Remote Sens. Environ., 110 (1), 59-78.

Fisher, R. A. (1923), Some factors affecting the evaporation of water from soil, J. Agron. Sci., 13, 121-143.

Flatt, R. J. (2002), Salt damage in porous materials: How high supersaturations are generated, J. Cryst. Growth, 242, 435-454.

Flatt, R. J., F. Caruso, A. M. Aguilar Sanchez, G. W. Scherer (2014), Chemomechanics of salt damage in stone. Nat. Com., 5, 4823.

Fonseca, P.C., G. W. Scherer (2014), An image analysis procedure to quantify the air void system of mortar and concrete. Mater. Struct., 47, 10.1617/s11527-014-0381-9.

Grapsas, N., and N. Shokri (2014), Acoustic characteristics of fluid interface displacement in

drying porous media, Int. J. Multiphase Flow, 62, 30-36.

Guendouzi, M., and A. Mounir (2003), Water activity, osmotic and activitycoefficients of aqueous solutions of Li2SO4, Na2SO4, K2SO4, (NH4)2SO4, MgSO4, MnSO4, NiSO4, CuSO4, and ZnSO4 at T = 298.15 K, J. Chem. Thermodyn., 35(2), 209-220.

Guglielmini, L., A. Gontcharov, J. A. Aldykiewicz, and H. A. Stone (2008), Drying of salt solutions in porous materials: Intermediate-time dynamics and efflorescence, Phys. Fluids, 20, 077101.

Haghighi, E., E. Shahraeeni, P. Lehmann, and D. Or (2013), Evaporation rates across a convective air boundary layer are dominated by diffusion, Water Resour. Res., 49, 1602-1610.

Hidri, F., N. Sghaier, H. Eloukabi, M. Prat, S. Ben Nasrallah (2013), Porous medium coffee ring effect and other factors affecting the first crystallisation time of sodium chloride at the surface of a drying porous medium. Phys. Fluids., 25, 127101.

Huinink, H. P., L. Pel, and M. A. Michels (2002), How ions distribute in a drying porous medium: A simple model, Phys. Fluids, 14, 1389-1395.

Il'ichev, A. T., G. G. Tsypkin, D. Pritchard, and C. N. Richardson (2008), Instability of the salinity profile during the evaporation of saline groundwater, J. Fluid Mech., 614, 87-104.

Jardine, A., P. Speldewinde, S. Carver, and P. Weinstein (2007), Dryland salinity and ecosystem distress syndrome: Human health implications, EcoHealth, 4, 10-17.

Kowalski, S. J. (2000), Toward a thermodynamics and mechanics of drying processes, Chem. Eng. Sci., 55, 1289-1304.

Lehmann, P., S. Assouline, and D. Or (2008), Characteristic lengths affecting evaporative drying of porous media, Phys. Rev. E, 77, 056309.

Lightstone, J. M., T. B. Onasch, T. B., D. Imre (2000), Deliquescence, Efflorescence, and Water Activity in Ammonium Nitrate and Mixed Ammonium Nitrate/Succinic Acid Microparticles. J. Phys. Chem. A., 104, 9337-9346 (2000)

Liu, X. Y. (2000), Heterogeneous nucleation or homogeneous nucleation?, J. Chem. Phys. 112, 9949.

McCabe, W. L., J. C. Smith, and P. Harriott (2004), Unit Operations of Chemical Engineering, McGraw Hill, New York.

Nachshon, U., E. Shahraeeni, D. Or, M. Dragila, and N. Weisbrod (2011a), Infrared thermography of evaporative fluxes and dynamics of salt deposition on heterogeneous porous surfaces, Water Resour. Res., 47, W12519.

Nachshon, U., N. Weisbrod, M. Dragila, and A. Grader (2011b), Combined evaporation and salt precipitation in homogeneous and heterogeneous porous media, Water Resour. Res., 47, W03513.

Nassar, I. N., and R. Horton (1989), Water transport in unsaturated non-isothermal salty soil: II. Theoretical development, Soil Sci. Soc. Am. J., 53, 1330-1337.

Nassar, I. N., and R. Horton (1999), Salinity and compaction effects on soil water evaporation and water and solute distributions, Soil Sci. Soc. Am. J., 63, 752-758.

Nissan, A. H., W. G. Kaye, and J. R. Bell (1959), Mechansim of drying thick porous bodies during the falling rate period, A.I.Ch. E. J., 5, 103-110.

Norouzi Rad, M., and N. Shokri (2012), Nonlinear effects of salt concentrations on evaporation from porous media, Geophys. Res. Lett., 39, L04403.

Norouzi Rad, M., N. Shokri (2014), Effects of grain angularity on NaCl precipitation in porous media during evaporation. Water Resour. Res., 50, 2014WR016125.

Norouzi Rad, M., N. Shokri, and M. Sahimi (2013), Pore-scale dynamics of salt precipitation in drying porous media, Phys. Rev. E, 88, 032404.

Or, D., P. Lehmann, E. Shahraeeni, and N. Shokri (2013), Advances in soil evaporation physics—A review, Vadose Zone J., 12(4).

Pel, N., H. Huinink, and K. Kopinga (2002), Ion transport and crystallization in inorganic building materials as studied by nuclear magnetic resonance, Appl. Phys. Lett.,81, 2893.

Pel., L and T. A. Saidov, The thermodynamic and poromechanic crystallization pressure of sodium sulfate heptahydrate: an NMR study, Proceedings 5th Biot conference on pormechanics, Vienna, July 10-13, 2013

Petković, J., H. P. Huinink, L. Pel, K. Kopinga, and R. P. J. van Hees (2007), Salt transport in plaster/substrate layers, Mater. Struct., 40(5), 475-490.

Pitzer, K. S., J. C. Peiper, and R. H. Busey (1984), Thermodynamic properties of aqueous sodium chloride solutions, J. Phys. Chem. Ref. Data, 13,1-102.

Platt, J. C. (1999), in Advances in Kernel Methods: Support Kernel Machine, edited by B. Scholkopf, C. Burges, and A. J. Smola, chap. 12, 185 pp., MIT Press, Cambridge, Mass.

Prasad, A., D. Kumar, and D. V. Singh (2001), Effect of residual sodium carbonate in

irrigation water on the soil sodication and yield of palmarosa (Cymbopogon martinni) and lemongrass (Cymbopogon flexuosus), Agric. Water Manage., 50(3), 161-172.

Prat, M. (2002), Recent advances in pore-scale models for drying of porous media, Chem. Eng. J., 86, 153-164.

Prat, M. (2014), Evaporation from a Porous Medium in the Presence of Salt Crystallization. NATO Science Peace Secur: Env. Sec., 8, 223-229.

Rodriguez-Navarro, C., and E. Doehne (1999), Salt weathering: Influence of evaporation rate, super saturation and crystallization pattern, Earth Surf. Processes Landforms, 24, 191-209.

Sahimi, M. (1993), Flow phenomena in rocks: from continuum models to fractals, percolation, cellular automata, and simulated annealing, Rev. Mod. Phys. 65, 1393.

Saravanapavan, T., and G. D. Salvucci (2000), Analysis of rate-limiting processes in soil evaporation with implications for soil resistance models, Adv. Water Resour., 23, 493-502.

Sarmadian, F., A. Keshavarzi, and A. Malekian (2010), Continuous mapping of top soil calcium carbonate using geostatistical techniques in a semi-arid region, Aust. J. Crop Sci., (8), 603-608.

Scherer, G. W. (1990), Theory of drying, J. Am. Ceram. Soc., 73,3-14.

Scherer, G. W. (1999), Crystallization in pores, Cem. Concr. Res.,29,1347-1358.

Scherer, G. W. (2004), Stress from crystallization of salt, Cem. Concr. Res., 34, 1613-1624.

Schiro, M., E. Ruiz-Agudo, and C. Rodriguez-Navarro (2012), Damage mechanisms of porous materials due to in-pore salt crystallization, Phys. Rev. Lett., 109, 265503.

Schlunder, E.U. (1998), On the mechanism of the constant drying rate period and its relevance to diffusion controlled catalytic gas phase reactions. Chem. Eng. Sci., 43, 2685-2688.

Sghaier, N., M. Prat (2009), Effect of efflorescence formation on drying kinetics of porous media, Transport Porous Med., 80 (3), 441-454.

Sghaier, N., S. Geoffroy, M. Prat, H. Eloukabi, S. Ben Nasrallah (2014), Evaporation-driven growth of large crystallized salt structures in a porous medium, Phys. Rev. E., 90, 042402.

Shahidzadeh-Bonn, N., S. Rafai, D. Bonn, and G. Wegdam (2008), Salt crystallization during evaporation: Impact of interfacial properties, Langmuir, 24, 8599-8605.

Shimojimaa, E., R. Yoshika, and I. Tamagawa (1996), Salinization owing to evaporation from bare-soil surfaces and its influences on the evapora-tion, J. Hydrol.,178, 109-136.

Shokri, N. (2014), Pore-scale dynamics of salt transport and distribution in drying porous media, Phys. Fluids, 26, 012106.

Shokri, N., D. Or, (2013), Drying patterns of porous media containing wettability contrasts, J. Colloid Interface Sci., 391, 135-141.

Shokri, N., and D. Or (2011), What determines drying rates at the onset of diffusion controlled stage-2 evaporation from porous media?, Water Resour. Res., 47, W09513.

Shokri, N., G. D. Salvucci (2011), Evaporation from Porous Media in the Presence of a Water Table, Vadose Zone J., 10 (4), 1309-1318.

Shokri, N., P. Lehmann, and D. Or (2010), Liquid phase continuity and solute concentration dynamics during evaporation from porous media- pore scale processes near vaporization surface, Phys. Rev. E., 81, 046308.

Shokri, N., P. Lehmann, P. Vontobel, and D. Or (2008), Drying front and water content dynamics during evaporation from sand delineated by neutron radiography, Water Resour. Res., 44, W06418.

Shokri, N., M. Sahimi, and D. Or (2012), Morphology, propagation dynamics and scaling characteristics of drying fronts in porous media, Geophys. Res. Lett., 39, L09401.

Smith, J. M., H. C. Van Ness, and M. M. Abbott (2004), Introduction to Chemical Engineering Thermodynamics , McGraw-Hill, New York.

Smits, K. M., V. V. Ngo, A. Cihan, T. Sakaki, and T. H. Illangasekare (2012), An evaluation of models of bare soil evaporation formulated with different land surface boundary conditions and assumptions, Water Resour. Res., 48, W12526.

Tsui, N., R. J. Flatt, G. W. Scherer (2003), Crystallization damage by sodium sulphate, J. Cult. Herit., 4, 109-115.

Van Brakel, J. (1980), Mass transfer in convective drying, in Advances in Drying, vol. 1, edited by A. S. Mujumdar, pp. 217-267, Hemisphere, Washington, D. C.

Van der Heiden, G. H. A., R. M. W. van Bijnen, L. Pel, and H. P. Huinink, Moisture transport in heated concrete, as studied by NMR, and its consequences for fire

spalling, Cement Concr. Res., 37 (6), 894-906.

Veran-Tissoires, S., M. Marcoux, and M. Prat (2012a), Discrete salt crystallization at the surface of a porous medium, Phys. Rev. Lett., 108, 054502.

Veran-Tissoires, S., M. Marcoux, and M. Prat (2012b), Salt crystallisation at the surface of a heterogeneous porous medium, Europhys. Lett., 98, 3400.

Veran-Tissoires, S., and M. Prat (2014), Evaporation of a sodium chloride solution from a saturated porous medium with efflorescence formation, J. Fluid Mech., 749, 701-749.

Walters R. H., B. Bhatnagar, S. Tchessalov, K. Izutsu, K. Tsumoto, S. Ohtake (2014), Next Generation Drying Technologies for Pharmaceutical Applications. J. Pharm. Sci., 103, 2673-2695.

Yiotis, A. G., A. G. Yiotis, A. G. Boudouvis, A. K. Stubos, I. N. Tsimpanogiannis, and Y. C. Yortsos (2004), Effect of liquid films on the drying of porous media, A. I. Ch. E. J., 50 (11), 2721-2737.

Yiotis, A. G., D. Salin, E. S. Tajer, and Y. C. Yortsos (2012), Drying in porous media with gravity-stabilized fronts: Experimental results, Phys. Rev. E., 86, 026310.

Yiotis, A.G., I. N. Tsimpanogiannis, A.K. Stubos, Y. C. Yortsos (2007) Coupling between internal and external mass transfer during drying of a porous medium. Water Resour. Res., 43, W06403.

Zahnge, C., L. Li, D. Lockington (2014), Numerical study of evaporation-induced salt accumulation and precipitation in bare saline soils: Mechanism and feedback. Water Resour. Res., 50, 2013WR015127

Zhao, P., S. Ge, D. Ma, C. Areeprasert, K. Yoshikawa (2014), Effect of Hydrothermal Pretreatment on Convective Drying Characteristics of Paper Sludge. ACS Sustainable Chem. Eng., 2, 665−671.

Appendix A

Numerical Solution of the Convection Diffusion Equation

To determine the onset of precipitation using Convection Diffusion Equation (CDE) in both chapters 2 and 3, we solve the CDE assuming a 1-D vertical solute transport to find the profile of concentration on the surface of the porous medium knowing that based on the Peclet numbers which are greater than 1, the precipitation will happen on the surface in form of efflorescence. We assume that the time the concentration passes the solubility limit as the onset of precipitation (assuming small super saturation).

The CDE with a 1D vertical transport will be:

$$\frac{\partial(\rho\varepsilon SC)}{\partial t} = \frac{\partial}{\partial z}(\rho\varepsilon SD^{*}\frac{\partial C}{\partial z}\rho\varepsilon SCU) \qquad (A.1)$$

with C(z, t) the mass fraction of salt, ε the porosity, D* the effective diffusion coefficient of solute in porous media, ρ the density of the solution, z the depth below surface, U the average velocity of the liquid, t the time, and S the saturation.

Tt the boundaries, we assumed that the diffusive and convective fluxes are balanced, i.e., $UC - D^{*}\frac{\partial C}{\partial z} = 0$ at z = 0, L (L is the length of the column). We assumed negligible change in water saturation through the space, and also since the initial precipitation takes place during stage-1 evaporation, as a first order of approximation, we estimated the velocity term in the CDE by averaging the measured evaporation rate during stage-1 evaporation. Temporal change in liquid saturation is accounted as $S = 1 - \frac{e}{\rho L\varepsilon}$.

With the mentioned assumptions, we are able to solve the CDE which is a partial differential equation, using a first order one-sided finite difference method. If $\omega = C\varepsilon$ then the discretization of the problem will be

$$\omega_n^{i+1} = \omega_n^i + \frac{\Delta t}{b}\left(J_{n,n+1}^i - J_{n-1,n}^i\right) \qquad (A.2)$$

and

$$J_{n,n+1}^i = -\frac{D}{b}\left(\omega_n^i - \omega_{n+1}^i\right) + U_{n+1}^i \omega_{n+1}^i \qquad (A.3)$$

b is the parameter representing the length of each grid (i.e. distance between two points), superscripts (i and i+1) show the change in time, Δt is the time step. For the nodes on the boundaries: $n = 0$ and $n = m J_{-1,0}^i = J_{m,m+1}^i = 0$.

In order to have convergence in the results, parameter b should be chosen in a way that $\frac{b}{L} \ll 1$. More detailed solution can be find in Huinink et al., [2002]. The discretization in equations A.1 and A.2 were solved in MATLAB to find the distribution of solute concentration on the surface. Another outcome of the code could be the distribution of the solute through the porous media. The script written to solve this equation is presented in the following.

```
clear;
close all;
%
concen=[0.1 0.5 0.75 1 1.5 2 2.5 3 3.5];
hc=[3.50 4.1 3.2 3.12 3.6 2.82 2.41 2.38 3.03];
time=[30000 560000 400000 350000 180000 200000 190000 110000 90000];
rhoo=[0.9928 1.014025 0.997157757 1.024293746 1.05325 1.034212008
1.071290106 1.088411123 1.104680801];
Pe=[1.713992933 1.885489086 1.44652257 1.167428936 1.587220097 1.139114238
1.444283455 1.276887075 1.166307092]
for ii=5

D=0.000000001;
l=0.034;
b=l*0.005;
%dz/L=5*10^(-3)
dz=5*10^(-5);
%Ddt/b^2<0.5, dt=Delta t(s)
dt=2.9/5*0.5*dz.*dz./D;
%porosity
e=0.4;
% z=0:dz:l;
t=time(ii);   % 900000;
%Pe=1.77;
%h evaporation rate
% h=Pe(ii)*D*e/l;
rho= rhoo(ii)*1000; %density
h=hc(ii)/24/3600/1000; %h=3.026553497/rho/24/3600;
% ts=t/dt;
% zs=l/dz;
%t/dt=49200&l/dz=200
n=ceil(t/dt);
ro=zeros(201,n+1,'single');
%velocity
%u=zeros(201,n+1);
C0=concen(ii);%C0=3;%molality
M=58.443; % gr/mol
%ro(i,j+1)=ro(i,j+(dt/b)*((-(D/b)*(ro(i,j)+u(i+1,j)*ro(i+1,j))-(-
(D/b)*(ro(i-1,j)+u(i,j)*ro(i,j)))));
% for i=1:201
%     for j=1:n+1
%         u(i,j)=abs(h./(l*e-h.*(j-1).*dt).*((i-1).*dz-l));
%     end;
% end;
%u=abs(u);
cpercent=single(100*C0*M/(1000+C0*M));
ro(:,1)=single(cpercent*1000*0.4*0.35/100);
for j=1:n
    ro(1,j)=single(ro(2,j)/(1-h*l*dz/(D*(e*l-h*(j-1)*dt))));
    ro(201,j)=single(ro(200,j));
    for i=2:200
            uij=single(abs(h/(l*e-h*(j-1)*dt)*((i-1)*dz-l)));
            uipj=single(abs(h/(l*e-h*(j-1)*dt)*(i*dz-l)));
            %ro(i,j+1)=ro(i,j)+dt./dz*((-D./dz*(ro(i,j)-
ro(i+1,j))+u(i+1,j).*ro(i+1,j))-(-D./dz.*(ro(i-1,j)-
ro(i,j))+u(i,j).*ro(i,j)));
            ro(i,j+1)=ro(i,j)+dt/dz*((-D/dz*(ro(i,j)-
ro(i+1,j))+uipj*ro(i+1,j))-(-D/dz*(ro(i-1,j)-ro(i,j))+uij*ro(i,j)));
    end;
end;
```

```
for j=1:n
    i=ro(2,j)/1000/.4/.35;
    C(j)=i*1000*100/(100-100*i)/58.44;
end;
figure;
plot(C);
title(concen(ii));
ylim([concen(ii) 6.15]);
end
```

Appendix B

Support Vector Machines (SVMs) as a Tool for Image Segmentation

Support Vector Machines or SVMs is a classification (and/or regression) algorithm in Machine Learning. This algorithm tends to classify the data using linear dividing systems. For example if two sets of data as in Figure B.1 is given, the line AB could be used to divide the data into two distinguished sets.

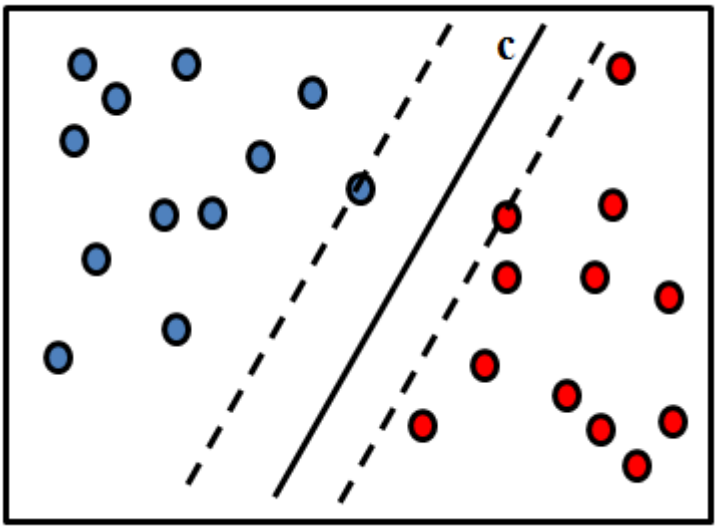

Figure B.1 Basic schematic presentation of a linear SVM with the dividing hyperplane (line c) and supporting hyperplanes (dash lines). Data points fallen on the supporting hyperplanes are support vectors.

In Figure B.1 the dividing line c (solid line) is called a hyperplane, dash lines are the supporting hyperplanes (parallel to the dividing hyperplane) and the data points fallen on the supporting hyperplanes are the support vectors which generally we are interested in finding. Depending on the problem, the distance between the dividing and supporting hyperplanes is

an optimization problem which determines how many support vectors are allowed to be fallen in the area between the two supporting hyperplanes. If dividing the data sets is not possible by one straight line (Figure B.2) then the data will be mapped to the space (Kernelling) using the function φ which is a Kernel function so a suitable hyperplane (plane C) can be found for classification.

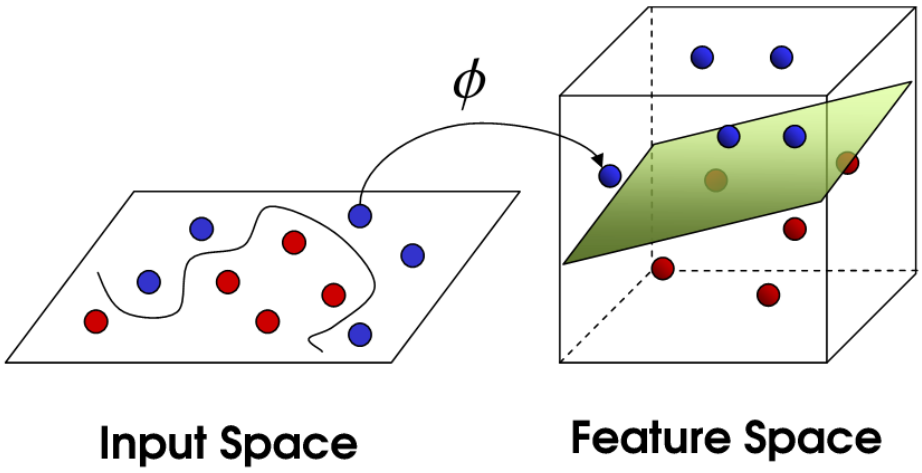

Figure B.2 To solve a non-linear SVM problem, it will be mapped to a space using a function (Kernel), here φ, so that the hyperplane could be find as a plane (here plane C).

Using different data sets (training sets) with specified characterization (for example color in this case), we will be able to train the machine so it learns how to classify the new set of data without knowing which category each point falls to. In this thesis however, the SVM algorithm was not developed from the scratch but it was used through the MATLAB Machine Learning toolbox. The method and parameterization is explained in the followings.

The problem in our case is to segment the 2D grayscale cross sections to an image with three distinguished phases of solid, liquid and gas. Ideally this would be possible using open source softwares such as Image-J or using thresholding, where the minimums in the gray value

histogram are found to separate three distinguished peaks or regions of phases (Figure B.3). However depending on the quality of scanning which changes by the quality of the machine and change in the surrounding of the object (as the energy received by the object is constant), the minimums may not be as easy to determine and there might be many local minimums which make the segmentation subjective to human errors. Using SVMs on the other hands, machine learns about the segmentation by seeing samples of original and segmented images and learning how to segment a new image.

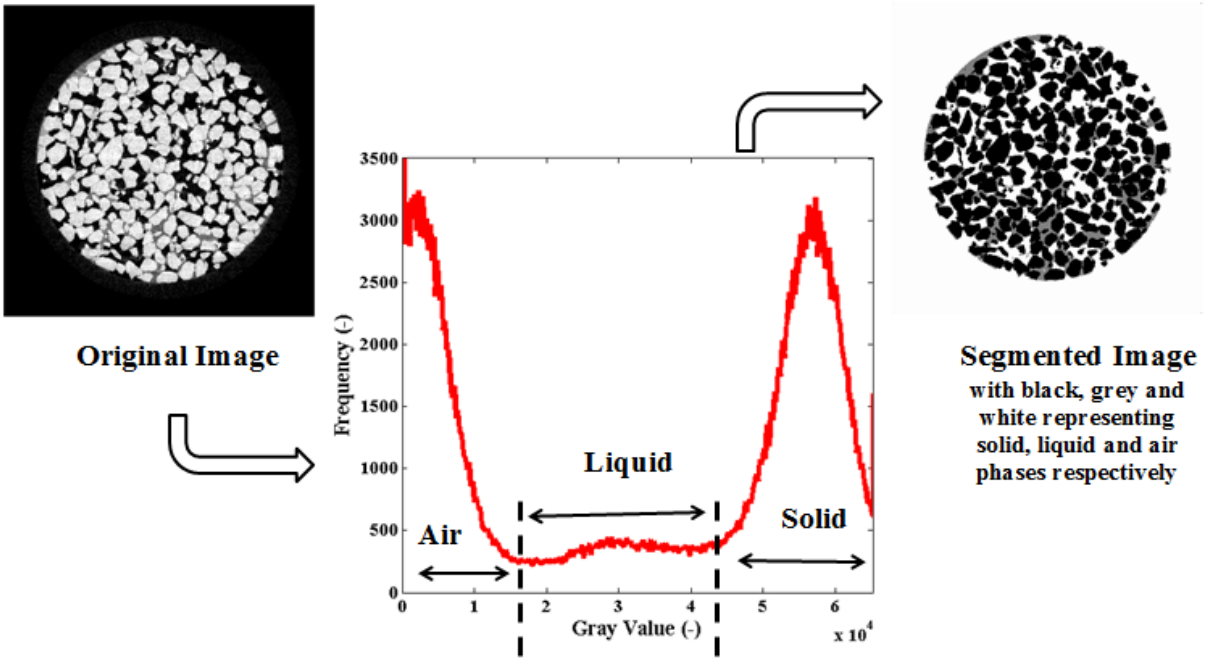

Figure B.3 General process of image segmentation based on gray value histogram. In this case, histogram shows two distinguished minimums so the phases could be easily distinguished. If too many local minimum exist in the histogram, separating the zone for each phase would be more challenging.

For training set, we feed the code with about 1% of the whole data set. To do that we segment a handful images manually (this can be done via ImageJ). The quality of the segmented image should be the best, all the required pre-processing and post-processing may be applied

for this segmentation but the outcome should be the most perfect segmentation possible. These segmented images along with their original gray scale image (without any processing) will be then be fed to the code. The parameters that can be seen and compared for the classification are the coordinates of a pixel (i.e., the location on the 2D cross section and the number of the cross section along the column which shows the depth) and its gray value.

Using these information we try to make two classifiers for air and solid such that, the machine decides a pixel is air or non-air, and solid or non-solid which leaves the pixel of non-air and non-solid as the liquid. When the training process is over, using the classifiers we can segment the new set of un-segmented images. The kernel function used in this method was a polynomial kernel and the optimization method was sequential minimal optimization (SMO). The detailed code which was written for this purpose is presented in the following.

```
clear
close all

radius=0;

pics==%Training images >> Array of 2D cross section numbers (depth)

t1=%Array of first threshold (air-liquid)
t2=%Array of second threshold

stacks=stack;
%stacks=[3 5 6 7 8    9 10 11 13 14     15 16 17 18 19     20 21 22 23 24
26 27 28 29 30     31 32 33 34 35];

image_name=sprintf('file address',stacks(1),pics(1));

image=imread(image_name);
r=321; %%% for lower section of the column
rr=2*(r+15);
pic=pics(1);
yy=775+floor(pic/90); xx=1270+floor(pic/60); %%%S
cut=image(xx-r+50:xx+r+50-1,yy-r+50:yy+r+50-1);
% figure, imshow(cut);
yy=floor(length(cut(:,1))/2);
xx=floor(length(cut(:,1))/2);
final=cut;
for k=1:length(cut(:,1))
    for j=1:length(cut(:,1))
        if (k-xx)^2+(j-yy)^2>r^2
            final(k,j)=0;
        else
            final(k,j)=cut(k,j);
        end
    end
end
image=final;

l=length(image(:,1))/3;
w=length(image(1,:))/3;
```

```
% % % % % % TRAINING
x0=1;y0=1;
[svm_air1,svm_sand1]=TrainSVMSegmenterS(pics, stacks, radius, t1, t2,
x0,y0,l,w);
x0=l ;y0= 1;
[svm_air2,svm_sand2]=TrainSVMSegmenterS(pics, stacks, radius, t1, t2,
x0,y0,l,w);
x0=2*l ;y0= 1;
[svm_air3,svm_sand3]=TrainSVMSegmenterS(pics, stacks, radius, t1, t2,
x0,y0,l,w);
x0=1 ;y0=w ;
[svm_air4,svm_sand4]=TrainSVMSegmenterS(pics, stacks, radius, t1, t2,
x0,y0,l,w);
x0=l ;y0=w ;
[svm_air5,svm_sand5]=TrainSVMSegmenterS(pics, stacks, radius, t1, t2,
x0,y0,l,w);
x0=2*l ;y0=w ;
[svm_air6,svm_sand6]=TrainSVMSegmenterS(pics, stacks, radius, t1, t2,
x0,y0,l,w);
x0=1 ;y0=2*w ;
[svm_air7,svm_sand7]=TrainSVMSegmenterS(pics, stacks, radius, t1, t2,
x0,y0,l,w);
x0=l ;y0=2*w ;
[svm_air8,svm_sand8]=TrainSVMSegmenterS(pics, stacks, radius, t1, t2,
x0,y0,l,w);
x0=2*l ;y0=2*w ;
[svm_air9,svm_sand9]=TrainSVMSegmenterS(pics, stacks, radius, t1, t2,
x0,y0,l,w);

% [svm_air,svm_sand]=RLTrainSVMSegmenterS(pic, stack, radius, t1, t2,
x0,y0,l,w);
    stack_value=0;
 for pic=150:1900%:1848%:1860 %647 752, 1610

%         stacktobesegmented(j)
%        pic
%         segmented=image;
        x0=1;y0=1;

[image,segmented1]=SegmentWithGivenSVMS(pic,stack_value,radius,svm_air1,svm
_sand1,x0,y0,l,w);

         x0=l;y0=1;

[image,segmented2]=SegmentWithGivenSVMS(pic,stack_value,radius,svm_air2,svm
_sand2,x0,y0,l,w);

        x0=2*l;y0=1;

[image,segmented3]=SegmentWithGivenSVMS(pic,stack_value,radius,svm_air3,svm
_sand3,x0,y0,l,w);

        x0=1;y0=w;

[image,segmented4]=SegmentWithGivenSVMS(pic,stack_value,radius,svm_air4,svm
_sand4,x0,y0,l,w);

        x0=l;y0=w;
```

```
[image,segmented5]=SegmentWithGivenSVMS(pic,stack_value,radius,svm_air5,svm
_sand5,x0,y0,l,w);

        x0=2*l;y0=w;

[image,segmented6]=SegmentWithGivenSVMS(pic,stack_value,radius,svm_air6,svm
_sand6,x0,y0,l,w);

        x0=1;y0=2*w;

[image,segmented7]=SegmentWithGivenSVMS(pic,stack_value,radius,svm_air7,svm
_sand7,x0,y0,l,w);

        x0=l;y0=2*w;

[image,segmented8]=SegmentWithGivenSVMS(pic,stack_value,radius,svm_air8,svm
_sand8,x0,y0,l,w);

        x0=2*l;y0=2*w;

[image,segmented9]=SegmentWithGivenSVMS(pic,stack_value,radius,svm_air9,svm
_sand9,x0,y0,l,w);


 filename=sprintf('file address',stack_value,stack_value,pic);
    segmented=uint8(zeros(3*l,3*w));

    for i=1:l
        for j=1:w
            segmented(i,j)=segmented1(i,j);
            segmented(i+l,j)=segmented2(i,j);
            segmented(i+2*l,j)=segmented3(i,j);
            segmented(i,j+w)=segmented4(i,j);
            segmented(i+l,j+w)=segmented5(i,j);
            segmented(i+2*l,j+w)=segmented6(i,j);
            segmented(i,j+2*w)=segmented7(i,j);
            segmented(i+l,j+2*w)=segmented8(i,j);
            segmented(i+2*l,j+2*w)=segmented9(i,j);
        end
    end
%     imshow(segmented);
    segmented=fiximage(segmented);
    imwrite(segmented,filename,'tiff');
end
```

```
function [svm_air, svm_sand] = TrainSVMSegmenterL(pic, stack, radius, t1,
t2,x0,y0,l,w)

 image_name=sprintf('file address',stack(1),pic(1));

image_orig=imread(image_name);
r=321; %%% for lower section of the column
rr=2*(r+15);
pics=pic(1);
yy=821+floor(pics/447); xx=550+floor(pics/71);%%%L
cut=image_orig(xx-r+50:xx+r+50-1,yy-r+50:yy+r+50-1);
% figure, imshow(cut);
yy=floor(length(cut(:,1))/2);
xx=floor(length(cut(:,1))/2);
final=cut;
for k=1:length(cut(:,1))
    for j=1:length(cut(:,1))
        if (k-xx)^2+(j-yy)^2>r^2
            final(k,j)=0;
        else
            final(k,j)=cut(k,j);
        end
    end
end
image=final;
image=image(x0:x0+l-1,y0:y0+w-1);
image=im2uint8(image);
image_length=length(image(:,1));
image_width=length(image(1,:));
diam=2*radius+1;
%sample_columns=4+diam*diam;
sample_columns=4;
num_pixels=image_length*image_width;
num_samples=length(pic)*num_pixels;
sample_probability=0.05;
sample_size=uint32(num_samples*sample_probability*2);
train=zeros(sample_size,sample_columns);
is_air=uint8(zeros(sample_size, 1));
is_sand=uint8(zeros(sample_size, 1));
%is_water=uint8(zeros(sample_size, 1));
index = 0;
for i=1:11 %%%%%%%%%%%%%%%%%

    image_name=sprintf('file address',stack(i),pic(i));

    image=imread(image_name);
pics=pic(i);
y0=1420+floor(pics/71); x0=950;%%%M
cut=image(x0-r+50:x0+r+50-1,y0-r+50:y0+r+50-1);
% figure, imshow(cut);
y0=floor(length(cut(:,1))/2);
x0=floor(length(cut(:,1))/2);
final=cut;
for k=1:length(cut(:,1))
    for j=1:length(cut(:,1))
        if (k-x0)^2+(j-y0)^2>r^2
            final(k,j)=0;
        else
            final(k,j)=cut(k,j);
```

```
        end
    end
end
image=final;
    image=im2uint8(image);
    image=medfilt2(image);

% image=n;

    image=image(x0:x0+l-1,y0:y0+w-1);
    segmented=SegmentWithGivenThreshold(image,t1(i),t2(i));
    segmented=fiximage(segmented);
    for x=1:image_length
        for y=1:image_width
            if rand < sample_probability
                index = index + 1;
                train(index, :) = ConstructDataPointForSVMSegmenter(image,
pic(i), stack(i), radius, x, y);
                if segmented(x,y)==0
                    is_air(index)=-1;
                    is_sand(index)=1;
              %      is_water(index)=-1;
                elseif segmented(x,y)==128
                    is_air(index)=-1;
                    is_sand(index)=-1;
               %     is_water(index)=1;
                else
                    is_air(index)=1;
                    is_sand(index)=-1;
                %    is_water(index)=-1;
                end
            end
        end
    end
end
index
sample_size
train(index+1:sample_size,:)=[];
is_air(index+1:sample_size,:)=[];
is_sand(index+1:sample_size,:)=[];
%is_water(index+1:sample_size,:)=[];
disp('constructed training data');
length(train)

%options=optimset('Algorithm','interior-point-
convex','Display','iter','MaxIter',1000);
options=statset('Display','iter','MaxIter',500000);
svm_air = svmtrain(train, is_air,'method','SMO','options',options,
'kktviolationlevel',0.00, 'tolkkt', 0.01,'kernel_function', 'polynomial');
disp('trained first svm');
svm_sand = svmtrain(train, is_sand,'method','SMO','options',options,
'kktviolationlevel',0.00, 'tolkkt', 0.01,'kernel_function', 'polynomial');
disp('trained second svm');
%svm_water = svmtrain(train, is_water,'method','SMO','options',options);
%disp('trained third svm');
% svm_air=single(svm_air);
% svm_sand=single(svm_sand);
end
```

```
function [data] = ConstructDataPointForSVMSegmenter(image, image_number,
stack, radius, x, y)
diam=2*radius+1;
%data=zeros(1,4 + radius);
data=zeros(1,4);
image_length=length(image(:,1));
image_width=length(image(1,:));
data(1,1) = x;
data(1,2) = y;
data(1,3) = image_number;
%data(1,4) = stack;
%for k=1:diam
%    for l=1:diam
%        x2=x-radius-1+k;
%        y2=y-radius-1+l;
%        val=-100;
%        if x2>=1 && x2 <= image_length && y2 >= 1 && y2 <= image_width
%            val = image(x2,y2);
%        end
%        data(1, 4+(k-1)*diam+l) = val;
%    end
%end
data(1,4) = image(x,y);
val = 0;
num = 0.0;
%for k=x-1:x+1
 % for l=y-1:y+1
  %   if k >= 1 && k <= image_length && l >= 1 && l <= image_width
   %    val = val + image(x,y);
    %   num = num + 1.0;
     %end
  %end
%end
%data(1,5) = val / num;
%data=single(data);
end
```

```
function [image,segmented] = SegmentWithGivenSVML(pic, stack, radius,
svm_air, svm_sand, x0,y0,l,w)


image_name=sprintf('E:\\Texture 2nd round\\done\\stacks\\copied to
cluster\\%d\\MNR_texture_16bit%2.4d.tif',stack,pic);

image_orig=imread(image_name);
r=321; %%% for lower section of the column
rr=2*(r+15);

yy=821+floor(pic/447); xx=550+floor(pic/71);%%%L
cut=image_orig(xx-r+50:xx+r+50-1,yy-r+50:yy+r+50-1);
% figure, imshow(cut);
yy=floor(length(cut(:,1))/2);
xx=floor(length(cut(:,1))/2);
final=cut;
for i=1:length(cut(:,1))
    for j=1:length(cut(:,1))
        if (i-xx)^2+(j-yy)^2>r^2
            final(i,j)=0;
        else
            final(i,j)=cut(i,j);
        end
    end
end
image=final;

    image=im2uint8(image);
    image=medfilt2(image);

% image=n;

image=image(x0:x0+l-1,y0:y0+w-1);

image_length=length(image(:,1));
image_width=length(image(1,:));
num_pixels=image_length*image_width;
filtered_image=medfilt2(image);
diam=2*radius+1;
sample_columns=3+diam*diam;
svm_input=zeros(num_pixels,sample_columns);

for x=1:image_length
    for y=1:image_width
        index=(x-1)*image_width + y;
        svm_input(index,:) =
single(ConstructDataPointForSVMSegmenter(filtered_image, pic, stack,
radius, x, y));
    end
end


disp('constructed test input');
result_air=svmclassify(svm_air, svm_input);
disp('classified air');

result_sand=svmclassify(svm_sand, svm_input);
```

```
disp('classified sand');
%result_water=svmclassify(svm_water, svm_input);
%disp('classified water');
segmented=uint8(zeros(image_length,image_width));

for x=1:image_length
    for y=1:image_width
        index=(x-1)*image_width + y;
        if result_sand(index)==1 && result_air(index)~=1
            segmented(x,y)=0;
        elseif result_sand(index)~=1 && result_air(index)==1
            segmented(x,y)=255;
        else
            segmented(x,y)=128;
        end
    end
end
end
```

Appendix C

Modified Figures

In this chapter, modified figures (as mentioned in the text) are presented. Names of the figures are started by C and followed by its actual number in the text except for the first figure (Figure C.1) which was not presented in the text.

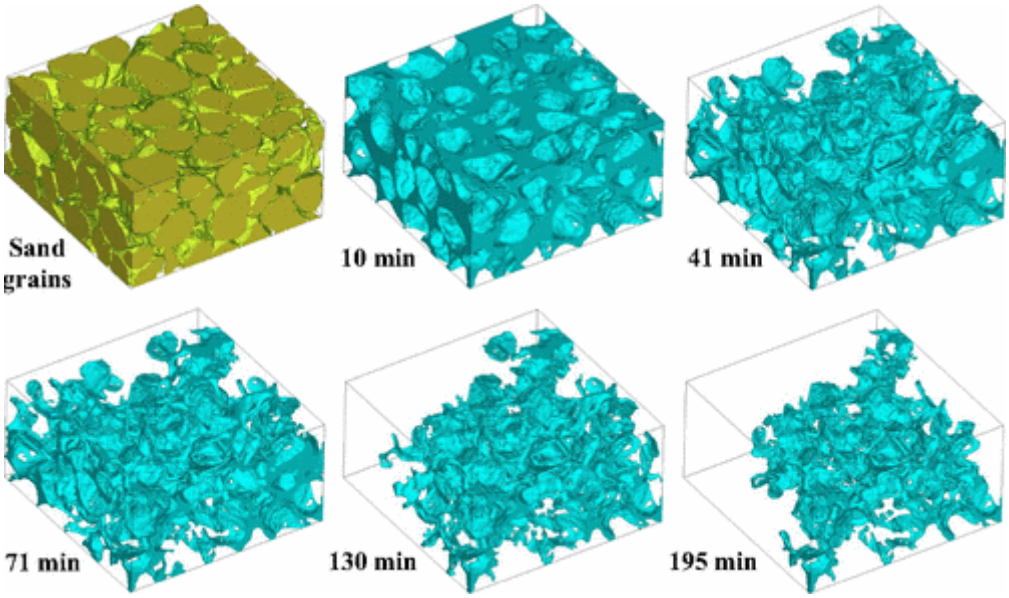

Figure C.1 "Liquid-phase distribution during evaporation from sand column using x-rays from synchrotrons. The arrangement of sand grains and liquid phase within the first scanned block ($3.3\times3.3\times1.7$ mm^3) is shown for five time steps. Isolated liquid clusters were filtered out to highlight continuous liquid phase only. In course of evaporation, water content decreases without breaking phase continuity" (Shokri *et al.*, 2010).

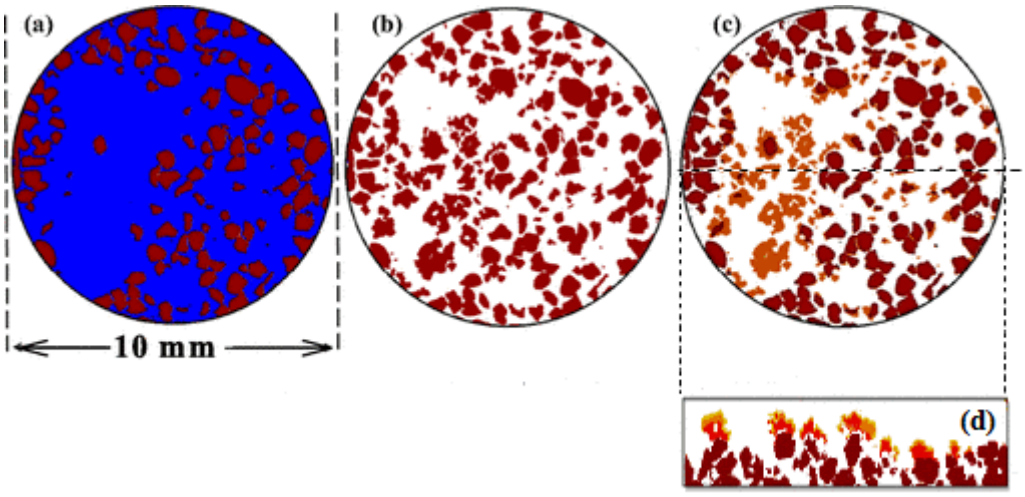

Figure. C. 3.1 (a) A typical horizontal cross section above the surface, taken at the beginning of the experiment, illustrating the liquid [blue (dark gray)] and solid [brown (medium gray)] phases. (b) The same cross section after 17 h, showing the distribution of the solid [brown (medium gray)] and air (white) phases. (c) The image constructed by comparing the solid phases in (a) and (b) with the difference [orange (light gray)], corresponding to the precipitated salt. (d) A typical vertical close-up of the surface of the sand column saturated with 4 Molal NaCl solution, constructed by the same method as in (c) and applied to all cross sections. The spectrum of orange to yellow (medium to light grey) indicates the addition of precipitated salt in each scan. Brighter colours indicate longer times.

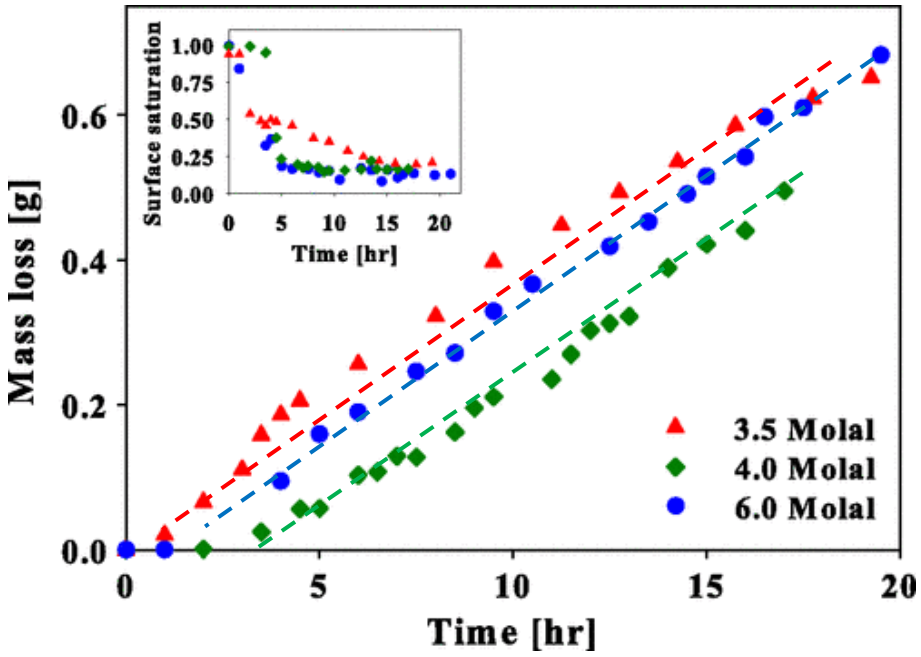

Figure C.3.2 "Cumulative mass of liquid water removed by evaporation from the sand columns, initially saturated with various NaCl solutions. The notably lower water evaporation from the 4.0 Molal solution might be due to the lower atmospheric demand. Although the evaporative demand was nearly constant during each round of the experiment, the relative humidity and temperature inside the x-ray chamber could not be controlled precisely. The inset shows the near surface (the top 0.5 mm) water saturation, confirming the presence of liquid at the surface during the entire course of the experiments". (Norouzi Rad *et al.* 2013)

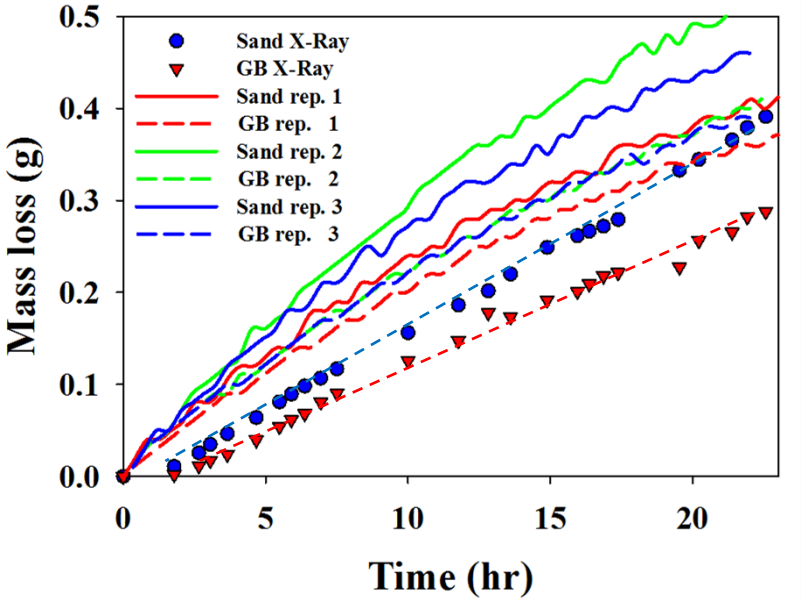

Figure C.4.3. "Cumulative mass of liquid water removed by evaporation from the columns packed with sand and glass beads initially saturated with NaCl solution. The symbols correspond to the cumulative mass loss measured during the experiments with X-ray microtomography determined from image analysis. In addition, three repetitions (written as rep. in the legend) were performed in the lab to measure the evaporation rate using digital balances to check the reproducibility of the observed behavior, *i.e.*, higher evaporation from sand pack compared to the glass beads. The solid and dash lines indicate the data measured using the balance. The slight difference in the measured cumulative mass loss in each round is due to the slight fluctuation of the evaporative demand during each round affecting the evaporative mass losses during stage-1 evaporation". (Norouzi Rad *et al.*, 2014)

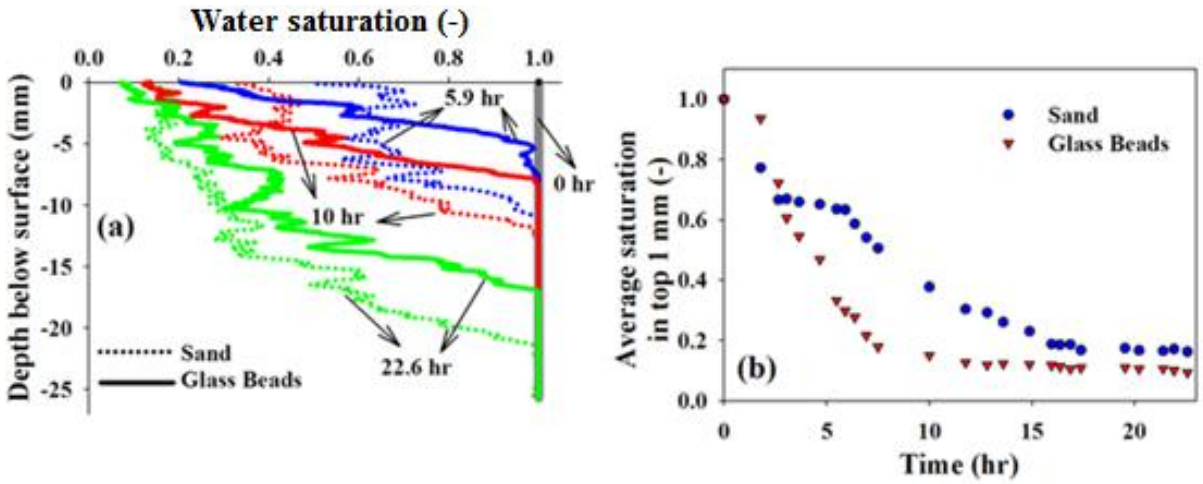

Figure C.4.5. "(a) Water saturation profiles at different times from the onset of the evaporation experiments in the columns packed with sand and glass beads. (b) The average water saturation over the top 1 mm of the sand and glass beads columns confirming the presence of water close to the surface during the entire course of our experiments in both cases and also higher water saturation in the case of sand compared to glass beads." (Norouzi Rad *et al.*, 2014)